Center for the Advancement of Natural Discoveries using Light Emission

Hrach Toneyan

TIME-LENS INDUCTION, SIMILARITON- AND SOLITON- SHAPING TYPE PROCESSES FOR FEMTOSECOND LASER PULSE MANIPULATION AND CHARACTERIZATION

PhD thesis

Specialization U.04.20 “Charged particle beam physics and accelerator technology”

Scientific supervisor:

Prof. Levon Mouradian

Yerevan 2018

Contents

Introduction **3**

Chapter 1: Literature review and overview of thesis **9**

1.1 Spectron and dispersive Fourier transformation 9

1.2 Nonlinear-dispersive similariton 10

1.3 Spectral interferometry for femtosecond signal characterization 12

1.4 Direct measurement of femtosecond pulses 15

1.5 Spectral compression and pulse self-compression 17

1.6 Overview of the thesis 21

Chapter 2: Spectral compression of femtosecond laser radiation **25**

Introduction 25

2.1 Classic technique of spectral compression 26

2.2 All-fiber spectral compression 29

2.3 Similaritonic spectral compression 31

2.4 Spectral compressor for spectrotemporal imaging of femtosecond pulses 35

Conclusion 46

Chapter 3: Spectral analogue of solitonic compression: spectral self-compression **47**

Introduction 47

3.1 Dispersion characterization of negatively curved hollow-core fiber 48

3.2 Experimental demonstration of the process of spectral self-compression 53

3.3 Numerical modelling of spectral self-compression 58

Conclusion 61

Chapter 4: Similaritonic and spectronic techniques of femtosecond pulse diagnosis **62**

Introduction 62

4.1 Spectral characteristics of nonlinear-dispersive similariton 63

4.2 Measurement of similariton bandwidth for femtosecond pulse duration determination 76

4.3 Numerical study of spectron phase peculiarities 78

Conclusion 89

Summary and Acknowledgements **90**

References **92**

List of abbreviations **102**

Introduction

The generation and acceleration of ultrashort high brightness electron beams are one considered as very important problems for the development of accelerator- based basic and applied researches. The laser driven technologies are the most promising approaches to reach the aforementioned goals. In high energy physics this is the development of advanced accelerator technology based on laser plasma wake field accelerators or laser dielectric concepts for future linear colliders [1-4]. For the applied research this is the laser driven ultrashort electron beam generation for ultrafast sciences and the creation of Free Electron Lasers [5-6]. The ultrafast lasers with tunable parameters are also powerful tools in advanced accelerators for beam parameters measurements and shaping of electron beams [7; 8].

In all these accelerator technologies, the generation, shaping and characterization of ultrafast laser pulses of sub-picosecond and femtoseconds duration in Infrared (IR) and Ultraviolet (UV) wavelength ranges are the key issues to succeed in goals.

The problem of pulse characterization in femtosecond time scale encouraged the use of adaptive optics, Fourier optics, spectral interferometric methods, etc. The narrowing of the laser pulse spectrum, or spectral compression (SC), which occurs due to the nonlinear effect in fibers, is of interest in the context of signal analysis and synthesis [9; 10]. Ultrafast laser sources are used in fields like femtochemistry, femtobiology, ultrafast spectroscopy, optical telecommunication, nonlinear optics, spectroscopy of ultrafast events, biophysics, photochemistry, etc. These fields require laser pulse measurement and manipulation tools for everyday operations. The generation and shaping of spectron, soliton and similariton pulses, and temporal lensing [11] brings some solutions to these urgent problems. Similariton pulses, due to their characteristics of linear chirp and broad spectrum are used in compression of ultrashort pulses, pulse characterization and manipulation. As the information is transferred from spectral to temporal domain in the spectron shaping process, these pulses are used in real-time registration of spectrum and other problems. Soliton and soliton-type pulses have broad applications in telecommunication and pulse manipulation problems.

The thesis consists of introduction to the subject, four chapters, summary, and a list of references. This includes 102 pages and 45 figures, including 112 references to scientific publications.

In the introduction, the brief overview of the topic of thesis, the overview of the chapters, the defending statements and the list of publications related to the work are presented.

In the first chapter, the review of the literature related to the topic of thesis is presented. In addition, the current unsolved problems related to the topic, the objectives of work, its scientific novelty and practical significance are presented.

Second chapter describes the studies aimed at the development and experimental demonstration of a compact prototype of spectrotemporal imaging (STI) device. This technique of imaging and direct measurement of femtosecond pulses, based on the process of SC, has the advantages, compared to its alternatives currently used in laboratories, which are the high resolution and the self-referencing performance of the device. The technique was implemented in a laboratory version, which showed the advantages compared to its alternatives. The research presented in this chapter is directed towards the development, design and experimental demonstration of a commercial prototype of the device with a compact footprint (30x30cm), which allows the practical use of the technique as a powerful instrument for ultrashort pulse characterization. Also, the classic, all-fiber and similaritonic techniques of femtosecond laser radiation SC is demonstrated experimentally. The classic technique enables high spectral brightness output due to its energetic efficiency, while the similaritonic technique allows achieving a much higher ratio of compression. For the all-fiber technique, a hollow-core fiber (HCF) was used, followed by a single-mode fiber (SMF). This allows to reach compact sizes of spectral compressor. The HCF was also used as a dispersive medium in the parallel scheme for both STI and wavelength-tunable SC.

Third chapter describes the first experimental demonstration of the spectral self-compression (self-SC), the spectral analog of pulse self-compression. Two experiments were performed, with use of an HCF in the first one, and a standard telecom SMF in the

second one, as a medium for self-SC. In the case of the use of HCF, the laser pulses with 800nm central wavelength were coupled into the fiber. A 1.3x self-SC was observed at the output of the fiber. In the second experiment, the amplified ultrashort laser radiation at 1030nm was used to generate the broadband supercontinuum in a YAG crystal. The supercontinuum was then filtered, keeping the part above 1300nm, and the resulting spectrum was coupled into a 600-m long SMF to achieve self-SC. At the output, a 4.1x compression of the spectrum was registered.

Fourth chapter consists of two studies: experimental and numerical investigation of similariton spectral characteristics, aimed at development of ultrashort pulse duration determination technique; and numerical study of the phase peculiarities in the process of spectron pulse shaping. In the study of similariton spectral characteristics, the dependence of the bandwidth from the input pulse duration was investigated experimentally and numerically for a variety of pulses with different shapes and durations. Experimentally, these pulses were coupled into a piece of SMF where the nonlinear-dispersive (NL-D) similariton was generated, and the spectral width and average power of the coupled radiation was measured. A general relation between the bandwidth of similariton and duration of test pulse is revealed, which allows the easy measurement of the pulse duration, with use of standard optical laboratory equipment, as an alternative to the autocorrelation technique. Moreover, the numerical analysis of the process of spectron pulse shaping shows, that additionally to the spectron pulse intensity profile repeating the spectral shape, the phase information is also transferred from spectral to temporal domain. This process is studied for the bell-shape regular pulses, multiple-peak pulses, pulses with sinusoidal modulation of intensity and phase, and two-peak pulses with initial self-phase modulation (SPM). The lengths of dispersive media on which the phase mimicking occurs are compared for the variety of test pulses.

The summary is concluding the main results of the research included in the thesis.

In the studies, the main method of research was the experiment, supported by the numerical modelling.

Defending statements:

1. With the use of an hollow-core fiber (2m HCF-800B) as an anomalous dispersion medium, followed by a standard single-mode fiber with normal dispersion (1m 780HP) as a nonlinear medium, an all-fiber temporal lensing based on the self-phase modulation is performed (sequential setup) for spectral compression of femtosecond pulses (8.4x, 800nm central wavelength). In the similariton-based temporal lensing setup with sum-frequency generation (parallel setup) of femtosecond pulse spectrotemporal imaging, the replacement of prism or grating pair with the HCF also provides the successful performance of the method.
2. The self-interaction of an 800nm central wavelength femtosecond laser pulse in an hollow-core fiber (2m HCF-800B), under the combined impact of strong anomalous dispersion and weak Kerr nonlinearity, leads to the spectral self-compression (30% spectral narrowing, along with the increasing of autocorrelation duration from 150fs to 1.3ps), in accordance with to the theoretical prediction of spectral analogue of soliton pulse compression.
3. The duration of a femtosecond laser pulse can be determined by coupling the radiation into a single-mode fiber, generating a nonlinear-dispersive similariton, and measuring its spectral width and pulse energy.
4. In the process of spectron pulse shaping, in the far field of dispersion, information (signal modulations) is transferred from spectral to temporal domain not only for field amplitude, but also for phase. As a result, a pulse is shaped, which reproduces the intensity spectral distribution, and its phase reproduces the initial spectral phase (in addition to the dispersion-induced parabolic phase).

The experimental studies presented in this thesis are done at CANDLE Synchrotron Research Institute and Yerevan State University. The scientific supervisor of thesis is Prof. L. Mouradian.

List of publications related to the work:

1. H. Toneyan, A. Zeytunyan, R. Zadoyan, and L. Mouradian “Classic, all-fiber, and similaritonic techniques of spectral compression”, Journal of Physics: Conference Series 672 012016 (2016).
2. H. Toneyan, “Experimental Techniques of Spectral Compression of Femtosecond Radiation”, Armenian Journal of Physics, 10 (3), pp. 108-111 (2017).
3. H. Toneyan, M. Sukiasyan, A. Zeytunyan, V. Tsakanov and L. Mouradian, “Designing the femtosecond optical oscilloscope”, Journal of Physics: Conference Series 673 012016 (2016).
4. V.M. Tsakanov, et al. "AREAL Test Facility for Advanced Accelerator and Radiation Source Concepts", Nuclear Instruments and Methods in Physics Research A, 829, pp. 284-290 (2016).
5. A.N. Kolyadin, G.K. Alagashev, A.D. Pryamikov, L. Mouradian, A. Zeytunyan, H. Toneyan, A.F. Kosolapov, I.A. Bufetov, “Negative curvature hollow-core fibers: dispersion properties and femtosecond pulse delivery”, Physics Procedia, vol.73, pp.59 – 66 (2015).
6. H. Toneyan, K. Manoukyan, M. Sukiasyan, A. Kutuzyan, L. Mouradian, “Spectral Characteristics of Nonlinear-Dispersive Similariton Generated in Single-Mode Fiber without Gain”, Armenian Journal of Physics, 10 (4). pp. 192-198 (2017).
7. Н. Карапетян, Г. Тонеян , А. Кутузян , М. Сукиасян , В. Аветисян, Д. Гулканян, К. Апресян , Л. Мурадян, “Численное Исследование Процесса Формирования Спектрона: Фазовые Особенности”, Известия НАН Армении, Физика, т.53, No2, с.173–180 (2018).
8. H.Toneyan, A. Zeytunyan, L. Mouradian, V. Tsakanov, F. Louradour, A. Barthelemy, R. Zadoyan, “8x, 12x, and 23x Spectral Compression by All-Fiber, Classic, and Similaritonic Techniques” Frontiers in Optics (FiO) 2014, FW4D.5 (October 19-23, 2014, Tucson, Arizona, USA).
9. H.Toneyan, M. Sukiasyan, A. Zeytunyan, V. Tsakanov and L. Mouradian, “Designing the Femtosecond Optical Oscilloscope”, 3rd International Symposium on Optics and its Applications, p.108 (oral presentation, 1-5 October, 2015, Yerevan, Armenia).

10. L. Mouradian, A. Grigoryan, A. Kutuzyan, G. Yesayan, M. Sukiasyan, H. Toneyan, A. Zeytunyan, A. Barthelemy, “Spectral Analogue of the Soliton Effect Compression: Spectral Self-Compression” Frontiers in Optics (FiO) 2015, FW3F.3 (October 18-22, 2015, San Jose, CA, USA).
11. H.Toneyan, M.Sukiasyan, V.Avetisyan, A.Kutuzyan, A.Yeremyan, and L.Mouradian, "Solitonic Self-Spectral Compression of Noisy Supercontinuum Radiation"- Frontiers in Optics 2016, OSA Technical Digest , Rochester, New York, United States, 17–21 October , JW4A.44 (2016).
12. K.Manoukyan, H.Toneyan, A.Zeytunyan, and L.Mouradian, "Simple Similaritonic Alternative to the Autocorrelation Technique for Determination of Femtosecond Laser Pulse Duration"- 25th Annual International Laser Physics Workshop (LPHYS’16), Yerevan, Armenia July 11-15, P.S8.4 (2016).
13. N.Karapetyan, H.Toneyan, A.Kutuzyan, and L.Mouradian- "Spectron’s phase peculiarities: numerical study"- 5th International Simp. Optics & its appl.ications, 25-28 July,2016 Yerevan-Ashtarak, Armenia July 11-15, p. 113 (2016).
14. K.Manukyan, M.Sukiasyan, H.Toneyan, A.Zeytunyan, and L.Mouradian, "Simple Diagnostics of Femtosecond Pulses by the Use of Nanosecond Oscilloscope"- Frontiers in Optics 2017, OSA Technical Digest, Washington D.C, United States, 17–21 September, JTu3A.62 (2017).
15. N. Karapetyan, H. Toneyan, A. Kutuzyan, L. Mouradian, “Numerical analysis of spectron phase peculiarities”, IONS Balvanyos 2017, pp. 116-117, Balvanyos, Romania (2017).

CHAPTER I

LITERATURE REVIEW AND OVERVIEW OF THESIS

1.1 Spectron and dispersive Fourier transformation

Spectrons are pulses, which have a temporal intensity profile that repeats the profile of the spectrum, in a temporal analogy with Fraunhofer diffraction [12]: they are shaped, when a pulse passes through long enough dispersive medium. Spectrons provide dispersive Fourier transformation (DFT), a method which demonstrates interesting applications [13]. The concept of space-time duality is used for ultrashort pulse characterization and processing, overcoming the speed limitations of traditional optical devices. DFT allows the mapping of the spectrum of test pulse on the temporal domain [14]. This allows the real-time single-shot measurement of the spectrum by the use of an oscilloscope. The DFT is done by passing the pulse through medium with group-velocity dispersion (GVD). The application of DFT in spectroscopy allowed the identification of dynamics of spectrum in absorption and Raman spectroscopy [15]. This led to the first registration of optical rogue waves [16] and allowed the demonstration of a stable type of coherent white light generation – the stimulated supercontinuum generation [17].

The large GVD, required for spectron generation, can be reached through various methods. The most known ones are through the implementation of a dispersive delay line (DDL), consisting of a pair of prisms or gratings with a reverse mirror. Other interesting solutions are the use of fiber Bragg gratings [18; 19], SMF in the absence of nonlinearity, hollow-core fibers, chromo-modal dispersion [20], etc. In particular, the chromo-modal dispersion uses a pair of gratings to apply spatial distribution of spectrum in the beam. This beam is then coupled into a multimode fiber with a lens, resulting in the angular distribution of spectrum in the multimode fiber. The different wavelengths are traveling through different modes of the fiber, resulting in a huge stretching of the output pulse (up to nanosecond domain). The final duration of the pulse depends on the angle of insertion

and the core size of the multimode fiber, but not on the spectral width of the pulse, in opposite to the classical DDL.

1.2 Nonlinear-dispersive similariton

The NL-D similaritons [11; 21; 22] generated in a passive SMF recently show a variety of applications in the problems of femtosecond signal characterization and processing. NL-D similaritons are self-shaped when an ultrashort pulse passes through an SMF. The combined impact of the second order of dispersion and Kerr nonlinearity in an SMF results in a pulse with interesting properties. In the first step of the NL-D similariton shaping, the input pulse is reshaped into a pulse with flat top profile. In the further length of the fiber, the pulse obtains linear chirp due to the GVD of the fiber, which results in a pulse profile that repeats the profile of the spectrum. This linear chirp depends (linearly) on the length of the fiber where in which NL-D similariton is shaped, but not on the initial pulse parameters. The resulting pulse has a near-parabolic spectral and temporal shape [11].

NL-D similariton has a variety of important applications [11; 21; 22] in ultrafast laser science. Some of those applications are listed below:

Compression of NL-D similariton pulses. Similariton pulses are used in pulse compression techniques, due to the linear chirp and smooth bell-shaped profile of the similariton pulse. Similariton pulses were compressed down to 14fs duration [23], with a potential of compression of as low as 6fs. This result can be enhanced with the use of a hybrid DDL consisting of a combination of prisms and gratings, which allows the more precise compensation of high-order dispersion.

Similariton-based chirped CARS microscopy and spectroscopy. The use of broadband femtosecond pulses in CARS microscopy with pulse chirping and spectral focusing provides both high contrast of image and tunability of the spectrum [24]. Another approach is based on periodical modulations of the amplitude of a broadband pulse, in a resonance with medium Raman oscillations [25]. These setups can be simplified with the use of a single laser source through the application of NL-D similariton.

Femtosecond pulse characterization through the solution of reverse problem of generation of the NL-D similariton. The NL-D similariton has a linear chirp, which depends only on the fiber parameters in which it was shaped, and can be easily calculated. Thus, the similariton temporal and spectral profiles can be measured by only recording the spectrum of the NL-D similariton. The initial pulse shape can be recovered if the reverse dynamics of propagation through the fiber is numerically calculated for the measured NL-D similariton. Thus, a short piece of fiber and a software can be an alternative to FROG technique [26-28].

Self-referencing spectral interferometry based on similaritons. The classic spectral interferometry is using the interference of the test and a reference pulse in a spectrometer, which results in beating in spectrum. These beating carry information on the difference of the spectral phases of two pulses. The application range of this technique is limited by the need of reference pulse, with the bandwidth larger or equal to the one of the test pulse, meaning that a single laser source cannot be used for the measurement of test pulse that undergoes nonlinear impact. This technique is improved by the application of NL-D similariton as a reference pulse [21; 29]. The similariton is generated from a portion of the test pulse in an SMF, thus providing the self-referencing performance of the technique. As the linear chirp of similariton is easily calculated from the length of SMF, the spectral phase of the test pulse can be calculated from the registered spectral beatings.

Similariton-induced time lens for pulse spectrotemporal imaging. This technique provides the conversion of pulse temporal profile to the spectral domain, both for the intensity and phase. The time-to-frequency Fourier Transformation is done by the temporal lens, in an analogy with the space to wavevector transformation done by a spatial lens. The direct and real-time temporal measurements were done by the spectral imaging of the pulse based on the aberration-free similariton-based temporal lensing. This leads to the development of the ultrafast optical oscilloscope [29; 30], with the resolution given by the spectral width of NL-D similariton: it is ~5fs for an 80-THz bandwidth similariton [9; 31-35].

Spectral focusing by similariton-induced temporal lens. In an analogy with the beam collimation in the spatial domain, the similariton-induced temporal lens provides SC, which is aberration-free due to the parabolic shape of the similariton central energy carrying part.

In this method, the pulse is first stretched in the DDL. The accumulated phase is then compensated in a quadratic nonlinear process (e.g. sum- or difference-frequency generation, CARS, etc.). It is done by applying a positive parabolic phase to the pulse in the nonlinear process. For this, the NL-D similariton, generated from a portion of the test pulse, is used as a reference pulse. Experimentally, this technique of SC has shown effective and aberration-free SC in sum-frequency generation (SFG) process. This type of SC can be used in CARS spectroscopy to increase its resolution.

Control of signal spectrum in the similariton-induced temporal lens. The setup of SC done by similariton-induced temporal lens also has the capability of controlling the central wavelength of the generated signal. It is done by applying a temporal delay between the two pulses, which participate in the SFG process. The combination of SC and frequency tuning can be applied in resonant spectroscopy and in telecommunication.

1.3 Spectral interferometry for femtosecond signal characterization

The most commercialized and well-known technique of femtosecond signal characterization is the FROG [26-28] technique. FROG uses virtually any nonlinear-optical effect and it is based on registration of signal spectrum versus the temporal delay between the two replicas of the input pulse. The resulting 3D pattern of intensity depending from the frequency and delay is known as pulse's spectrogram. The iterative retrieval procedure then allows to reconstruct the phase and intensity profiles of the pulse, thus giving the complex field, i.e. completely characterize the pulse. The resolution of such measurements is theoretically limited by the response time of the nonlinear medium.

The XFROG [36; 37] technique is a cross-correlation-based alteration of FROG [26-28], which allows the simultaneous measurement of the amplitude and phase of two ultrashort pulses with different central wavelengths. The two pulses have to be derived from a single mode-locked laser in order to match the repetition rate of the pulses. A $KNbO_3$ crystal is used for the sum-frequency-mixing of two (mid-IR and near-IR) pulses [37]. The spectrum of sum-frequency-mixing signal is registered by a spectrometer for different time delays between the two pulses. The pulse data is retrieved from the registered spectra using iterative numerical procedures.

The GRENOUILLE [38] technique is a simplified setup of FROG. It uses a Fresnel biprism to replace the beam splitter, delay line and beam-combining optics. The setup uses a thick second-harmonic generation (SHG) crystal, which gives stronger signal. The use of biprism results in non-sensitive alignment of the setup, which makes the use of the device much simpler. Cylindrical lenses are placed after the thick SHG crystal, and the resulting beam is imaged using a CCD camera. The beam registered by the camera has the full single-shot trace of intensity vs wavelength (vertical) and intensity vs delay (horizontal).

Spectral interferometry is another powerful approach for ultrafast laser pulse diagnostics. The classic technique of spectral interferometry is done by coupling the two beams (test and reference) into the spectrometer, where the interference in the spectrum is registered [39]. The beatings in spectrum carry the information on the difference of the spectral phases between the test and reference pulses. After subtracting the known phase of the reference pulse (usually laser pulses without any interactions with medium), the test pulse spectral phase is revealed, which can be applied on the spectrum in order to receive the complex field of radiation i.e. completely characterize the signal. This basic method of spectral interferometry has a major drawback, it cannot operate when the test pulse has broader spectrum than the signal. To overcome this limitation, several upgraded methods of spectral interferometry have been developed, such as SPIDER [40-42], SPIRIT [43; 44], and SORBETS [45], as well as the similariton based spectral interferometry [11; 21].

SPIDER (spectral phase interferometry for direct electric field reconstruction) [40-42] is a single-shot self-referencing interferometric technique, which provides the amplitude and phase measurement of ultrashort laser pulses. It uses nonlinear frequency mixing to generate a replica of test pulse with a spectral shear. The interferogram is then measured using an integrating detector. The amplitude and phase of the pulse are then reconstructed from the interferogram. The use of two-dimensional detector array allows the measurements to have single-shot performance. SPIDER technique is suited also for ultraviolet and infrared pulse characterization.

Spectral interferometry resolved in time (SPIRIT) [43; 44] is another method for pulse amplitude and phase measurements based on spectral shearing interferometry. In this

method, a standard spectrometer is used to display the input pulse's spectrum in various positions on a spatial axis. The shear plate is inserted into the system, before, after or inside the spectrometer. This creates the replica of the test pulse, with a slight shift in space, which overlaps the original spectrum on the spatial axis. The two spectra are placed close to each other, so that they almost entirely overlap each other. The spatial beatings that occur in this setup carry the information on the spectral phase of the test pulse. A streak camera is used to register the pattern of those beatings. Another way of registration is the clipping of a single temporal slice of the spatiotemporal interference. Time gating is done through noncollinear SFG from the test signal and a shorter pulse. In most of the cases, taking part of the signal at the input of the system is enough for the time gating, meaning that the technique is self-referencing. For the single-shot performance, the gate beam has to be broadened to fully cover the test spectrum. The SPIRIT technique is capable of characterizing the pulses both in single-shot and repetitive regime.

Superposition of optical radiation and beatings to extract the time signals (SORBETS) [45] measures the spectral phase of the test pulse through the superposition of two shifted replicas of the spatial representation of test pulse spectrum. The resulting spectral beatings are registered at each point of the spectrum. The generated beatings have low frequency, which allow the recording of signal by a fast linear detector. The setup allows to give the spatial shift as small as needed, which allows to temporally resolve the signal by a detector. The setup is also capable to measure the spectral phase of a single pulse

The methods mentioned above (SPIDER; SPIRIT; SORBETS) have the advantage of non-iterative measurement of the spectral phase (compared to FROG technique [26-28]), with the drawback of having more complex implementation.

The similariton-based self-referencing spectral interferometry [11; 21] is another interferometric technique for femtosecond signal analysis. In this method, a part of the signal is coupled into an SMF, where a reference NL-D similariton [11] is generated, with broad spectrum and linear chirp, given by the fiber dispersion only. Both pulses are then coupled simultaneously into the spectrometer, where the spectral beatings occur. As the similariton pulse always has larger spectrum compared to the signal, it will always cover the entire spectrum of the pulse under test. The registered spectral beating pattern carries

the information on the difference of the spectral phases of the test and similariton pulses. Due to the linear chirp of the similariton pulse, which does not depend on the seed pulse, it is easy to calculate the spectral phase of the test pulse, which is then applied on its spectrum to get the complex field of the test pulse i.e. completely characterize the signal. This method combines the advantages of both the classic spectral interferometry and spectral shearing interferometry, with its simplicity and self-referencing performance.

A technique of real-time spectral interferometry [46] uses a combination of spectral interferometry and dispersion-induced real-time Fourier transformation, demonstrating single-shot complete pulse characterization with a temporal resolution of ~400fs on a record span of ~350ps (900x record span and resolution ratio). The measurements update rate were up to 17MHz. This fiber-optics-based method uses balanced Fourier-transform spectral interferometry scheme [47; 48], combined with real-time optical Fourier transformation [49; 50]. It is based on measurement of the energy density of interference pattern between the test pulse and a known reference pulse (with spectral width larger than the one of the test pulse).

Another interesting solution to the spectral phase measurement of ultrashort pulses is the recently developed MIIPS [51; 52] technique. This technique is not based on interferometry and does not require a reference pulse. It adaptively changes the spectral phase using the feedback from the second harmonic signal. It is done through the shaping of shortest possible pulse from the test pulse, which is corresponding to the second harmonic signal with maximal intensity.

1.4 Direct measurement of femtosecond pulses

All of the mentioned diagnostic methods are based on the determination of the spectral phase of signal, and completely characterize it. In order to perform femtosecond pulse direct measurement, the temporal information has to be transferred into the space or frequency domain. The measurements can also be performed, if the information is transferred into temporal domain within a measurable scale, thus “zooming” the pulse to measureable scales. For this approach, the 103x upconversion time microscope is

demonstrated [53], with a 300fs resolution and measurements is done on a 5.7ps span. The setup consists of three parts. In the first and last parts, the test pulse is passing through a grating-pair based DDL to obtain linear chirp. In the middle part of the setup, an SFG crystal, in which sum-frequency is generated from the test and a pump pulse, which is also linearly chirped. The SFG signal then passes through the second DDL, and the signal with temporal magnification is measured.

The silicon-chip based ultrafast optical oscilloscope [54] demonstrates direct and single-shot measurement of subpicosecond pulses, 220fs temporal resolution. The measurements here are performed on a temporal span of up to 100ps. It uses complementary metal-oxide semiconductor (CMOS)-compatible electronics and optics, and SMF. This technique applies phase shift by using four-wave mixing. In the experimental setup, the test pulse passes through an optical fiber, while the pump pulse passes through a fiber with double the value of dispersion. Afterwards, the two pulses are combined in a nanowaveguide, where four-wave mixing is done. The resulting spectra is registered with a spectrometer, and has the shape of the input pulse. The spectral width of the pump pulse and the dispersive element's length determine the length on which the device records and its resolution.

Another promising alternative to the femtosecond pulse registration problem is the similariton-based spectrotemporal imaging (STI) technique [9; 30-35]. STI provides direct measurement of femtosecond pulses. The setup also provides SC and frequency tuning on the second harmonic wavelength. STI uses similariton pulses [22], generated in a passive SMF, linear chirp, as a reference pulse for the temporal lens. The test pulse passes through a DDL, where spectron is generated. Those two pulses participate in the SFG process, which results in a pulse with a spectrum, repeating the initial pulse shape. This technique has the advantage of self-referencing performance, as the similariton is generated from the portion of test pulse. It also provides fine spectral tuning along with strong aberration-free SC [23-25; 29]. This spectrum can be tuned in frequency domain, which is done by giving temporal delay between the similariton and test pulse. This leads to compressed spectrum which has wavelength, depending on the delay between the two pulses.

1.5 Spectral compression and pulse self-compression

The nonlinear process of SC [55-58], the spectral analogue of pulse compression, occurs when the laser pulses pass first through a dispersive medium with negative dispersion, and then receive impact of nonlinearity in the second medium, for example, through SPM [9], usually by passing through an SMF. In the process of SC, the dispersive impact stretches the pulse and applies negative linear chirp, which is then compensated by the SPM in the SMF, and results in a pulse with compressed spectrum. This technique shows applications in various fields, based on the spatiotemporal analogy and the time lens concept [11; 59].

The principle of SC is based on the compensation of the parabolic dispersion-induced phase by the nonlinear phase (via e.g. SPM). The phase given by the SPM depends on the pulse shape. For Gaussian or sech pulses, the central energy carrying part of the pulse is parabolic. The difference from parabolic shape results in side lobs in the compressed spectrum. To overcome this unwanted effect, an amplitude-modulated SC was done [59]. In this study, pulse shaper was used to form the linearly negatively chirped parabolic pulses, which were then compressed in a photonic crystal fiber (PCF). The parabolic shape of the pulse provided the aberration-free SC of the pulse. This resulted in 8.7x SC, which corresponded to pulse, which exceeds the Fourier transform limit by 20%.

Another promising result for SC of picosecond pulses was achieved through an all-fiber configuration of spectral compressor [60], operating at the telecommunication wavelengths. In this study also, the pulse shaper was used for the shaping of parabolic pulses. SMF was used to give the initial linear chirp to the pulse. The pulse then passed through a kilometer-long highly nonlinear fiber, where the SPM phase compensates the initial phase from SMF. This resulted in a 12x SC factor, with aberration-free spectrum, due to the parabolic shape of the pulse.

The similariton-based SC technique [30] also shows an effective SC process, due to similariton-induced temporal lensing. In this case, the pulse is split into two parts. The linear negative chirp is obtained by the first pulse in a DDL. The second pulse is coupled into an SMF, where an NL-D similariton is generated, with flat central energy carrying part

and linear positive chirp. This similariton is then used for time lens induction in the process of SFG. The SFG signal is spectrally compressed, due to the compensation of two chirps in the process of its generation. This technique of SC is also aberration-free, due to the linear chirp of the similariton. It also has the opportunity of spectral tuning in the spectral range of similariton, which typically exceeds the spectral width of the seed pulse by a factor of 10. The tuning is done simply by changing the spatial delay between the two pulses, which results in interaction of the dispersive pulse with sides of the similariton, instead of the center, resulting in change of the central wavelength of SFG signal.

These techniques of SC have a wide spectrum of promising applications. They can be used in resonant spectroscopy [9; 10], generation of dark solitons [61], femtosecond signal undistorted delivery due to the lowering of the dispersive impact of medium [62], and the D-scan method of material characterization, a temporal analog of Z-can technique [63].

An experimental demonstration of technique for cancelling of spectral broadening caused by nonlinearity, using phase modulation was reported in paper [64]. This technique uses sinusoidal phase modulations in temporal domain to effectively cancel the chirp gained from SPM. The experiments were performed both for passive and amplifying fiber. In this experiments, an all-fiber configuration was used, with a continuous wave external cavity laser at 1550nm, matched with the wavelengths used in telecommunication. A lithium-niobate modulator was used to modulate the intensity of the radiation, with a 20GHz bandwidth. Thereafter, repetition rate was reduced to 100MHz and phase modulation was applied to the pulses. The radiation was then coupled into the fiber, which had pure nonlinear impact with an ignorable dispersion. This technique can be interpreted as spectral focusing (SC), where the initial sinusoidal phase modulation is canceled by the nonlinear impact in the fiber. This method can be useful in application in high-power pulse amplification, for pulses with ~10ps duration.

An interesting method of signal manipulation in picosecond time scale was reported in paper [65]. An all-optical tunable delay was demonstrated in a fiber, with use of dispersive element and two nonlinear elements and filters. The 3.5ps laser pulses were given a continuous delay over a range equal to 1200 times the width of the pulse. This method can

be used in telecommunication networks, where buffering or delaying of information is needed. Compared to other techniques based on “slow light” using laser-induced resonances [66], or techniques which use four-wave mixing to achieve the delay [67], this techniques has much simpler setup. It uses the Mamyshev regenerator [68] to achieve wavelength conversion. The spectrum is broadened through SPM in a 1km of highly nonlinear fiber. Afterwards, the pulse is amplified, and a tunable bandpass filter is used to cut the required part of the spectrum. The pulse then propagates through a 4km long dispersive fiber, where delay is applied. This delay depends on the chosen wavelength, thus giving the control over it. The delayed pulse is then again amplified and coupled into a 2km long highly nonlinear fiber. After SPM broadens the spectrum, the desired part of it is filtered to return to the initial central wavelength of the test signal. Experimentally, this method has shown the delay of up to 4ns for a 3.5ps pulse.

Another hot topic of contemporary laser physics are the optical solitons [69]. They are shaped when the pulse propagates through a medium with both negative dispersion and nonlinearity. Fundamental soliton propagates through medium without changing its parameters, given that the seed pulse had specific energy and shape. In the case if the dispersive impact of the medium is equal to the impact of nonlinearity, and the pulse has sech-shape, the fundamental solitons are shaped. In the case of fundamental solitons, the width of the pulse is inverse proportional to its amplitude. If the dispersive and nonlinear impacts are close, but not equal to each other, or in case if the pulse form is not sech-shaped, but is bell-shaped, the fundamental soliton is still generated [70], after passing some length in the nonlinear-dispersive medium. This makes solitons very useful in practical applications.

Pulse soliton-effect self-compression [70] is a new promising application of PCF. It is based on combined action of negative dispersion and SPM in a single material. This process is related to the generation of high-order soliton, which show periodical pulse narrowing and spectrum broadening, followed by pulse stretching and spectrum narrowing. The soliton-effect self-compression is achieved when the pulse exits the fiber in the compressed state. It was demonstrated experimentally [71] in a commercial PCF with 2.3μm core diameter tapered [72-75] down to 980nm size. Using this fiber, the 70fs pulses

were self-compressed down to 6.8fs few-cycle duration. In another study [75], the soliton-effect self-compression down to a single-cycle was reported. It uses Kagome fiber as the medium for self-compression, for pulses with up to 100μJ energy level. The Kagome fiber has a large core filled with gas under pressure, which is used as the medium for nonlinear interaction. The large core and absence of silica allows scaling the power input of the system, allowing the generation of self-compressed pulses with high pulse energy, without damaging the fiber. The setup operates in a modified solitonic regime, when a shock wave enhances the broadening of the spectrum. The 20x self-compression resulted in generation of 4.5fs pulse, under the 5fs optical cycle duration, with a gigawatt peak power at the output of the fiber.

Similarly to the pulse soliton-effect self-compression, the SC in a single medium is reported in paper [76]. Here, the 102.8x SC was experimentally demonstrated through soliton propagation in a dispersion-increasing fiber. The setup used a 1km long dispersion-increasing fiber, with relation of dispersion value at the input and output equal to 22.5. The 69fs nearly transform-limited laser pulse was coupled into the fiber, which resulted in the 102.8x self-compression of the spectrum. This spectrum can also be wavelength tuned in the range of 115nm by changing the coupled pulse power. Additionally, by negatively chirping the input pulse and choosing the coupling power within a specific range, structured spectral self-compression is observed in the process of soliton fission [77], with two distinct bright peaks.

Dark solitons are pulses which have an intensity dip on a constant background, generated in the region of positive dispersion. If the dip in the intensity goes down to zero at its center, the pulse is referred as a fundamental dark soliton or a black soliton. In this case, the pulse has a phase jump equal to π at the central part. The generation of dark soliton requires pulse shaping in amplitude and phase domains, as laser sources do not provide pulses with such characteristics.

The first experimental observation of dark solitons was done for picosecond pulses at 600nm central wavelength [78]. Paper [79] reports the experimental demonstration of femtosecond duration dark soliton generation. The generation of dark soliton train in an optical fiber was demonstrated experimentally in paper [80]. In this technique, two visible

pulses with a temporal delay are co-propagating in a long fiber. The streak camera at the exit of the fiber registered the formation of picosecond duration dark solitons. A synchronously pumped, cavity-dumped dye laser was used as the source of radiation in this experiment. The 2ps pulses were sent into a Michelson interferometer to shape pairs of pulses with equal intensities and controllable delay between each other. The output pulse pairs were coupled into a polarization preserving SMF with length of 100m. The picosecond dark solitons were registered at the output of the SMF, using a streak camera. A dark soliton communication setup is theoretically described, using Raman scattering to compensate the absorption in SMF [81]. Experimental and theoretical research also revealed that a dark soliton in a fiber with absorption are scattered and attenuated less than in a usual fiber [81-84]. Dark solitons are reported to undergo compression while amplified [81]. If the gain coefficient is low, the adiabatic amplification occurs. Raman amplification can be used to achieve adiabatic amplification.

The experimental study of nonlinear propagation of a picosecond duration near infrared dark soliton in a 1km long SMF was reported [85]. The 5.3ps dark pulse was shaped on the 36ps background, which was then propagated in a kilometer long SMF. Those pulses propagate without distortions, in a regime corresponding to the generation of fundamental dark soliton. The experiment used 850nm central wavelength pulses generated by a Ti:Sapphire laser system. The more stable nature of dark solitons over the bright (usual) solitons on long propagation distances makes their use in telecommunication networks with amplification more appealing.

1.6 Overview of the thesis

Unsolved problems: Thus, the laser techniques and methods in their current state yield variety of solutions to the problems of ultrashort pulse diagnostics and measurements. The ultrashort pulse shaping through SC has also seen recent advances. Both of these directions of laser science are of interest in context of laser laboratory everyday operation and telecommunication. Despites the variety of important researches done in these fields, there are number of unsolved problems in these directions. Namely:

- The spectrotemporal imaging technique of ultrashort pulse characterization, which is an important and promising alternative in this field, has no compact and practical setup and design.
- Although the nonlinear process of femtosecond pulse spectral self-compression is studied numerically, there is no experimental demonstration and deep analysis of the process.
- Despite the new promising techniques of ultrashort pulse measurement, auto-correlator remains the most practical solution to everyday diagnostics of laser systems.
- Although the shaping of a spectron pulse is well studied, the phase peculiarities of this process are not researched.

Objectives of the work: The importance of problems of femtosecond laser pulse characterization and manipulation, particularly, the determination of pulse duration, shape and phase, defines the importance of the experimental and numerical studies included in thesis. The objectives of the work include the following:

- Study of the spectrotemporal imaging aimed at the development of compact commercial prototype of the device.
- Study of SC with the use of new high-tech materials.
- Study of soliton shaping-type processes, specifically, experimental studies aimed at the demonstration of the process of spectral self-compression.
- Study of the spectral peculiarities of similariton pulses with prospective of diagnostics of the initial femtosecond pulse.
- Study of spectron-type processes (dispersive Fourier transformation), specifically, investigation of the spectron phase peculiarities.

The scientific novelty of the work is represented in the results achieved for the problems of ultrafast optics, photonics and laser physics, particularly, in the following results important for the ultrafast pulse characterization and manipulation:

- The hollow-core fiber (HCF-800B) was used as a dispersive delay line, replacing the prism / grating pair, in the temporal lensing setup. Experimentally, the use of hollow-core fiber in the sequential setup resulted in an 8.4x SC. In the parallel setup, 11x SC and spectrotemporal imaging were registered at the sum-frequency wavelength.
- The process of spectral self-compression, the spectral analogue of pulse soliton self-compression, is demonstrated experimentally for the first time. A 30% spectral narrowing was registered for self-interaction of pulses with 150fs autocorrelation duration and 800nm central wavelength in a hollow-core fiber (2m-long HCF-800B), with growth of autocorrelation duration to 1.3ps. A more effective spectral self-compression (4x) was registered for radiation in our initial studies, in a long single-mode fiber for a part of supercontinuum spectrum.
- The relation between the duration of femtosecond pulse and the spectral width of NL-D similariton generated from it was studied both experimentally and numerically for pulses with different shapes and durations. Pulses with various shapes (Gaussian, sech, asymmetric, multi-peak and compressed pulses) and chirps were studied numerically, which resulted in revealing of the general relation between the duration of pulse of any shape and the spectral width of similariton generated from it. Experimentally, this relation was confirmed for Gaussian, two-peak and compressed pulses, which, by passing through dispersive delay lines of various lengths, had different durations and shapes.
- The transfer of information from frequency to time domain for phases in the process of spectron generation was studied using methods of numerical modelling, for various initial pulses. The necessary conditions for the process are revealed for asymmetric, two-peak and three-peak pulses, as well as for the pulses with amplitude or phase modulations of spectrum, and two-peak pulses with initial self-phase modulation.

Practical significance: The results of experimental and numerical studies presented in the thesis are of interest for problems of registration and manipulation of pico-femtosecond laser pulses, as well as for the needs of telecommunication, complete characterization of ultrashort pulses, CARS spectroscopy, and other urgent problems. The results are of

specific importance for their use in the design and enhancement of new methods of laser pulse diagnostics. In particular:

- The all-fiber setup of spectral compressor, due to the use of hollow-core fiber, significantly reduces the device sizes. The further advancements in this direction are expected by the splicing of hollow-core and single-mode fibers, for the implementation of the device in a united fiber. Such an integral device of SC is of interest for contemporary technological applications, such as similariton lasers, CARS spectroscopy, etc.
- The experimental study of the method of similaritonic spectrotemporal imaging has resulted in the development of prototype of the device for diagnostics of laser systems. It the current state, it has sizes of 30x30cm, and is easy in use. Moreover, the possibility of replacement of diffraction gratings by a hollow-core fiber is demonstrated experimentally, which reduces the sizes of the device, making its use in laser laboratories more practical. Compared to its alternatives, the device has an order of magnitude lower cost, while providing direct and high-resolution measurements of femtosecond laser pulses.
- The relation between the pulse duration and the bandwidth of an NL-D similariton generated from it in a passive single-mode fiber allows to perform the simple measurement of similariton spectral width instead of the complicated measurement of femtosecond pulse duration. As the method uses a single-mode fiber and standard equipment of optics laboratories, its implementation in laser pulse diagnostics is much simpler and significantly cheaper, compared to its alternatives.
- The transfer of phase information from temporal to spectral domain in the process of spectron shaping can be used for complete characterization of femtosecond pulses through the measurement of spectron phase by the sum-frequency generation. Spectral phase, together with the measured spectrum, gives the complete characterization of the complex field of the signal. This technique is an alternative to the spectral interferometric methods and devices, which are used for the signal complete characterization in femtosecond time scale.

CHAPTER II

SPECTRAL COMPRESSION OF FEMTOSECOND LASER RADIATION

Introduction

In this chapter, the experiments of SC through various techniques are presented, alongside with the design and experimental study of compact prototype of the STI device.

The nonlinear process of spectral narrowing, or SC [25; 56], is of interest, due to the its various applications. The process is the temporal analogue of diffracted beam collimation. The pulse is first stretched in a dispersive delay line, obtaining negative linear chirp. Afterwards the chirp is compensated in the nonlinear medium (e.g. fiber), which has the role of light-induced temporal lens, leading to spectral narrowing, or in the analogy to diffraction, beam collimation. This light-induced time lens, similarly to the usual lens, has more general function of Fourier transformation, meaning that the temporal information at the setup input is converted to the spectral domain, which leads to various applications in femtosecond signal registration and manipulation problems. STI is used for the direct real-time measurements of femtosecond pulses [9; 30]. SC is used in applications, such as: femtosecond pulse undistorted delivery [62]; fine frequency tuning [30]; resonant spectroscopy [58]; providing of high spectral brightness for CARS (coherent anti-Stokes Raman scattering) and stimulated Raman scattering microscopy. Recently, 8.7x SC of negatively chirped parabolic pulse generation was demonstrated, with the advantage of aberration-free SC, due to the optimal parabolic shape of the pulse [59]. Also, the 12x SC in an all-fiber setup was reported [60], with use of kilometer-long optical fiber. Experimental results of SC through classical, all-fiber and similaritonic techniques are reported in this section.

The most popular and commercialized techniques of femtosecond signal characterization is FROG [26]. This method and its modifications provide accurate determination of signal phase and amplitude profile, by registration of high-resolution spectrograms and decoding of the temporal information through iterative procedures.

Spectral interferometric techniques, such as SPIDER [40-42], SPIRIT [43; 44] and SORBETS [45], provide non-iterative recovery of spectral phase (and thus temporal shape of the pulse). One of the most advanced techniques of ultrashort pulse characterization is MIIPS [51], which uses adaptive mirror system for phase cancelation and transform-limited pulse shaping, by using of the feedback from second harmonic signal intensity.

The femtosecond signal characterization techniques described above are not direct in terms of pulse form recovery, as they operate by retrieving the spectral phase, measuring the spectrum, and then calculating the complex temporal field via Fourier transformation, and thus having the intensity temporal distribution (i.e. pulse). An example of direct measurement technique of pulse shape is the silicon-chip-based ultrafast oscilloscope, which provides temporal resolution of ~200fs [54]. In terms of temporal resolution, more promising is the STI in the similariton induced time lens [9; 31-34].

This section covers the studies aimed at development of commercial prototype of the STI device. Additionally, the research toward the development of real-time STI technique is described.

2.1 Classic technique of spectral compression

The nonlinear effect of SC occurs when a pulse is passing through a medium with GVD, followed by a medium with SPM. The GVD parabolically modulates the spectral phase:

$$\tilde{A}_{out}(\omega) = \tilde{A}_{in}(\omega)\exp[-i\omega^2(z/L_D)/2]. \quad (2.1)$$

Here, $\tilde{A}_{out}(\omega)$ is the Fourier image of the pulse slowly varying amplitude $A(t)$ passed through a dispersive medium, z is the propagation distance, and $L_D = (\beta_2 \Delta\omega_0^2)^{-1}$ is the characteristic dispersive length (β_2 is the coefficient of second order dispersion, $\Delta\omega$ is the bandwidth). The equation for SPM for bell-shaped (e.g. Gaussian) pulse has similar form, in temporal domain:

$$A_{out}(t) = A_{in}(t)\exp[i\beta_0 n_2 |A_{in}(t)|^2 z] \approx A_{in}(t)\exp[iz/L_{NL}]\exp[-it^2(z/L_{NL})] \quad (2.2)$$

Here $A_{out}(t)$ is the slowly varying amplitude of the pulse and $L_{NL} = (\beta_0 n_2 I_0)$ is the characteristic nonlinear length (β_0 is the wave number, n_2 is the nonlinearity coefficient). Opposite to the pulse temporal compression, which requires the pulse to undergo SPM followed by the GVD, the SC requires the pulse to obtain GVD, followed by SPM. For pulses, which first impacted by GVD and then by SPM, the field at the output of the system will be described as followed:

$$A(t) \propto \tilde{A}_{in}(\omega)|_{\omega=Ct} \exp\{i[\varphi_D(t) + \varphi_{NL}(t)]\}. \quad (2.3)$$

Here, the spectron approximation for GVD impact is considered; $\varphi_D(t)$ and $\varphi_{NL}(t)$ are the phases from GVD and SPM respectively. The ideal chirp cancelation for a bell-shaped pulse will occur when $\ddot{\varphi}_D + \ddot{\varphi}_{NL} = 0$, resulting in *s*-times stretched output transform-limited pulse, which means *s*-times compressed spectrum. In practice, the phase from SPM of a bell-shaped pulse is compensating the phase from GVD only partially, in the central part of the pulse, where it has parabolic shape.

Experimentally, the classic setup of SC consists of a dispersive delay line (DDL) [25], which provides negative dispersion, and a single-mode fiber (SMF) as a nonlinear medium for SPM. A DDL consisting of 3.75m separated SF11 prism pair with the reverse mirror, followed by 92-cm long Newport F-SE 780nm SMF for SPM were used (fig. 2.1a).

The initial radiation was at 800nm central wavelength with 11.3nm spectral bandwidth (fig. 2.1b). The radiation first passed through the prism pair, where it was stretched and obtained linear negative chirp. A standard ThorLabs fiber launching system was used to couple the radiation into the SMF. The laser (Gaussian) pulses are close to parabolic in their central energy carrying part, which leads to parabolic phase (positive linear chirp) from the SPM in the SMF. This positive linear chirp is added to the negative one from the DDL, resulting in chirp compensation, which leads to the spectral narrowing of the signal. The input 11.3nm bandwidth was compressed down to 0.92nm (fig. 2.1c) at the output of the system, with a compression factor of 12.3. The side lobes in the compressed spectrum are because of the uncompensated parts of the final chirp, as the Gaussian pulse is close to parabola only in the central part. The duration of output pulse measured by an autocorrelator was ~2ps, close to the bandwidth limit.

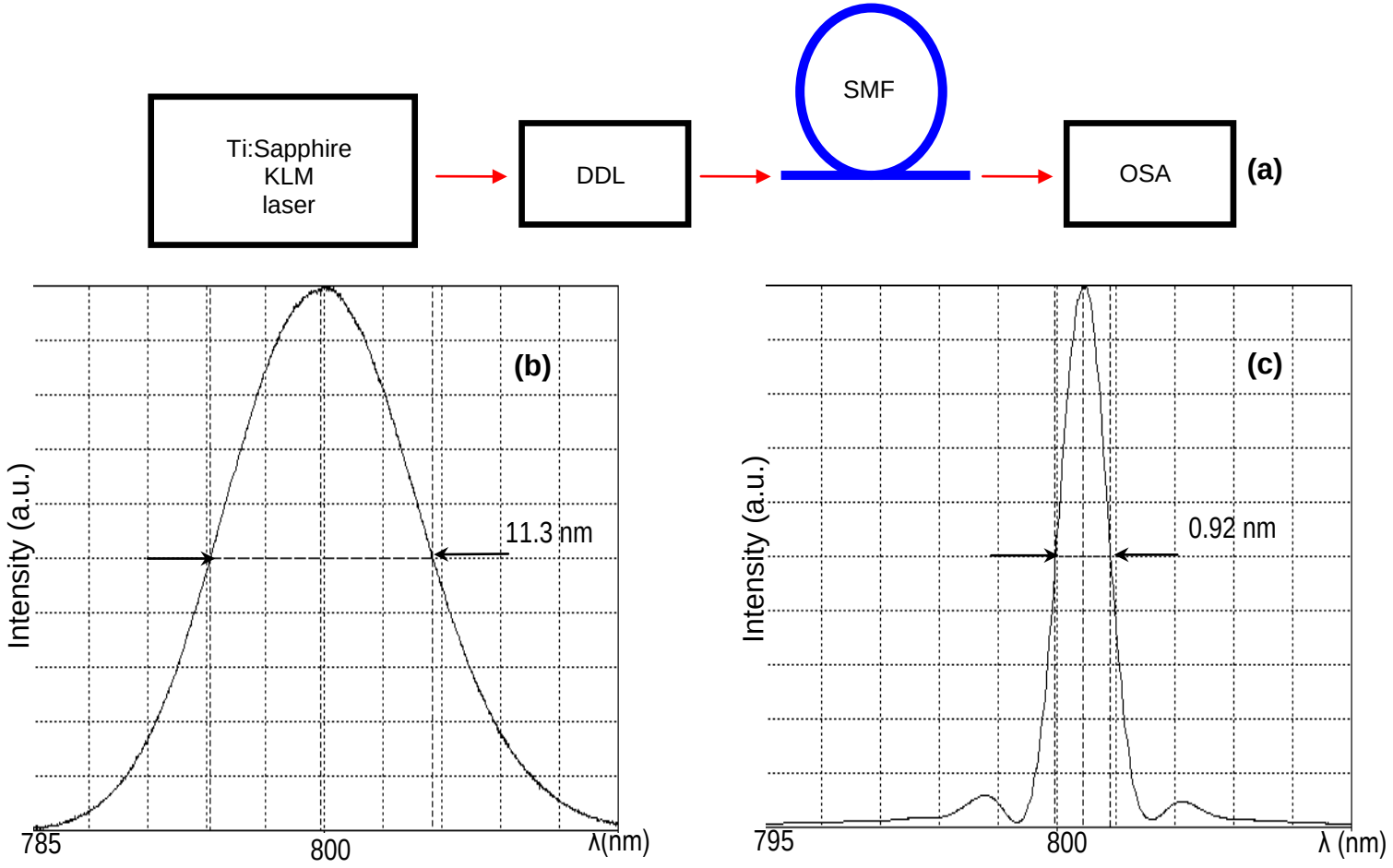

Figure 2.1. Experimental setup and results of SC through classic technique. (a) shows the setup, where Ti:Sapphire KLM laser is the Mira 900F + Verdi V10 laser system, DDL consists of SF11 prism pair, SMF is the Newport F-SE and OSA is the optical spectrum analyzer. The initial spectrum (b) had 11.3nm bandwidth and 800nm central wavelength. It is compressed down to 0.92nm bandwidth (c).

2.2 All-fiber spectral compression

To achieve a more compact size of SC setup, experiments were conducted aimed at the replacement of the prism pair DDL of the classic scheme with another fiber (all-fiber setup). The use of fibers in both parts of the spectral compressor (fig. 2.2a) allows reduction of large sizes of prism compressor (3.75m in the classic setup), theoretically down to the combined lengths of two fibers used (fig. 2.2a). To be able to replace the prisms with a fiber, this fiber has to have negative dispersion, and negligible nonlinearity. To test the all-fiber setup of SC, experiments with hollow-core fiber (HCF) were done. This type of fiber has air instead of the silica in core, and substructures around the core. The substructures around the core of HCF determine its dispersion, allowing the fiber to be designed to have negative dispersion at 800nm domain of wavelengths, which is not possible with conventional SMF. The air core of HCF also has negligible nonlinearity compared to SMF, allowing it to be used as a dispersive medium.

HCF ThorLabs HC-800B was used to pass to the all-fiber setup of the SC. The laser radiation was coupled in a 2m piece of this fiber. Afterwards, the output radiation from the HCF was coupled into a conventional SMF (Newport F-SE @780nm, 80 cm) (fig.2.2a). Compression of the initial 10.9 nm spectrum down to 1.3nm (fig. 2.2b,c) was obtained in this experiment, corresponding to 8.4x SC. At the input and output of the system, the average power was 1.5W and 0.4 W respectively. The side lobes of the compressed spectrum observed in figure 2.2c are caused by the high-order dispersion of HCF. To optimize the SC, the dispersion of HCF was changed by tuning of the central wavelength of the laser up to 808nm. This SC setup can be enhanced by the use of HCF designed specially to have only the second order of dispersion, which will lead to lesser side lobes, meaning more energy and spectral brightness can be concentrated in the central energy carrying part of the compressed spectrum. Another interesting enhancement of the setup can be splicing of the two pieces of fibers. With use of more compact fiber couplers, this can lead to more compact setup, practically limited only by the size of spliced fibers.

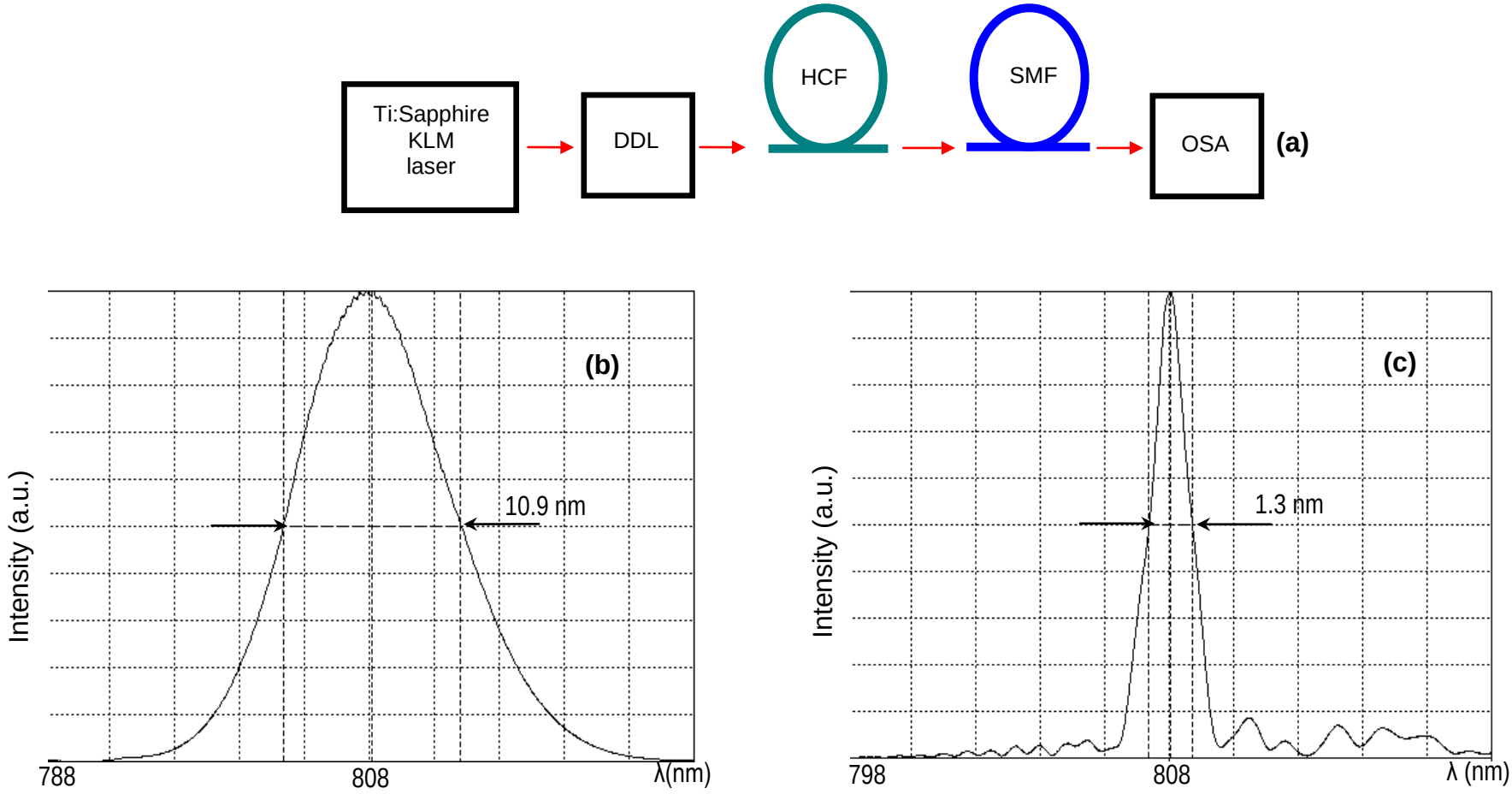

Figure 2.2. Experimental setup and results of SC through all-fiber technique. (a) shows the setup, where Ti:Sapphire KLM laser is the Mira 900F + Verdi V10 laser system, HCF is the hollow core fiber, SMF is the Newport F-SE and OSA is the optical spectrum analyzer. The initial spectrum (b) had 10.9nm bandwidth and 808nm central wavelength. It is compressed down to 1.3nm bandwidth (c).

2.3 Similaritonic spectral compression

To upgrade the SC setup with features of wavelength tunability and aberration free compression, and also to enhance the compression ratio, the similaritonic (parallel) technique of SC was implemented. The main difference of this setup from the previous ones is the way the phase is added to the signal after it passes through the DDL. In the classic and all-fiber setups, the stretched pulses pass through a SMF, where in process of SPM the chirp form the DDL is compensated, resulting in SC at the output of the fiber. In the similaritonic technique of SC, the phase addition is done through the process of SFG. The stretched pulses from the DDL are focused on an SFG crystal with the reference signal. In this case, the reference signal is the NL-D, generated in a passive fiber without gain. In the process of SFG, the two fields are multiplied. The similariton has flat top in the duration range of DDL pulse, and linear chirp, meaning that in the result of the field multiplication, the output pulse has the same shape as the pulse at the output of the DDL. Additionally, the field multiplication leads to the chirp of the output signal being the sum of chirps of two pulses involved in the SFG. The length of the fiber in which the similariton is generated, and the DDL are chosen so that they provide chirps with same values and opposite sigh, resulting in the chirp compensation in SFG process.

Mathematically, the pulse dispersed in DDL has a $\Delta t_d = s\Delta t_0$ duration (s is the stretching factor), and temporal amplitude of:

$$A_d(t) \propto \tilde{A}_0(\omega)|_{\omega=Ct} \exp[iC_d t^2/2]. \tag{2.4}$$

The similariton pulse has parabolic phase given by the fiber dispersion, and temporal amplitude of:

$$A_f(t) \propto |\tilde{A}_f(\omega)|_{\omega=Ct} \exp[iC_f t^2/2]. \tag{2.5}$$

In the SFG process, the two amplitudes are multiplied:

$$A_{out}(t) \propto A_d(t) \times A_f(t). \tag{2.6}$$

For the optimal compression, the following condition for chirps must be satisfied:

$$C_d + C_f = 0. \tag{2.7}$$

At the output of the system, the pulse is s-times stretched and is transform-limited (chirp from DDL pulse is compensated by the similariton chirp), meaning that the final spectrum will have bandwidth of $\Delta\omega = \Delta\omega_0/s$.

Experimentally, the radiation from the femtosecond laser source was split into two parts, with 80% and 20% power ratio (fig. 2.3a). The low-power part then passed through a DDL, consisting of a pair of SF11 prisms with a reverse mirror (prism separation here was 3.5m). Here the signal obtains a negative linear chirp. The high-power beam was coupled into a 1.65m of standard SMF (Newport F-SPF PP@ 820 nm), where NL-D similariton, linear positive chirp and broad spectrum (with ~100nm spectral width) was shaped. Afterwards, the DDL and similariton pulses were focused by a lens on a beta-barium borate (BBO) crystal, which was used as the medium for SFG. In the crystal, the SFG-signal (solid blue line in figure 2.3a) has trajectory different from the second harmonics of two beams (dashed blue lines in figure 2.3a), which makes the separation of signal pulse easier. As a result, SC from 2.8nm initial spectrum (fig. 2.3b) down to 0.12nm spectral width was registered (fig. 2.3c), which corresponds to 23.3x SC. The compressed spectrum is at 394nm central wavelength. Here, the SC ratio was calculated for the frequencies, which is 4 time less than for the wavelengths.

Additionally, the similaritonic technique has the feature of aberration-free SC, which is due to the linear chirp of the similariton compensating the chirp from DDL with high precision. Another interesting feature of this setup is the tunability of the compressed spectrum. The central frequency of the output spectrum can be tuned in the range of the similariton spectral width at its second harmonic. It is done by giving spatial delay to one of the two beams.

Experiments with all-fiber similaritonic technique of SC were also performed. Here, the prism pair based DDL is replaced with a 2m piece of HCF (fig. 2.4a) used in the all-fiber SC setup. As a result, compression from 10nm at 801nm central wavelength (fig. 2.4b) down to 0.2nm at 400nm was observed (fig. 2.4c), which corresponds to 11x SC for frequencies. Although the original similaritonic technique is aberration free, there are side

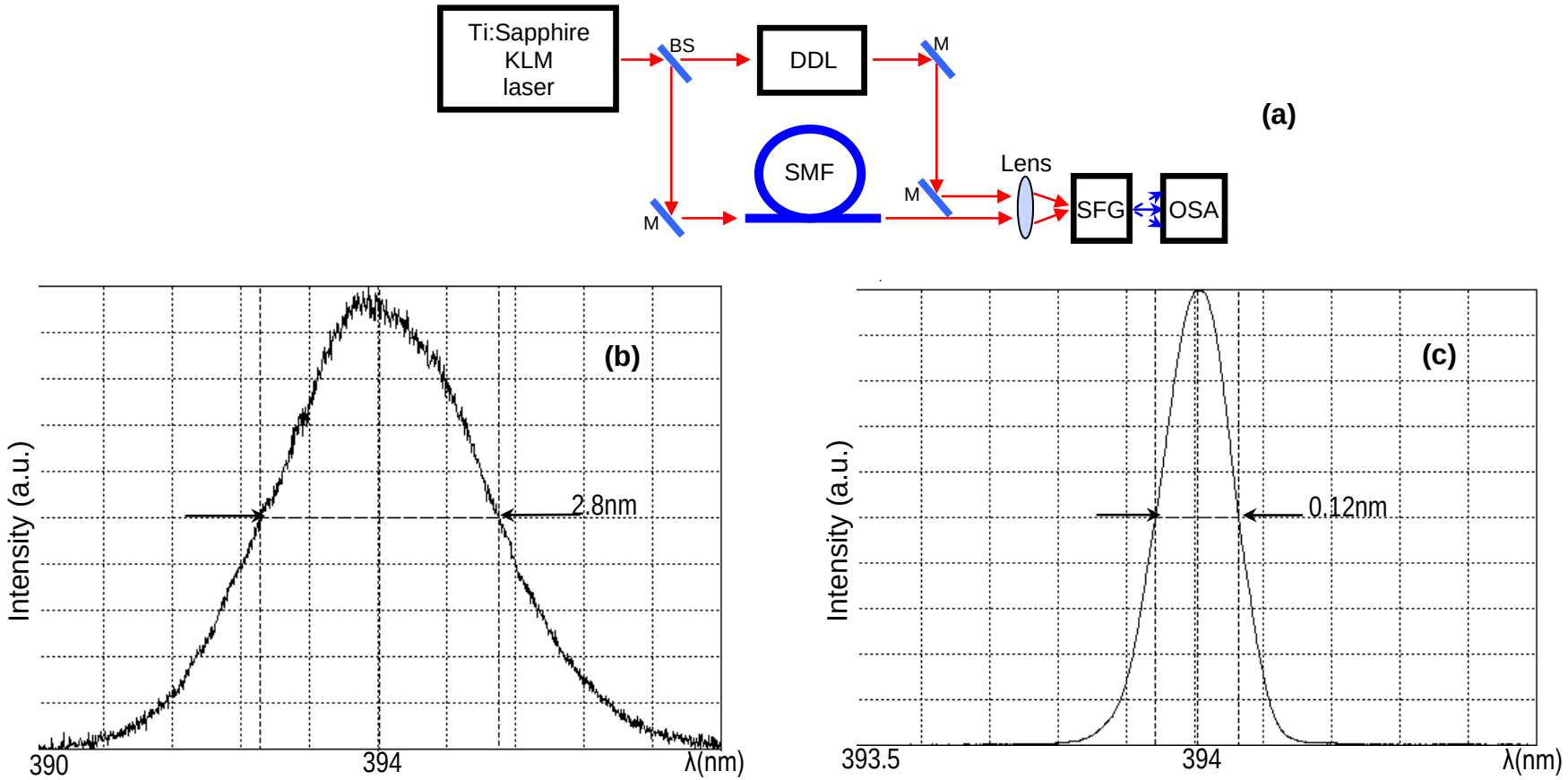

Figure 2.3. Experimental setup and results of SC through the similaritonic technique. (a) shows the setup, where Ti:Sapphire KLM laser is the Mira 900F + Verdi V10 laser system, DDL consists of SF11 prism pair, SMF is the Newport F-SPF and OSA is the optical spectrum analyzer. The initial spectrum (b) had 2.8nm bandwidth and 394nm central wavelength. It is compressed down to 0.12nm bandwidth at 400nm (c).

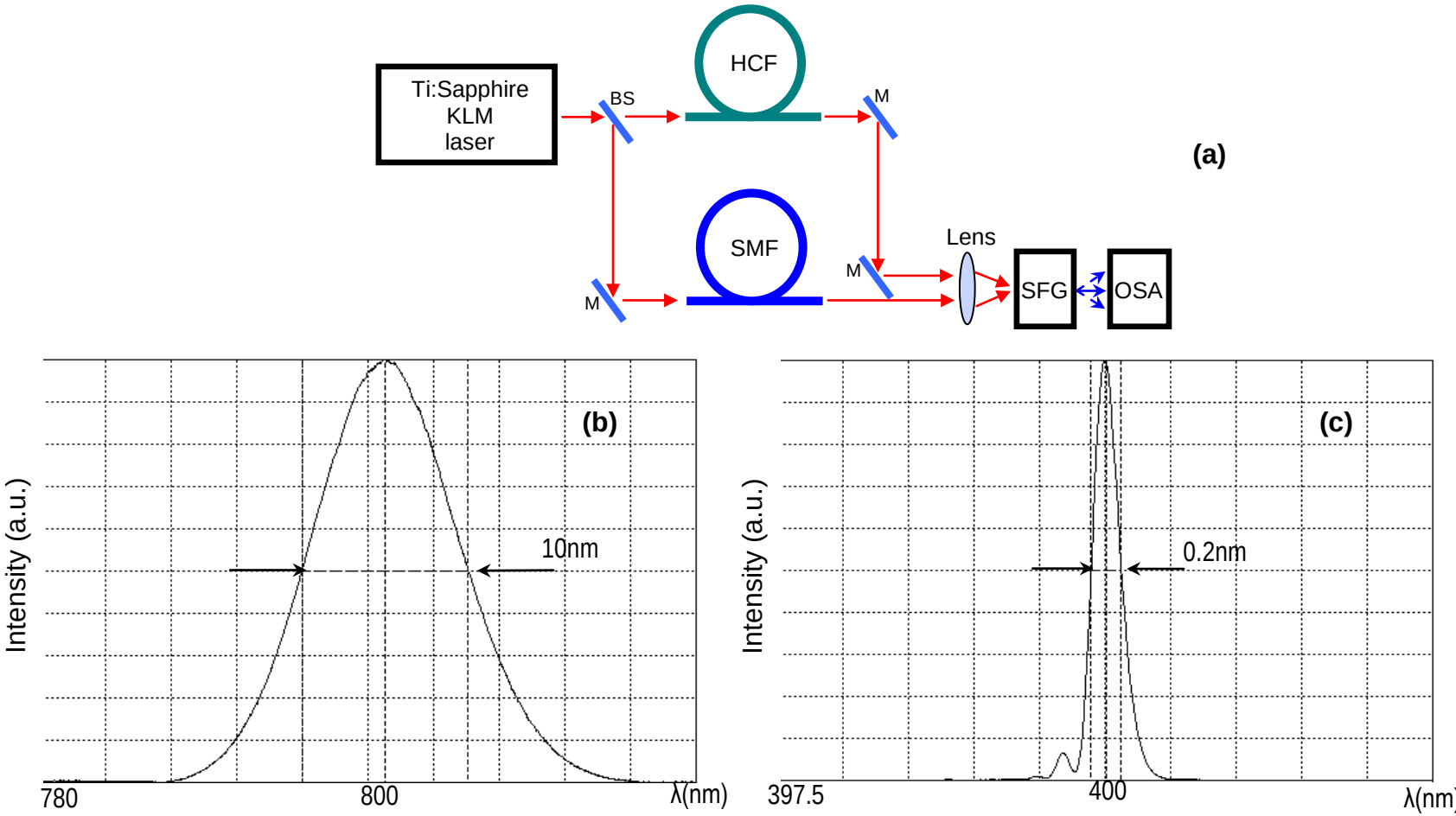

Figure 2.4. Experimental setup and results of SC through the all-fiber similaritonic technique. (a) shows the setup, where Ti:Sapphire KLM laser is the Mira 900F + Verdi V10 laser system, HCF is the HC-800B hollow-core fiber, DDL consists of SF11 prism pair, SMF is the Newport F-SE and OSA is the optical spectrum analyzer. The initial spectrum (b) had 10nm bandwidth at 801nm central wavelength. It is compressed down to 0.2nm bandwidth at 400nm (c).

lobes in the compressed spectrum in this configuration, caused by uncompensated high order dispersion of HCF.

2.4 Spectral compressor for spectrotemporal imaging of femtosecond pulses

The similariton-based aberration-free SC technique has more general function of Fourier transformation from temporal to spectral domain. For this, the signal is split into two parts, from which a spectron pulse is shaped and an NL-D similariton is generated [11]. Afterwards, the fields of spectron and NL-D similariton are multiplied in the SFG process. Mathematically the spectron and similariton spectral amplitudes are described as

$$\tilde{A}_d(\omega) = \tilde{A}_0(\omega) exp[-i\phi_d(\omega)], \tag{2.8}$$

$$\tilde{A}_f(\omega) = |\tilde{A}_0(\omega)| exp[-i\phi_f(\omega)], \tag{2.9}$$

respectively, with their parabolic phases $\phi_{d,f} = \tilde{C}_{d,f}\omega^2/2$. The temporal amplitudes of the spectron and similariton are replicating the form of their respective pulse spectrum. Mathematically, this has following form:

$$A_d(t) \propto \tilde{A}_0(\omega) exp[-iC_d t^2/2], \tag{2.10}$$

$$A_f(t) \propto |\tilde{A}_f(\omega)| exp[-iC_f t^2/2]. \tag{2.11}$$

The scaling parameter here is $\omega = C_{d,f} t$.

For chirps with same magnitude and opposite signs

$$C_f = -C_d \equiv C, \tag{2.12}$$

the SFG-signal temporal profile repeats the spectral profile of the input pulse:

$$A_{SFG}(t) \propto A_d(t) \times A_f(t) \propto [\tilde{A}_0(\omega) \times |\tilde{A}_f(\omega)|]_{\omega=Ct} \propto \tilde{A}_0(\omega)|_{\omega=Ct}, \tag{2.13}$$

given that the similariton has flat spectral profile in the overlapping part of two spectra: $\Delta\omega_f \gg \Delta\omega_0$. This results in the SFG-signal spectral amplitude repeating the input pulse temporal amplitude ($\omega = Ct$):

$$\tilde{A}_{SFG}(\omega) \propto A_0(t) \tag{2.14}$$

and the SFG-signal spectrum intensity shape repeats the intensity profile of the signal pulse:

$$S_{SFG}(\omega) = |\tilde{A}_{SFG}(\omega)|^2 \propto |A(t)|^2 = I(t). \quad (2.15)$$

The temporal resolution of this STI technique is reverse proportional to the spectral width of the similariton, as it serves as transfer function of the time lens [30].

Experimentally, the same setup described in section 1.4 was used for the spectro-temporal imaging of the femtosecond pulses. Here also, the beam was split into two parts with 80%-20% power proportions. The high power beam was coupled into the SMF, where NL-D similariton is self-shaped. The low power beam passed through DDL, consisting of the 3.75-m separated pair of prisms with the reverse mirror. The parameters of both SMF (length) and prism pair (separation distance) are chosen so that both pulses have the same absolute values of chirp. Afterwards, the two beams are focused on a BBO crystal for the SFG. Two SHG signals and the SFG signal have different exit angles form the crystal, allowing their easy separation. The resulting SFG signal is then measured by an optical spectrum analyzer, where the image of the input signal temporal profile is depicted in the spectral domain. One of mirrors in the scheme is mounted on a translation stage, for accurate spatial delay manipulations, which allows the tuning of the central wavelength at which the sum frequency signal is generated.

Two- and thee-peak pulses were shaped at the input of the setup to test the performance of the technique. To do this, microscope glass (or two glasses for three-peak pulse shaping) was inserted inside a part of the laser beam. The refractive index difference between the glass and air provided the time delay for part of the radiation, which resulted in formation of multi-peak pulses. At the setup output the signal spectrum repeated the initial pulse shape (fig. 2.5a,c). To check the precision of measurements, the autocorrelation trace of the test pulse was also measured, and compared to the calculated autocorrelation trace of the registered spectral image. Figures 2.5 (b) and (d) are showing the comparison of these autocorrelations for two- and three-peak pulses respectively. The solid lines are standing for the measured autocorrelation of the test pulse, and the dashed lines are the calculated autocorrelations of the spectral images of the test pulses. For two-

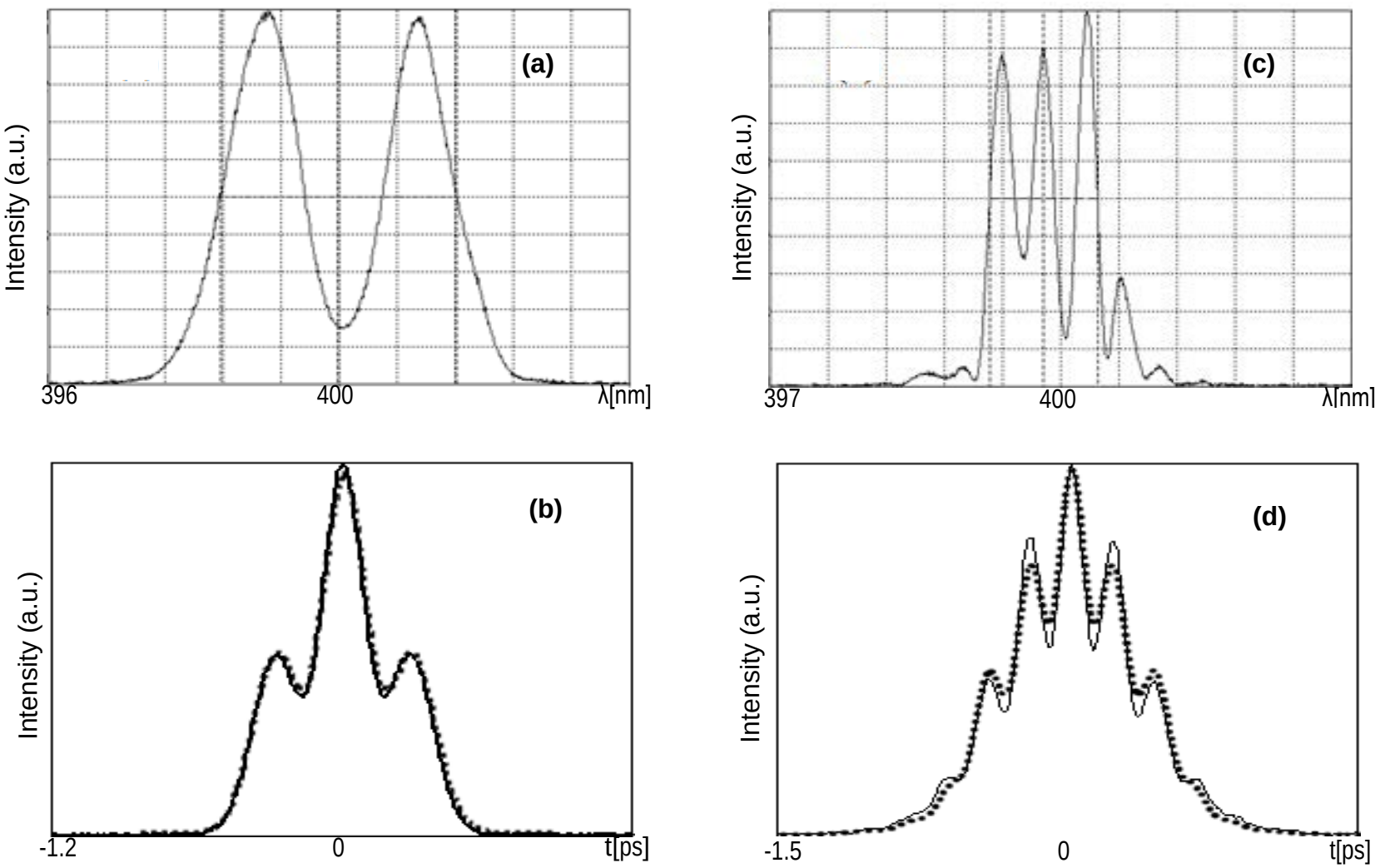

Figure 2.5. Experimental results of STI with the use of prism pair. Two- and three-peak test pulse images (a and c respectively) and comparison of autocorrelation traces of the signals and the registered images (b and d respectively).

peak pulses the matching of two curves is close to perfect. For three-peak pulses, the match is qualitative (figure 2.5c). These aberrations are caused by the fluctuations of the similariton shape generated from tree-peak pulses.

Comparative study of the STI technique and spectral interferometry was also performed. For this, the test pulse and the reference pulse, for which the laser pulse was used, were coupled into a fiber, which was inserted in the spectrometer, where the spectral beatings were registered. These beatings in the spectrum carry the information about the sum of phases of test and reference pulses. The test pulse phase was recovered by subtraction of the phase of reference pulse from the sum of phases. This phase is then put on the spectrum of the signal pulse, to recover the pulse shape. Figure 2.6 shows the spectrotemporal image of the two-peak pulse, the shape of the pulse recovered by spectral interferometry and the theoretical prediction of the pulse form based on the registered autocorrelation trace. As one can see, these curves are in a good agreement with each other. This STI setup has large sizes, because of the prism pair used, which had ~4m separation distance. To make the setup more compact and user-friendly, the commercial prototype of the device was designed. Figure 2.7 shows the 3D image of the compact setup. Here the prism pair was replaced with a grating pair, which allowed to reduce the ~4m length of DDL down to ~10cm. To reduce the sizes of the device and fit it on a 30x30cm plate, the fiber launching platform was also replaced by a ThorLabs Fiber Port Coupler. These two upgrades allowed to implement a compact, commercial prototype of the STI device. Figure 2.8 is the image of this device. Once closed by a box, it should have two holes for beam input and signal output, and 3 controllers for translation stages: for DDL length adjustment; signal arm length control; and output signal power adjustment. Moreover, this device can be used for similariton-based spectral interferometry, by simply replacing gratings with mirrors. Figure 2.9 shows the image of a two-peak pulse, obtained by the STI device, on the optical spectrum analyzer screen.

This prototype of device was tested by shaping of two-peak pulses with different peak values. Figure 2.10 shows the results of the experiment. Figure 2.10 (a) and (b) are for two-peak pulse with equal peak proportions and (c) and (d) are for two-peak pulse with

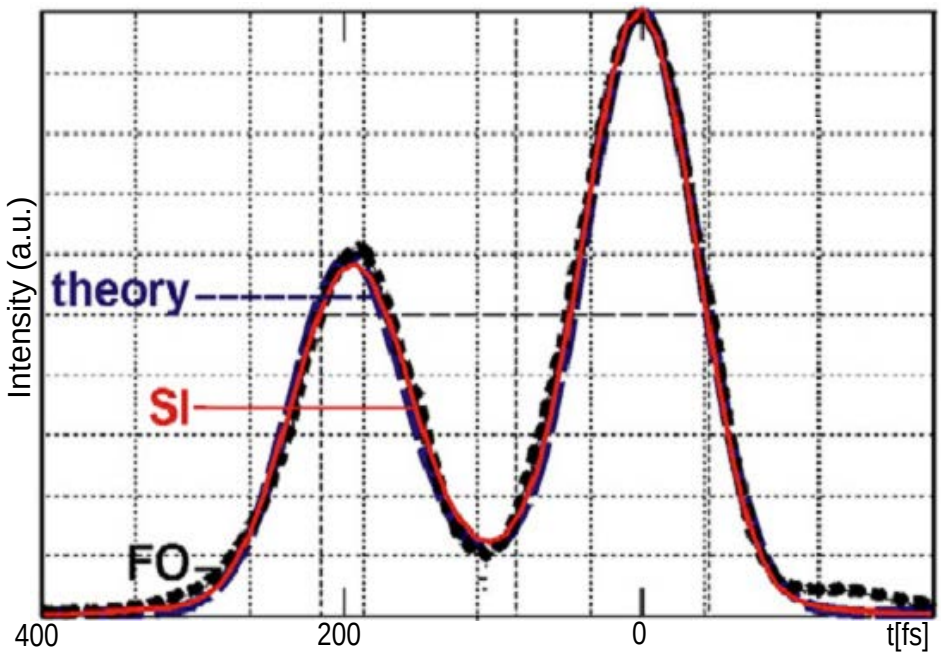

Fig. 2.6. STI image (black curve) of two-peak signal, spectral interferometric image (red curve), and theoretical prediction (blue curve).

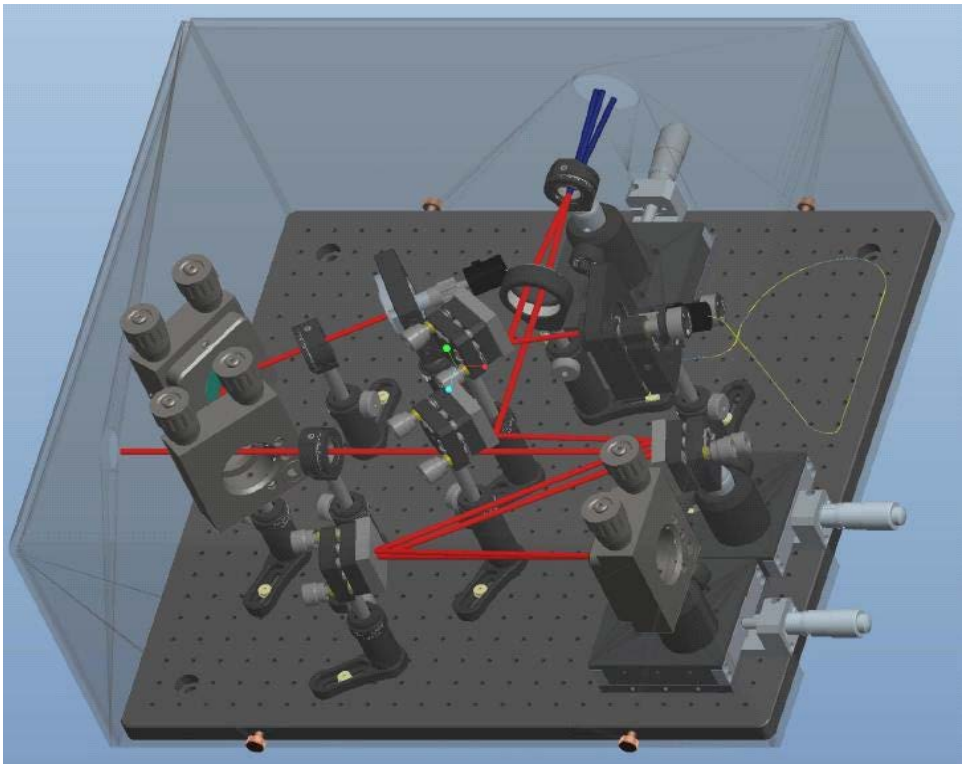

Fig. 2.7. 3D model of STI device. Red lines are showing the paths of similariton and spectron. Blue lines show the second harmonic radiation.

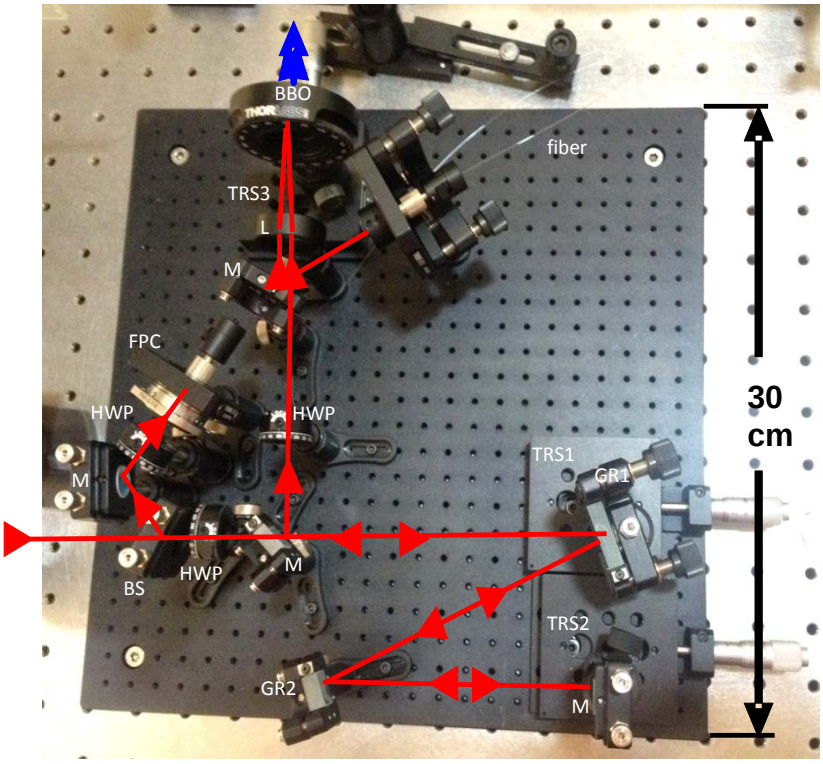

Fig. 2.8. Compact STI setup:

BS – beam splitter; M – mirror; HWP – half-wave plate; GR – grating; FPC – fiber port coupler; fiber – LMA5; L – lens; BBO – nonlinear SFG crystal; TRS – translation stage.

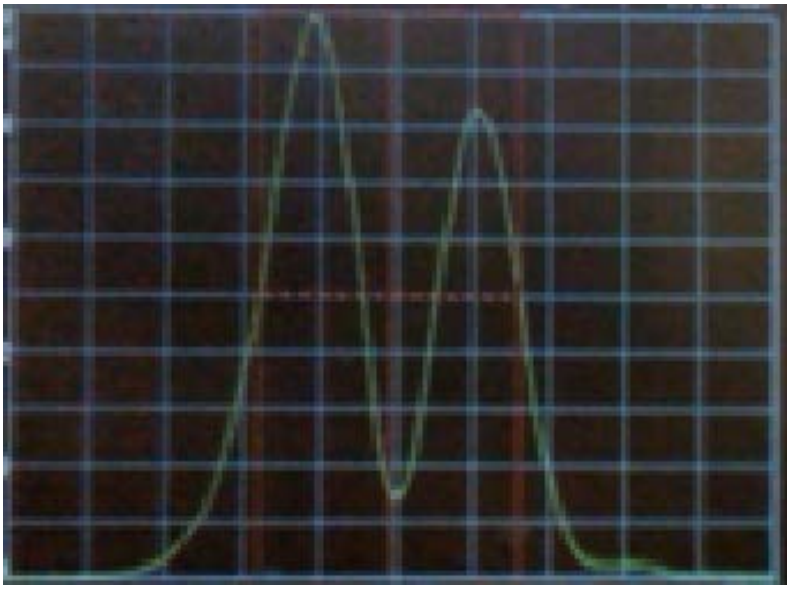

Fig. 2.9. Two-peak signal imaged on the screen of OSA through the STI device.

unequal peaks. (a) and (c) are the test pulse spectra, while (b) and (d) are the registered spectral images of the signal.

To further minimize the footprints of the proposed device, experiments were performed towards the all-fiber configuration. For this, the DDL in the setup was replaced by a HCF (HC-800B), which has negative dispersion at the laser wavelength and negligible nonlinearity due to its air core. Two-peak pulses with equal peaks were shaped at the entrance of the experimental setup to test its performance.

Figure 2.11 (a) and (b) show the test two-peak pulse spectrum, and the results of its STI in the all-fiber setup. The aberrations here are caused by the high-order dispersion in HCF, which cannot be compensated by the linear chirp of similariton. These aberrations can be avoided by the use of HCF with lower high-order dispersion. The amount of dispersion of the HCF was equalized to the chirp slope of the similariton by tuning of the wavelength of laser radiation. The output signal spectral width was taken as the reference: the SC is maximal when the two chirps compensate each other optimally.

Furthermore, experimental study was carried out towards the upgrade of the device with real-time performance. As the conventional spectrometers have averaging time close to 1s, the measurements done by a spectrometer are limited in time-resolution. To perform real-time measurements, one needs to do the measurement of the output signal through an electronic oscilloscope. For this, the signal pulse must be stretched up to nanosecond domain, as the resolution of conventional electronic oscilloscope is limited to this temporal domain. Furthermore, as the oscilloscope measures the pulse shape, but not the spectrum, the signal must be stretched in such a way, that it has a pulse repeating the signal spectrum shape. The generation of spectron pulse can be a solution to this problem. Spectron pulses have linear chirp, and the pulse shape repeats the shape of the spectrum, i.e. by measuring this pulse temporal form, one has the form of spectrum. To generate these pulses, the output signal has to pass through a DDL. The huge amount of stretching (from femtosecond to nanosecond domain) requires long fiber to be used (few kilometers). To overcome the huge DDL length requirements, experiments were performed with the chromo-modal dispersion (CMD) technique of pulse stretching [20]. For this, spectrum of the test pulse was projected to spatial domain by passing it through a pair of diffractive

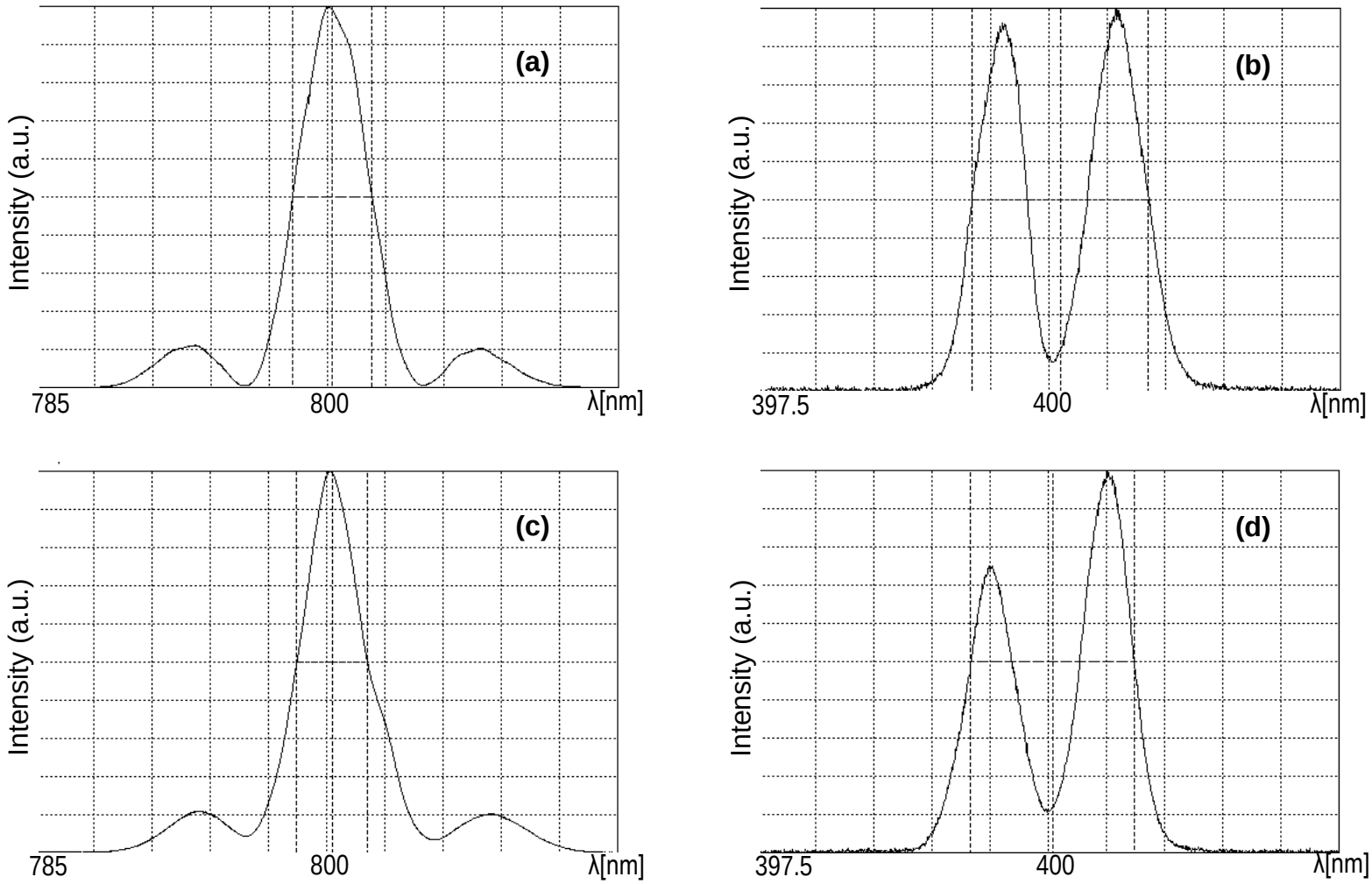

Figure 2.10. Two-peak signal imaged by the prototype of the STI device. Spectrum of the signal (a) and measured spectral image (b) of two-peak pulse with equal peaks. Spectrum (c) and image (d) of two-peak signal with unequal peaks.

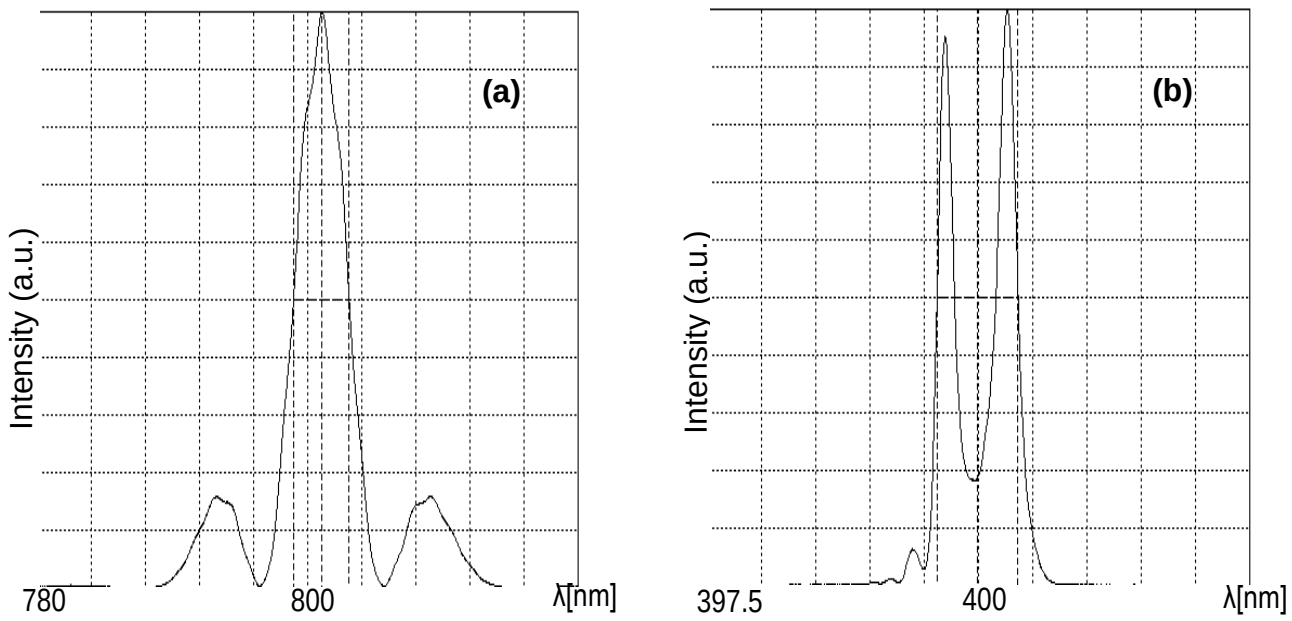

Fig. 2.11. Two-peak signal imaged by the all-fiber setup of STI device. (a) spectrum of two-peak signal with equal peaks and (b) signal image at the setup output.

gratings, without a reverse mirror. Thereafter, the beam with spatial distribution of the spectrum is focused by a lens. At the focus, the spatial distribution is transformed into angular distribution. A multimode fiber with big number of modes is put at the focus of the lens, and the radiation is coupled into it. As the spectrum of radiation is distributed in the angular domain at the focal point, the coupled radiation in the multimode fiber has also the spectral distribution, in the modes of the fiber. Because of the large number of modes (large diameter of core), different wavelengths are travelling different distances inside the multimode fiber. As a simple explanation, the small angle part of the beam is travelling through the central part of the multimode fiber, while the large angle part is reflected more from the sides, and thus it passes longer optical distance. This leads to huge stretching (up to few nanoseconds) of the pulse.

Experimentally, the method was tested on Gaussian and two-peak spectrum. For this, the radiation was first guided through a grating pair. After the input beam hits the first grating, it receives angular distribution of the spectrum. When this beam hits the second grating, the angular distribution is transferred to spatial distribution, and beam obtains spatial distribution of radiation spectrum. Thereafter, this beam was focused by a lens, with

one side of the beam passing through the middle of the lens, and the opposite side passing through its corner. A lens with 3cm focal length was used in this experiment. The multimode fiber, with core diameter of 200μm and 35m length, was put at the focus of the lens, and the radiation was coupled into the fiber.

Figure 2.12a shows the spectrum measured at the fiber input, and the pulse shape (red curve) measured at the output by an electronic oscilloscope. The CMD technique was also tested for two-peak spectrum. For this, a nail was put in the central part of the spectrum, after the grating pair (black curve in fig. 2.12b). Figure 2.12b (red curve) shows the image of the two-peak spectrum on electronic oscilloscope.

These results show qualitative agreement between the signal spectrum and measurements done by CMD method. However, the studies showed the problem with application of this method in real-time STI: the pulse energy requirement for the measurement is higher than could be provided by STI setup.

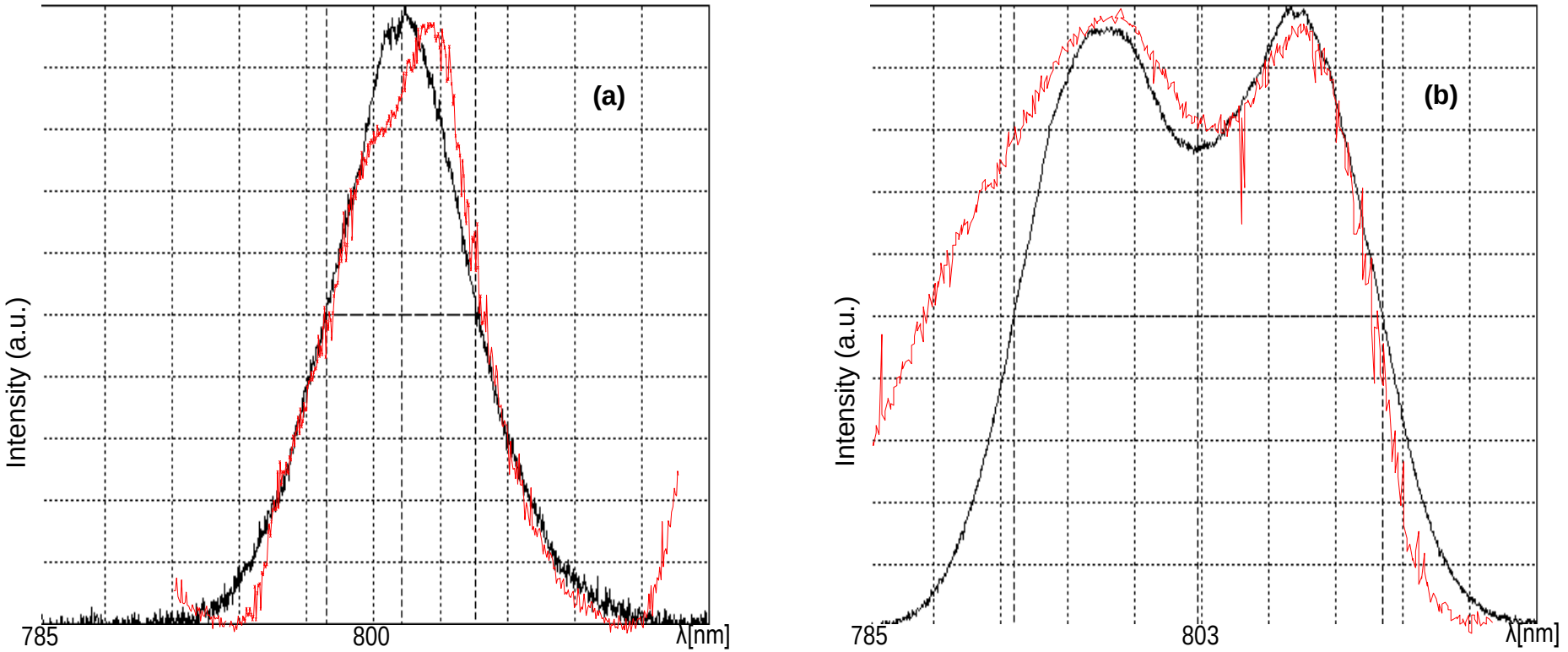

Fig. 2.12. Laser spectrum (a) and shaped two-peak spectrum (b) imaged by a spectrometer (black curve) and oscilloscope (red curve) by the use of CMD method.

Conclusion

This chapter is describing the comparative experimental study of three techniques of spectral compression. The results of studies are:

1. Demonstration of 12x spectral compression through the classical scheme of spectral compressor. This setup had high energetic efficiency, allowing it to be used instead of spectral filtering.
2. Demonstration of 8.4x spectral compression by the all-fiber setup. This setup allows to reduce the sizes of spectral compressor, especially if fiber splicing is performed. The technique has approximately the same power efficiency as the classical technique, with the drawback of strong side lobes as a result of uncompensated high order dispersion from HCF.
3. Demonstration of 23.3x spectral compression through similaritonic technique. This technique has the advantage of high ratio of spectral compression alongside with frequency tuning, at the signal second harmonic wavelengths. Another advantage of this technique is that it is aberration-free, due to linear chirp of the similariton, used as reference pulse. The drawback of the system is its low energetic efficiency.
4. Another application of similaritonic spectral compressor, the spectrotemporal imaging technique is experimentally demonstrated. The commercial prototype of the device is tested, with footprints of 30cm on 30cm, allowing user friendly performance of the device in laboratory conditions. The device is tested by imaging of two-peak pulses, and comparison of the results obtained by the technique to autocorrelation and spectral interferometric measurements. Additionally, a possible upgrade of the device to real-time performance is tested through pulse stretching by using of CMD method. The experiments in these directions showed promising results for pulse stretching up to few nanoseconds duration.

CHAPTER III

SPECTRAL ANALOGUE OF SOLITONIC COMPRESSION:
SPECTRAL SELF-COMPRESSION

Introduction

In this chapter, the first experimental studies on the spectral self-compression (self-SC) are described. This new effect is the spectral analog of the pulse solitonic compression.

The temporal effect of pulse temporal self-compression, supported by the technology of photonic crystal fibers and nanowires, recently demonstrates pulse compression of up to the fundamental frontiers of optics, generating down to one-two cycle pulses [71; 86; 87]. This process, associated with the shaping of high-order solitons (also called as soliton effect compression; solitonic compression; soliton compression), occurs under the combined impacts of strong SPM and weak anomalous GVD [88; 89].

In this chapter, the studies of the spectral analogue of this process, the self-SC, under the conditions when the impact of anomalous GVD exceeds the impact of nonlinear SPM, are presented. The spectrotemporal analogy led to the invention of SC in a DDL followed by a nonlinear fiber [25; 56], a process with prospective applications in ultrafast optics and laser physics [62; 90]. In this system, the GVD of the DDL stretches and negatively chirps the pulse, and the SPM in the nonlinear fiber results in the chirp compensation and SC [25; 56]. For the self-SC process, the factors of GVD and nonlinear SPM are combined in a single material (e.g. fiber). As the self-SC process requires negative GVD, the radiation has to be in the range of anomalous dispersion of silica (>1300nm), to use a conventional SMF. Alternatively, photonic crystal fibers (PCF), such as hollow-core fiber (HCF), with anomalous dispersion in the given spectral domain can also be used. The dispersion curve of this type of fiber depends on its substructure, allowing to fabricate fibers with desired dispersion curve.

In the frames of research described in this chapter, dispersion curve of an HCF is studied, which served as a background for conducting the first experiment aimed at the demonstration of self-SC in an HCF. Furthermore, to enhance the initial experimental results, and test the process in a conventional SMF, supercontinuum [91-100] with broad spectrum was generated. Part of its spectrum was cut and self-compressed in an SMF.

3.1 Dispersion characterization of negatively curved hollow-core fiber

As the process of self-SC requires negative dispersion, the use of HCF is of interest in frames of experimental demonstration of the process, in case if radiation is below 1300nm spectral domain. For this purpose, the dispersive characteristics of a type of HCF, called negatively curved hollow-core fiber (NCHCF), was studied.

Experimentally, the dispersion of an NCHCF was measured. The scanning electron microscope (SEM) image of the fiber microstructure is shown on the figure 3.1. It has a core diameter of 21μm, the eight capillaries around the core have 828nm wall thickness.

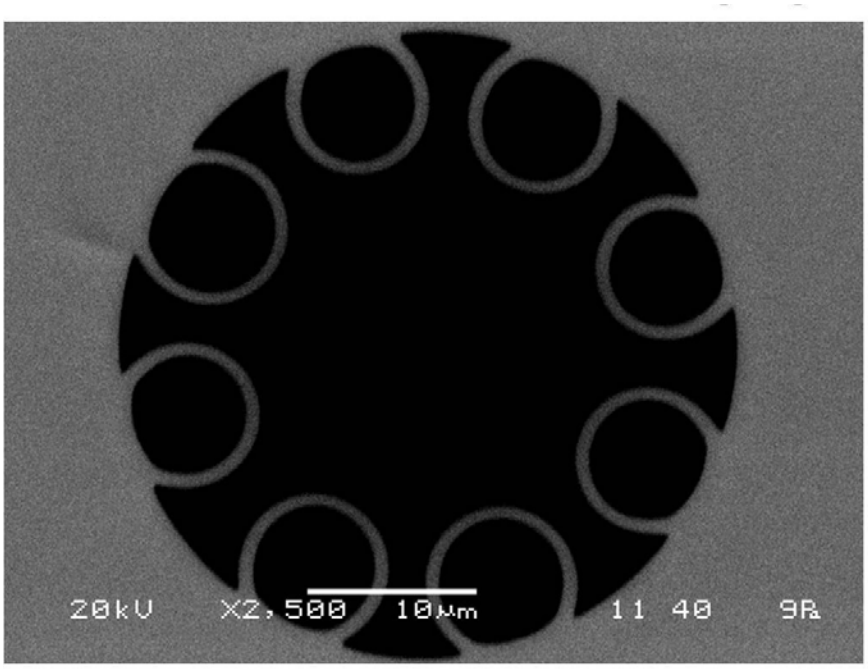

Figure 3.1. SEM image of NCHCF.

To study the dispersion characteristics of the NCHCF, spectral and autocorrelation measurements of femtosecond pulses at the input and output of this fiber were carried out. The measurements were done in 2 regimes of femtosecond laser operation: FWHM pulse

durations of 180fs (255fs AC duration), which corresponds to ~4-nm bandwidth; and of 125fs (180fs AC duration) with ~7nm bandwidth. A 20x (0.4 NA) microscope objective was used to couple the beam from the Coherent Verdi V10 + Mira 900F femtosecond laser system, with the following parameters of radiation: 1.3W average power at a 76MHz repetition rate, 748nm central wavelength. Also, different blocks of SF11 glass were added to compress the pulses at the fiber output, and with this to make sure that the fiber has anomalous dispersion. The length of the used fiber was 10m.

In the regime of 255fs AC duration, the average power of the laser radiation was 1.3W, and the average power at the fiber output was ~100mW. Figure 3.2 shows the spectra (a, c, e) and AC traces (b, d, f) of the pulses at the fiber input (fig. 3.2 (a, b)), at the fiber output (fig. 3.2 (c, d)), and at the fiber output when a 10-cm block of SF11 glass was added before (fig. 3.2 (e; f, line 1)) and after (fig. 3.2 (f, line 2) the fiber. After propagating through the fiber, the spectrum remains almost constant, and the duration of the AC trace increases from 255fs to 514fs (FWHM). The measured AC trace at the fiber input had 255fs duration (line 1 in fig. 3.2(b)), and the calculated Fourier-transform pulse of the measured spectrum had 236fs AC duration (line 2 in fig. 3.2(b)). This means that the laser gives slightly positively chirped pulses, with the amount of group delay dispersion (GDD) equal to +3,500fs^2. Thus, during the pulse propagation in the fiber, first takes place pulse compression due to the fiber anomalous dispersion, and after that takes place pulse dispersive stretching. A GDD=–22,900fs^2 was added on top of the spectrum to obtain the measured AC duration of 514fs at the fiber output. The GDD=$\beta_2 z$, where z=10m is the fiber length and β_2 is the second-order dispersion coefficient. Hence, β_2=–2,290fs^2/m (D=7,7ps/(nm*km)). Adding a 10-cm block of SF11 glass allowed to compress the pulses stretched in the fiber down to 280fs AC duration, proving that the pulse stretching took place due to the anomalous dispersion of the fiber. Moreover, SF11 glass added before and after the fiber gave roughly the same AC traces for the compressed pulse (lines 1 and 2 in fig. 3.2(f)). However, the durations of the initial and compressed pulses did not match, which presumably means that the induced chirp was not purely linear. The slight difference of the measured and calculated AC traces at the fiber output (lines 1 and 2 in fig. 3.2(d), respectively) also points out the presence of high-order dispersion.

The value of β_2 can be estimated by another rough method. For the propagation of transform-limited Gaussian pulses in a dispersive medium, we have $(\tau/\tau_0)^2 = 1 + (z/L_D)^2$, where τ_0 is the initial pulse duration (half-width at e^{-1} level), τ is the chirped pulse duration, and $L_D = (\beta_2 \Delta\omega_0^2)^{-1}$ is the dispersive length with the initial pulse bandwidth $\Delta\omega_0 = 1/\tau_0$. Further, β_2 can be calculated from this formula: $\beta_2 = [(\tau/\tau_0)^2 - 1]^{1/2}/[z\Delta\omega_0^2]$. In this regime, the value of β_2 is –2,390fs^2/m, which is in a good agreement with the pure experimental measurement β_2 = –2,290fs^2/m, without any assumptions for the pulse shape and chirp.

In the regime of 180fs AC duration, the average power of the laser radiation was 1.1W, and the average power at the fiber output was ~90mW. Figure 3.3 shows the spectra (a, c, e) and autocorrelation traces (b, d, f) of the pulses at the fiber input (fig. 2.3 (a, b)), at the fiber output (fig. 2.3 (c, d)), and at the fiber output when a 10-cm block of SF11 glass was also added before (fig. 2.3 (e; f, line 1)) and after (fig. 2.3 (e; f, line 2) the fiber. The AC duration increases from 180fs to 592fs. The measured AC trace at the fiber input had 180fs duration, and the calculated Fourier-transform pulse of the measured spectrum had 169fs AC duration. This means that the laser gave slightly positively chirped pulses, with the amount of GDD equal to +2,100fs^2. In this case, a GDD = –19,250fs^2 was added on top of the spectrum to obtain the measured AC duration of 514fs at the fiber output. Hence, β_2 = –1,925fs^2/m (D=6.5 ps/(nm*km)). Adding a 10-cm block of SF11 glass before and after the fiber allowed to compress the pulses stretched in the fiber down to 207fs AC duration. In this regime, the durations of the initial and compressed pulses also did not match, and there was a slight difference between the measured and calculated AC traces at the fiber output (lines 1 and 2 in fig. 3.3(d), respectively). According to the rough estimation method, in this regime for the second-order dispersion coefficient the value was β_2 = –1,850 fs^2/m.

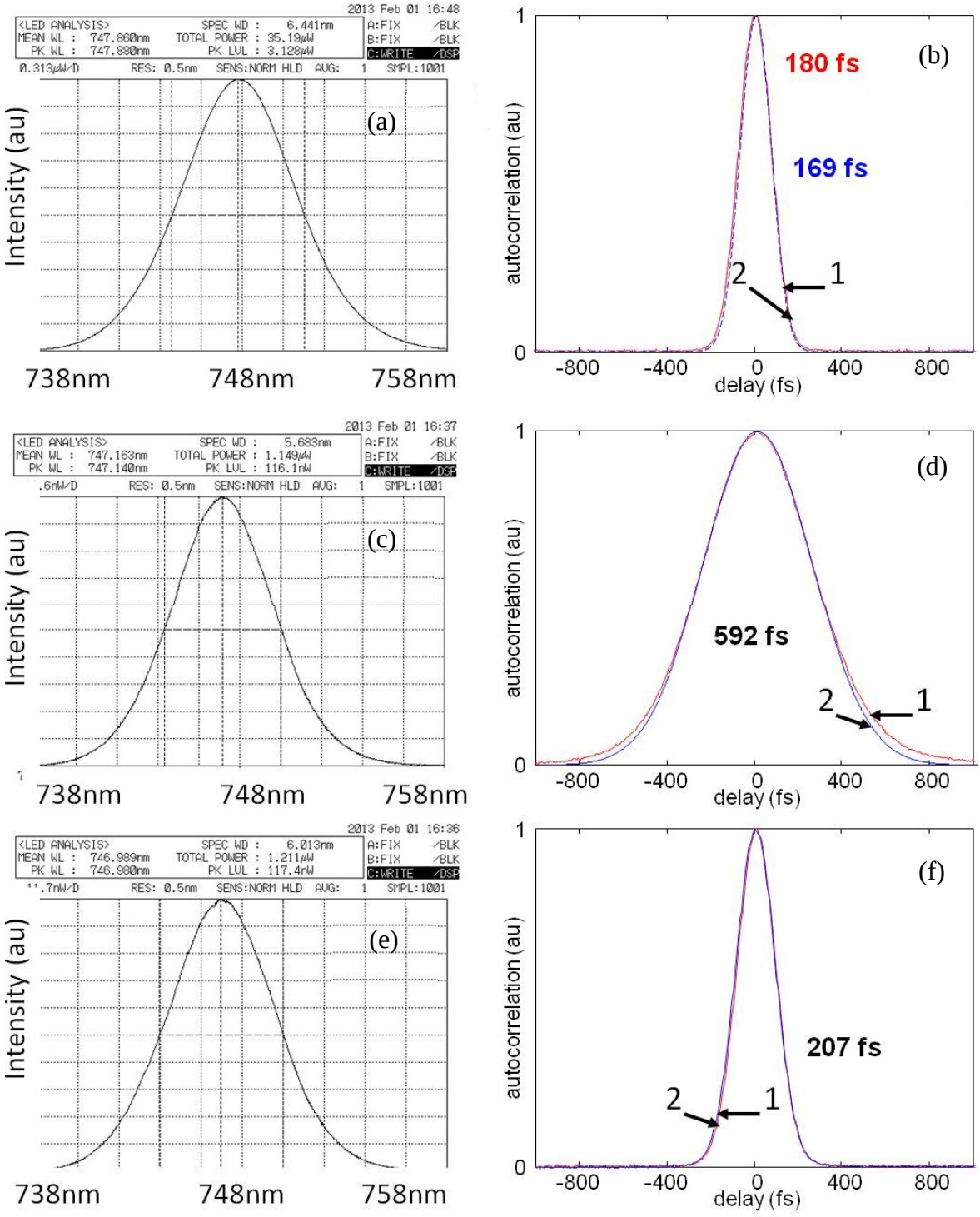

Figure 3.2. Experimental results of NCHCF dispersion measurements with 255fs AC duration. Here (a, c, e) are the spectra, and (b, d, f) are the AC traces.

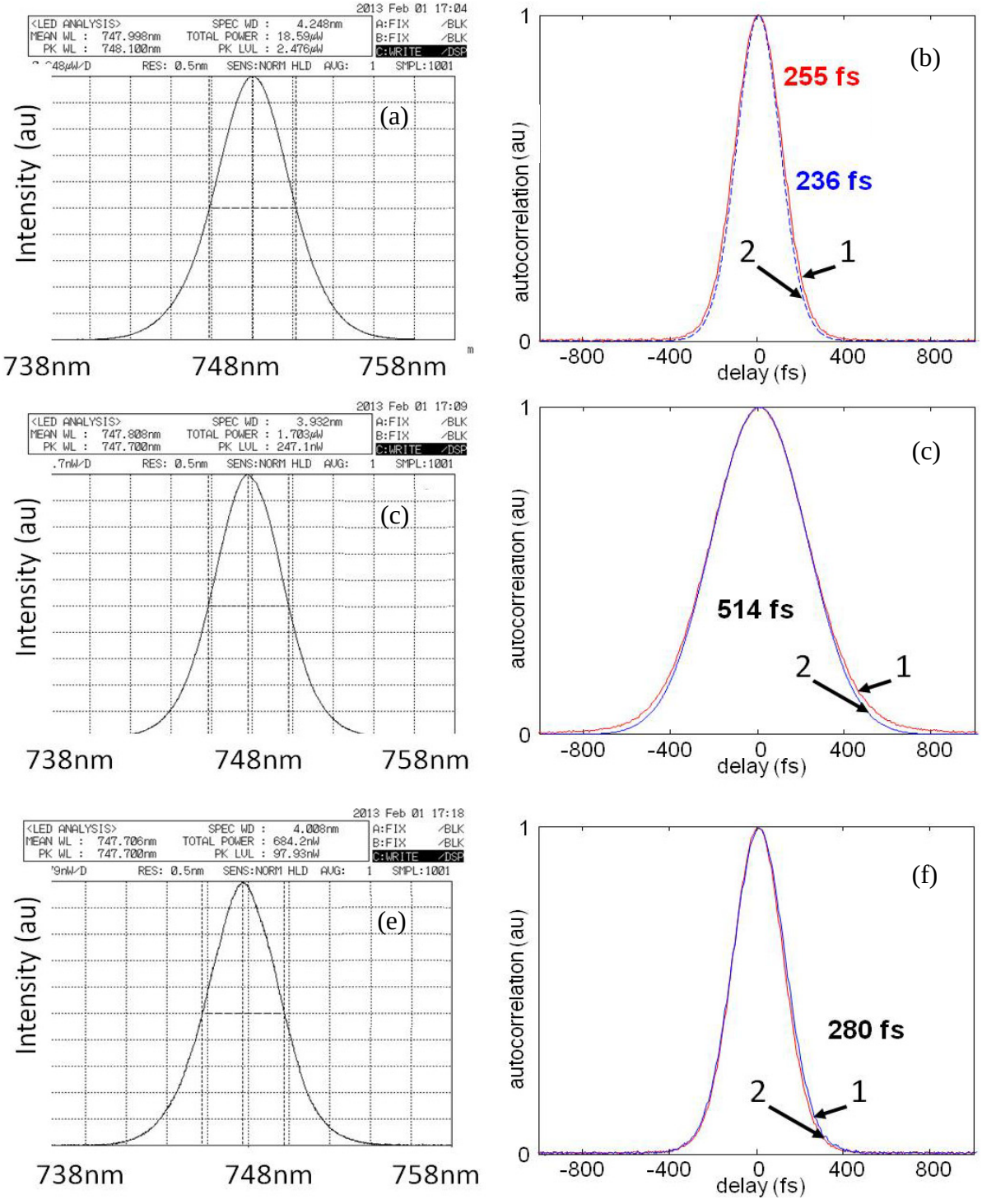

Figure 3.3. Experimental results of NCHCF dispersion measurements in 180fs AC duration. Here (a, c, e) are the spectra, and (b, d, f) are the AC traces.

3.2 Experimental demonstration of the process of spectral self-compression

Analytically motivating the process of self-SC, it can be useful to consider the analogy between the impacts of GVD in the spectral domain and nonlinear SPM in time domain. By comparing the expressions of the pulse slowly varying amplitude A and its Fourier image $\tilde{A}$, one can see that the GVD modulates the spectral phase parabolically (eq. 3.1), in same manner as SPM of a bell-shaped pulse modulates temporal phase in the central part of the pulse (eq. 3.2).

$$\tilde{A}(\omega, z) = \tilde{A}(\omega, 0)\exp[-i\omega^2(z/L_D)/2] \tag{3.1}$$

$$A(t, z) \approx A(t, 0)\exp(iz/L_{NL})\exp[-it^2(z/L_{NL})] \tag{3.2}$$

Here, the modulation "scale" for GVD is given by $L_D = (\beta_2 \Delta\omega_0^2)^{-1}$, the dispersive length of the medium, in comparison to one for SPM length, which is $L_{NL} = [\beta_0 n_2 |A(0,0)|^2]^{-1}$. In these equations, t is the "running" time and ω_0 is the central frequency, normalized to the initial pulse duration Δt and spectral bandwidth $\Delta\omega_0$, respectively. z is the propagation distance, n_2 is the nonlinear Kerr-coefficient.

Based on these equations, one can conclude that for the effect of self-SC to occur, pulse has to first obtain strong modulation of the spectral phase, induced by GVD, and afterwards only to obtain the impact of SPM, since for the solitonic pulse compression process, initial string SPM impact is required, followed by weaker GVD impact. Or, in terms of nonlinear and dispersive lengths, the solitonic pulse compression occurs in case when $L_{NL} < L_D$, while for the spectral analogue, $L_{NL} > L_D$ is required.

In the experimental study, the radiation of Coherent Verdi V10 + Mira 900F femtosecond laser system was used, which provides femtosecond radiation around 800nm central wavelength. As the dispersion of silica (and any standard SMF) is positive at 800nm wavelength domain, an HCF was chosen as a medium for demonstration of self-SC. ThorLabs HC-800B fiber was used, as it is designed to provide negative dispersion at 800nm spectral domain. The radiation was simply coupled into the 2m piece of HCF (fig. 3.4(a)). The spectrum, AC duration and the radiation power were measured at the output of the fiber. The coupling power was controlled via the neutral density filter. Use

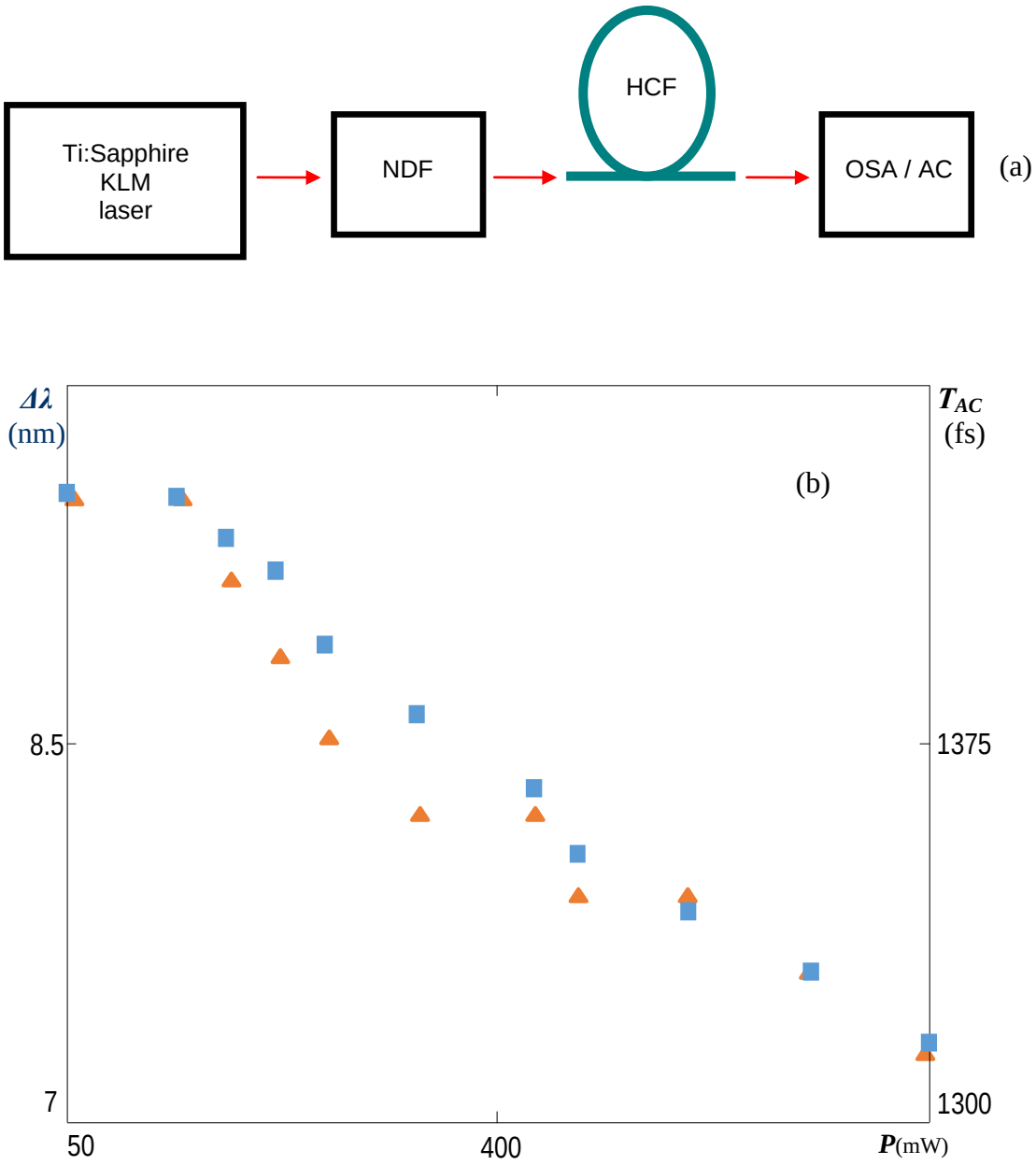

Figure 3.4. (a) experimental setup of self-SC in HCF, Ti:Sapphire KLM laser is the Mira 900F + Verdi V10 laser system, NDF is the neutral density filter, HCF is the ThorLabs HC-800B fiber, OSA is the optical spectrum analyzer and AC is the autocorrelator. (b) Experimental results of self-SC in HCF. The left and right vertical axis are standing for spectral width (squares) and autocorrelation duration (triangles) of compressed pulses, respectively. The horizontal axis stands for the power at the output of fiber.

of neutral density filter as a way of changing the coupled power ensures the beam trajectory remains the same when the power is changed.

Here, the spectral width of radiation at the entrance of HCF was 9.6nm at FWHM with 150fs pulse AC duration. It was self-compressed down to 7.4nm (fig. 3.4(b)) at the maximal coupled power (750mW). This corresponds to 1.3x self-SC. The AC duration of pulses with maximal self-SC was around 1.3ps. Figure 3.5(b) also shows that when the coupling power is lowered, the spectral width also grows, resulting in smaller amounts of self-SC. This, and the fact that the change of the input power did not change the trajectory of the beam, shows the nonlinear nature of the process. The small amounts of compression in this experiment was because of the low nonlinearity of the HCF. As it uses air instead of silica in the core, and thus, as the nonlinear medium, the impact of nonlinearity in this fiber was several orders of magnitude lower than the nonlinearity of conventional silica-core-based SMF. This result can be enhanced either by using significantly longer fiber, or by the use of conventional SMF. In the last case, the coupled radiation has to be above 1300nm spectral domain, as silica has negative dispersion needed for self-SC at this wavelengths.

To overcome the limitations of nonlinearity, experiment was conducted, aimed at achieving self-SC in a conventional SMF. As the silica has negative dispersion at wavelengths greater than 1300nm, the laser + amplifier system was used, which allows generation of supercontinuum in nonlinear crystals. The spectrum of this supercontinuum was then filtered, picking the part of the spectrum above 1300nm, which allowed the demonstration of self-SC in an SMF.

Experimentally, the radiation of Amplitude Systems femtosecond laser system with amplifier, providing 400fs pulse duration at 1030nm central wavelength. The radiation of amplifier was then focused on a YAG crystal, using a 3cm focal length lens, for supercontinuum generation (fig. 3.5(a)). The YAG crystal was chosen, as it provides best to our knowledge output at long wavelengths. The repetition rate of the amplifier here was set to 1kHz, to provide maximal average power for spectral measurements, without causing damage to the YAG crystal. The radiation power at the YAG crystal was controlled with a polarizing cube beamsplitter. The generated supercontinuum was then filtered with

a longpass filter, taking the spectral part above 1300nm. This spectrum passed through a neutral density filter, and was coupled into a standard telecom SMF with length of 600m (fig. 3.5(b)). The neutral density filter was used to adjust the power that was coupled into the fiber, in order to achieve the optimal compression for the given fiber length. Figure 3.6 (a) is the spectrum of radiation coupled into the SMF. Figure 3.6 (c) is the self-compressed spectrum, showing the 4.1x self-compression of the supercontinuum spectrum. Additionally, numerical modelling of the experimental result was done. Figure 3.6 (b) is the modelled spectrum at the entrance of SMF. Figure 3.6 (d) is the self-compressed spectrum, which is in a qualitative agreement with the experimental results.

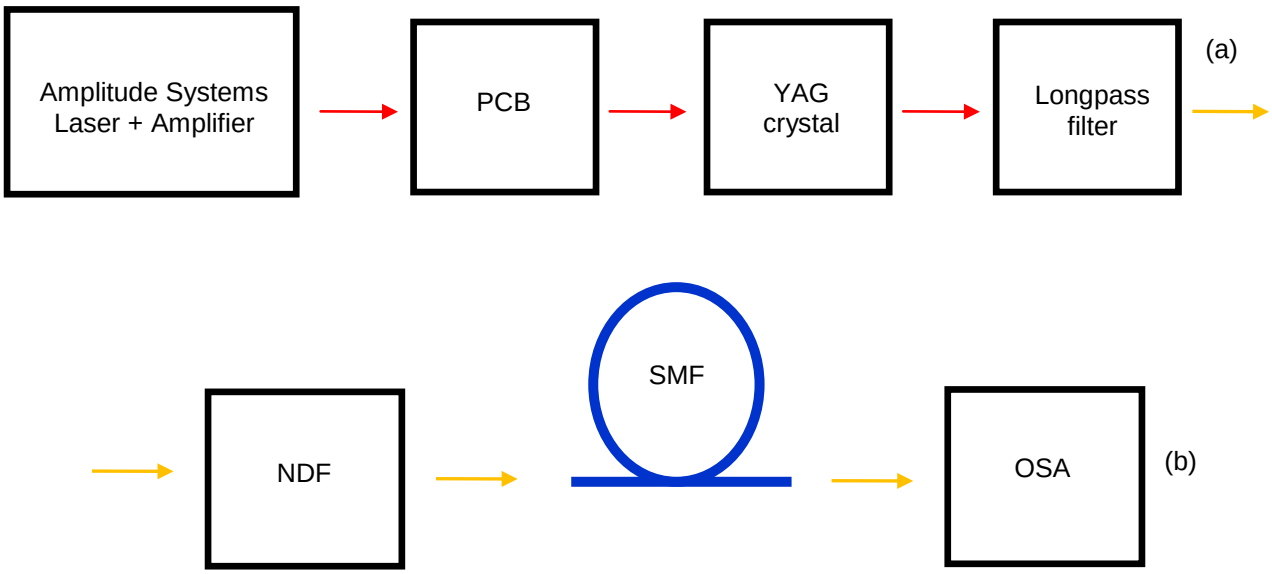

Figure 3.5. Experimental setup of self-SC of part of supercontinuum spectrum. (a) supercontinuum generation: here the PCB is the polarizing cube beamsplitter; YAG crystal is the yttrium aluminum garnet crystal. (b): self-SC: here NDF is the neutral density filter; SMF is the conventional single-mode telecom fiber with length of 600m; OSA is the optical spectrum analyzer.

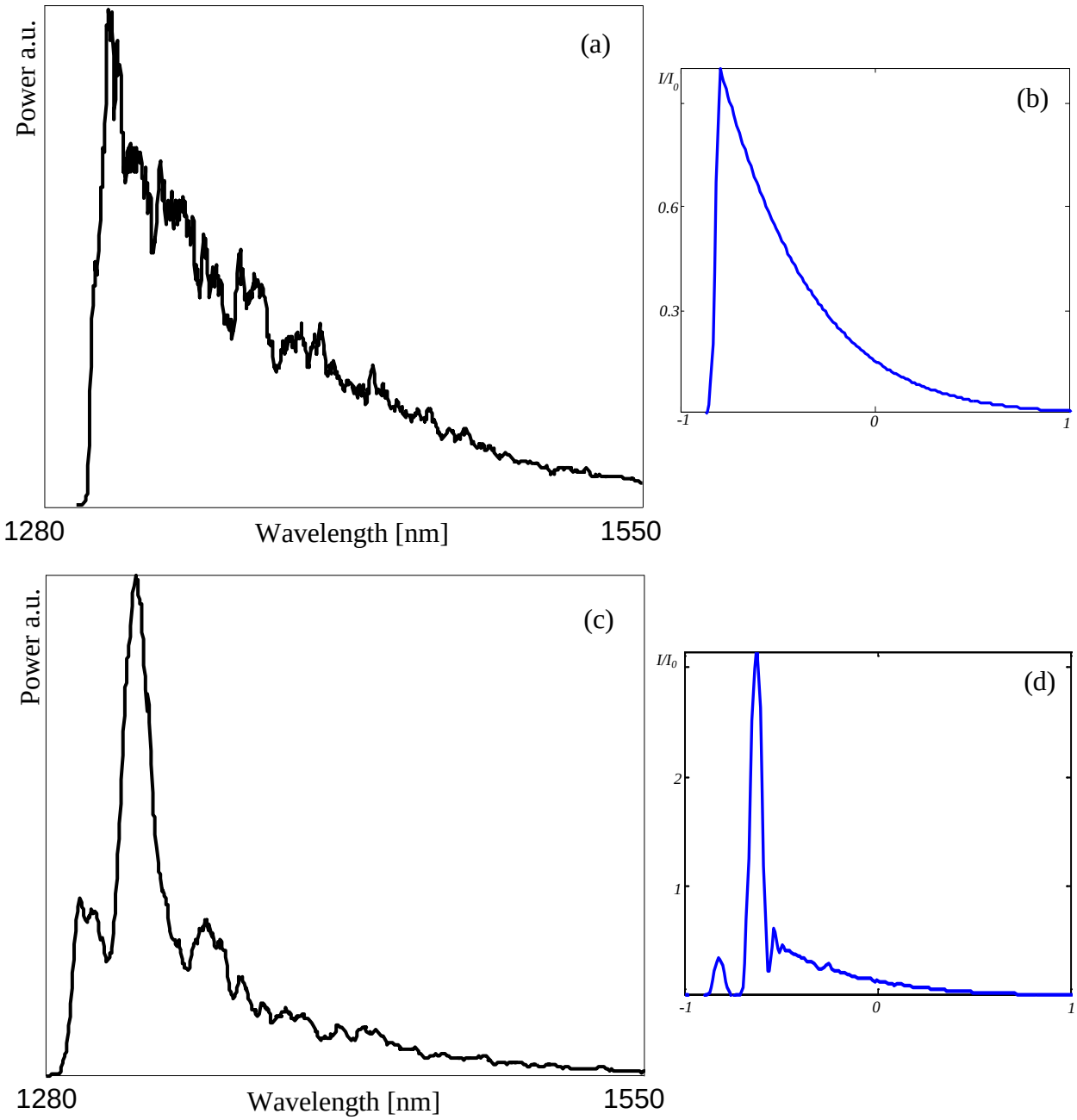

Figure 3.6. Experimental results of self-SC of part of supercontinuum spectrum. Supercontinuum spectrum cut at 1300nm (a), and self-compressed spectrum at the output of 600-m long SMF (c). (b) is the modelled initial spectrum and (d) is the modelled self-SC spectrum (d). Here I is intensity, and I_0 is initial peak intensity.

3.3 Numerical modelling of spectral self-compression

To have the complete physical pattern of the self-SC process and study its nature and peculiarities, numerical simulations were carried out, based on the solution of the nonlinear Schrödinger equation (NLSE), considering the factors of GVD and Kerr-nonlinearity, for both regular and noisy initial pulses.

Sech pulses were taken as an example of regular bell-shaped test pulse in these numerical studies. Figure 3.7 shows the results of numerical study. In figure 3.8 (a, b), the evolution of sech pulse and its spectrum are shown, during the propagation through fiber. As one can see, the process has clear repetitive nature: the spectrum compresses and broadens periodically throughout the propagation, while in opposite “phase” pulse is stretched and narrowed. This behavior is linked to the process of generation of high-order solitons. Figure 3.7 (c, d) shows the pulse and spectrum at the fiber input, and the pulse and spectrum at the length of fiber, where the first self-SC takes place. Here the nonlinear parameter is $\mathrm{R} = 0.6$ ($R = L_D/L_{NL}$) and the length of fiber where first compression takes place $\mathrm{f} = 30\mathrm{L_D}$. The self-SC ratio in fig 3.7 (d) is ~3x.

This research also shows, that the lower nonlinear coefficient is, the stronger compression may be observed. However, in order to obtain stronger compression, longer fiber is needed. This explains the low compression amount in the initial self-SC experiment with use of HCF, as the low nonlinearity of this fiber would require length of orders of magnitude longer, in order to optimally self-compress the spectrum.

Additionally, numerical studies of noisy signal self-SC process were carried out, based on the solution of the nonlinear Schrödinger equation. As the supercontinuum has noisy nature, the propagation of randomly modulated pulses in a medium with negative GVD and nonlinearity was numerically examined. For the pulses, the “signal + noise” model was used: $\mathrm{A(t)} = \mathrm{A_0(t)[1 + \sigma\xi(t)]}$, where $\mathrm{A(t)} = \mathrm{sech(t)}$ is the regular component of the pulse amplitude and the $\xi(t) = \xi_{Re}(t) + i\xi_{Im}(t)$ is a stationary complex noise with the σ amplitude, normal (Gaussian) distribution. 3D maps of the pulse and spectrum evolution in the fiber for a randomly modulated pulse show that self-SC is possible even for pulses

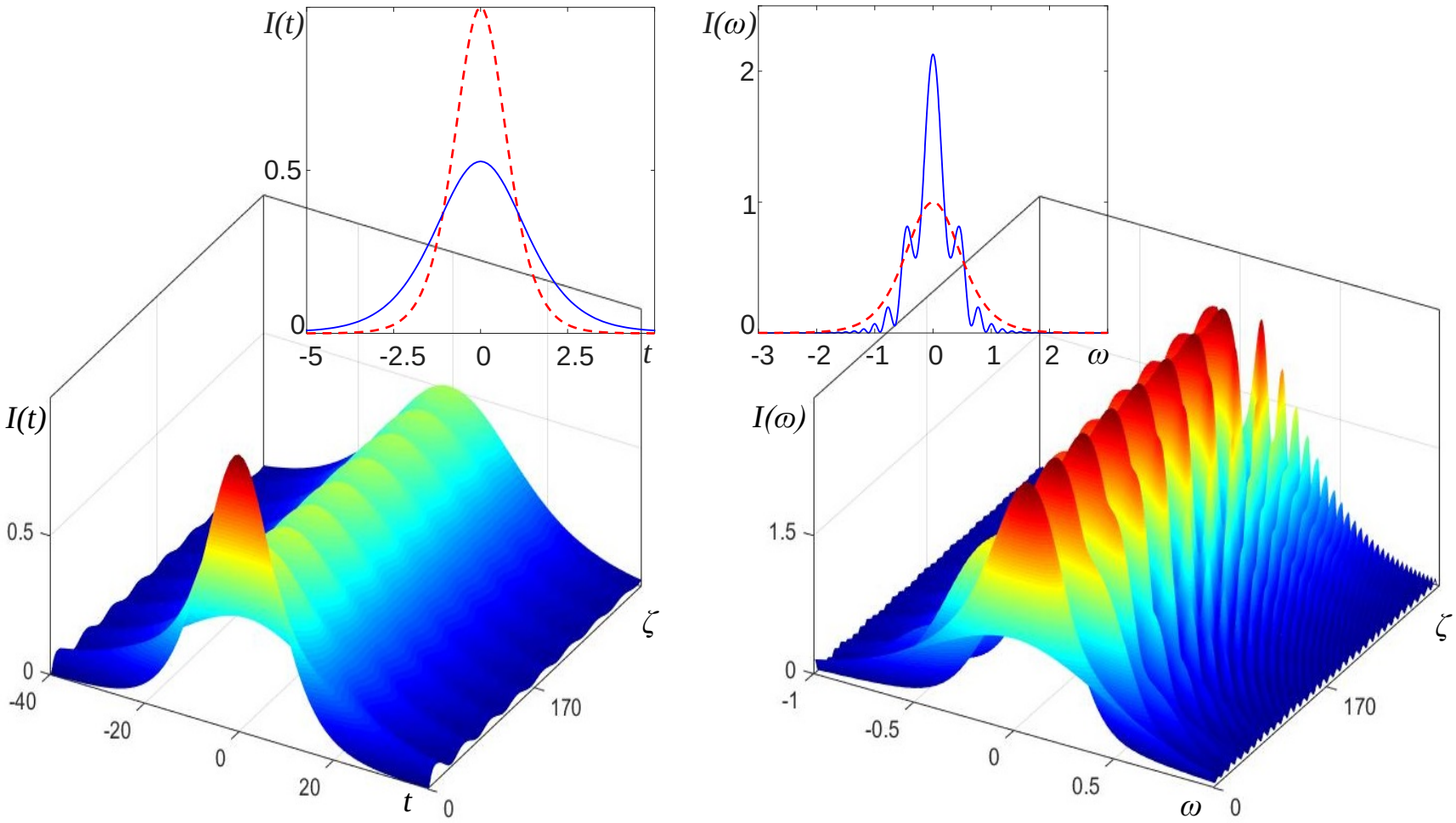

Fig. 3.7 Results of numerical study of self-SC of a sech pulse: 3D map of pulse (a) and spectrum (b) propagation, pulse profile at the input (c; dashed curve) and at the optimal spectral compression distance (c; solid curve), and spectral profile at the input (d; dashed curve) and at the optimal spectral compression distance (d; solid curve). Simulation data: $\mathrm{R} = 0.6$; $\mathrm{f} = 30\mathrm{L_D}$ (first compression).

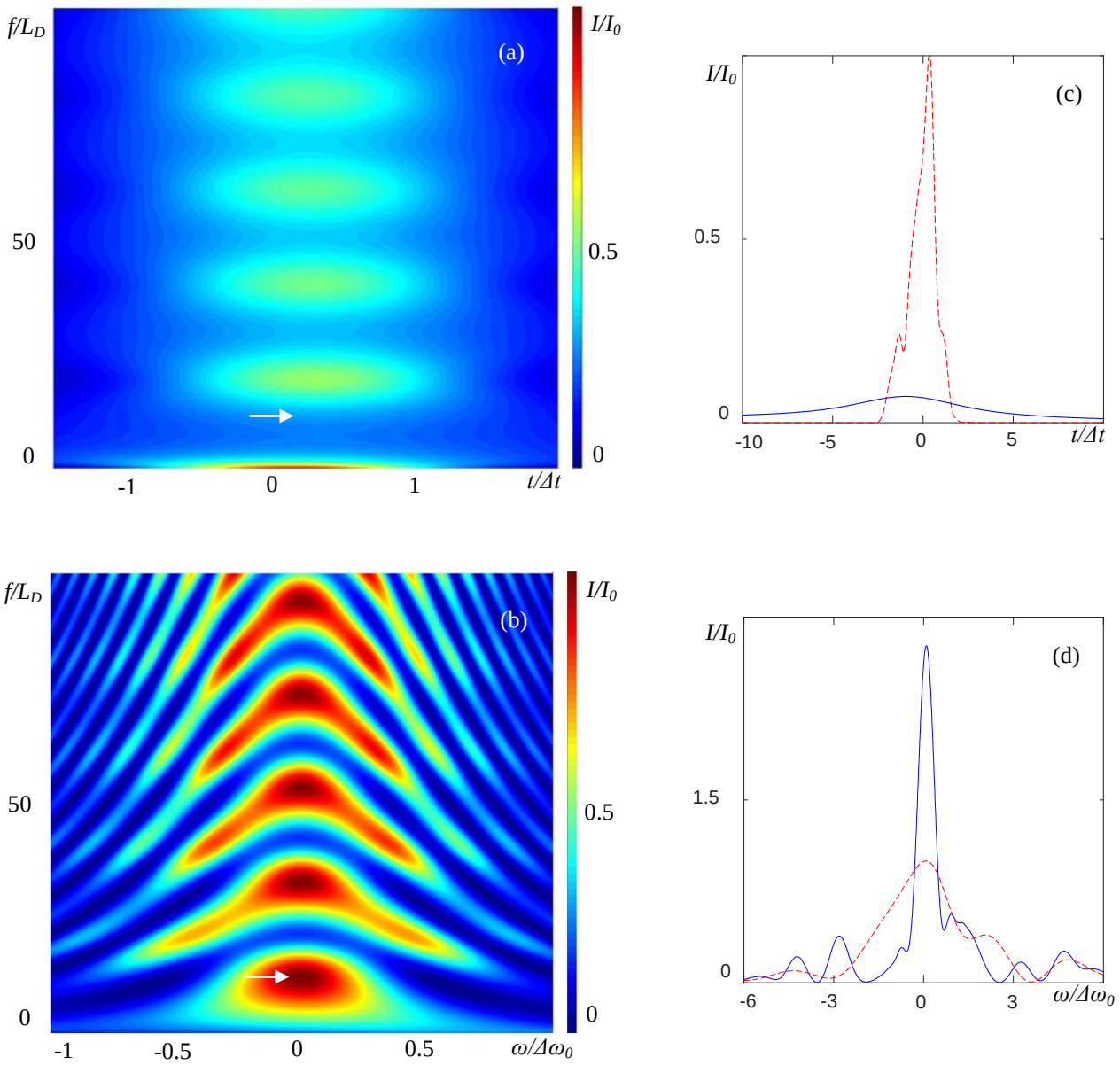

Fig. 3.8 Results of numerical study of self-SC of a randomly modulated pulse: 3D map of pulse (a) and spectrum (b) propagation, pulse profile at the input (c; dashed curve) and at the optimal self-SC distance (c; solid curve), and spectral profile at the input (d; dashed) and at the optimal self-SC distance (d; solid curve).

with noisy nature (fig. 3.8). Figure 3.8 (a,b) shows the periodic nature of this process, associated with high order solitons. The horizontal axis here are the time (a) and frequency (b). The vertical axis is the propagation distance in arbitrary units. The dashed

curves on the right side of figure 3.8 are the initial randomly modulated pulse and spectrum. The solid curves are the pulse and spectrum after the self-SC, at the point marked on the map with an arrow. The process of self-SC suppresses the noise, resulting in more coherent radiation at the output: the noisy pulse is “cleaned” out (fig. 3.8 (c,d)).

Conclusion

This chapter is representing the research, aimed at experimental demonstration of nonlinear effect of solitonic self-SC. The results of studies are:

1. 1.3x self-SC in an HCF is demonstrated for the first time. The self-SC was done at 800nm wavelength. The small compression factor because of the low nonlinearity of air core.
2. 4.1x self-SC in a conventional SMF is observed, with use of part of generated supercontinuum radiation, above 1300nm. This result also shows the possibility of compression of noisy radiation.

In addition, numerical studies were carried out to obtain a deeper understanding of the process. The modelling of self-SC of regular bell-shaped (sech) pulses shows the repetitive nature of the process, which is linked to the generation of high-order solitons. Moreover, the process was studied numerically for the pulses with random modulations of amplitude and phase. The results of these studies show, that self-SC of noisy pulses results in “cleaning” out the noises, and more coherent radiation.

CHAPTER IV

SIMILARITONIC AND SPECTRONIC TECHNIQUES OF

FEMTOSECOND PULSE DIAGNOSIS

Introduction

In this chapter, the experimental results of the similaritonic technique for determination of femtosecond pulse duration and the numerical studies of spectron phase characteristics are presented. For the first technique it is shown that the pulse duration can be found out by measuring the generated similariton spectral width. For the second topic, the research shows that the spectron transfers the information from spectral to temporal domain not only for the field amplitude, but also for the phase, and so, dispersive Fourier transformation takes place for the complex field of radiation.

Similaritons are pulses that maintain the shape of their temporal profiles during the propagation. The generation of similariton pulses with parabolic temporal, spectral and phase profiles was initially predicted by Anderson et al [101]. Later, such parabolic pulses were generated in fibers with gain or distributed dispersion [102-104]. The NL-D similariton of passive fiber (without gain) was generated under the combined impact of Kerr nonlinearity and second order of dispersion [105]. The NL-D similariton has the bell-shape spectral and temporal profiles and a parabolic phase (linear chirp), independent from the input pulse parameters.

It was experimentally checked, that the spectral bandwidth of the NL-D similariton generated from pulses with nearly Gaussian shape is proportional to the square root of the input pulse power [106]. In this study, the further investigation of this property of NL-D similariton is shown. It is done by testing the relation between the similariton bandwidth and seed pulse duration for various input pulse forms.

Spectrons are pulses for which the temporal intensity profile repeats the spectral profile. It is shaped when the pulse passes through long enough dispersive medium [11; 107], in a temporal analogy with the far field diffraction (Fraunhofer zone diffraction). The

spectron shaping process is well studied in context of dispersive Fourier transformation (DFT) [108; 109], or the real-time Fourier transformation [110; 111]. The DFT method uses dispersive element and a single-pixel photodiode for the real-time spectral measurements, thus avoiding the response time limitations of the traditional spectrometers [14]. This method has numerous applications, such as the real-time spectroscopy, fast real-time optical imaging, laser scanning, etc. Although the spectron shaping process is well known, the phase peculiarities of spectron are not studied in details. Such a study can be of interest, particularly, for spectral phase measurements and full characterization of femtosecond pulses, e.g., alternatively to methods of spectral interferometry. Full information on pulse spectral intensity and spectral phase allows the reconstruction of the complex temporal field of the femtosecond signal (temporal intensity profile and phase). This is done by the methods of spectral interferometry [24; 40-45] and spectral shearing interferometry [111].

The studies of spectron phase peculiarities allow to measure the spectral phase of the test pulse by the measurement of the spectron phase using SFG [112], as an alternative to interferometric techniques, which are more complicated technically. The goal of this research was the study of spectron phase peculiarities, specifically, finding the conditions, under which the spectron temporal phase reproduces the spectral phase.

4.1 Spectral characteristics of nonlinear-dispersive similariton

Here, both numerical and experimental studies of the spectral peculiarities of NL-D similaritons, in particular, the dependence of its spectrum from the input pulse duration are presented. During the numerical investigations, the generation of NL-D similariton in passive (without gain) optical fiber was numerically modeled. For this, the nonlinear Schroödinger equation and Fourier split-step method were used to numerically model the pulse propagation through the fiber. Dimensionless parameters were used to describe the pulse propagation through the fiber: $\zeta = z/L_D$ - dimensionless length, where z is the fiber length, $L_D = \Delta t_0^2/k_2$ is the dispersion length, Δt_0 is the duration of the input pulse, $k_2 = \partial^2 k/\partial\omega^2|_{\omega_n}$ is the parameter of the second order of dispersion, $R = L_D/L_{NL}$-

nonlinearity parameter, where $L_{NL} = (k_0 n_2 I_0)^{-1}$ is the nonlinear length, k_0 is the wave number, n_2 is the fiber nonlinearity coefficient, I_0 is the peak intensity. After the generation of NL-D similariton, the dependence of similariton bandwidth from the input pulse duration was studied. First, the input pulses without initial chirp were examined. For Gaussian input pulses, the similariton bandwidth is inversely proportional to the square root of the input pulse duration [11; 105; 106]. The coefficients of these dependences for pulses of various shapes were compared.

The numerical simulations showed that although the similariton bandwidth is proportional to the square root of the parameter R, the curve coefficients is different for the pulses with different shapes. Further detailed simulations showed that these coefficients depend linearly on the parameter $\Delta t_{TL} \Delta \omega_0$ of initial pulse, were $\Delta \omega_0$ is the initial pulse spectral width and Δt_{TL} is the duration of the transform limited (TL) input pulse. Taking into account this correction, the dependence of similariton bandwidth from the square root of R is normalized to get a relation independent from the input pulse shape:

$$\Delta \omega \sim \sqrt{\Delta t_{TL} \Delta \omega_0} \sqrt{E/\Delta t}, \tag{4.1}$$

where Δt is the FWHM duration and E is the input pulse energy.

Figure 4.1 shows the dependence of the similaritons spectral width from the parameter of nonlineaity R, for various shapes of initial pulse. Here, the X-axis is $\sqrt{R}$, and it's normalized on $\sqrt{\Delta \omega_0}$ for each initial pulse. In the left column, the shapes of initial pulses are shown.

The relation (4.1) is true only for transform-limited pulses. The duration of bell-shape pulses with spectral phase can also be measured independently of their shape. For this, the similariton spectral bandwidth has to be measured at its base, instead of FWHM. In this case, the relation (4.1) has more simple form

$$\Delta \omega_{base} \sim \sqrt{E/\Delta t}, \tag{4.2}$$

independently from the pulse shape. This gives the opportunity to easily retrieve the input pulse FWHM duration by measuring the spectral width at the base of the generated similariton spectrum.

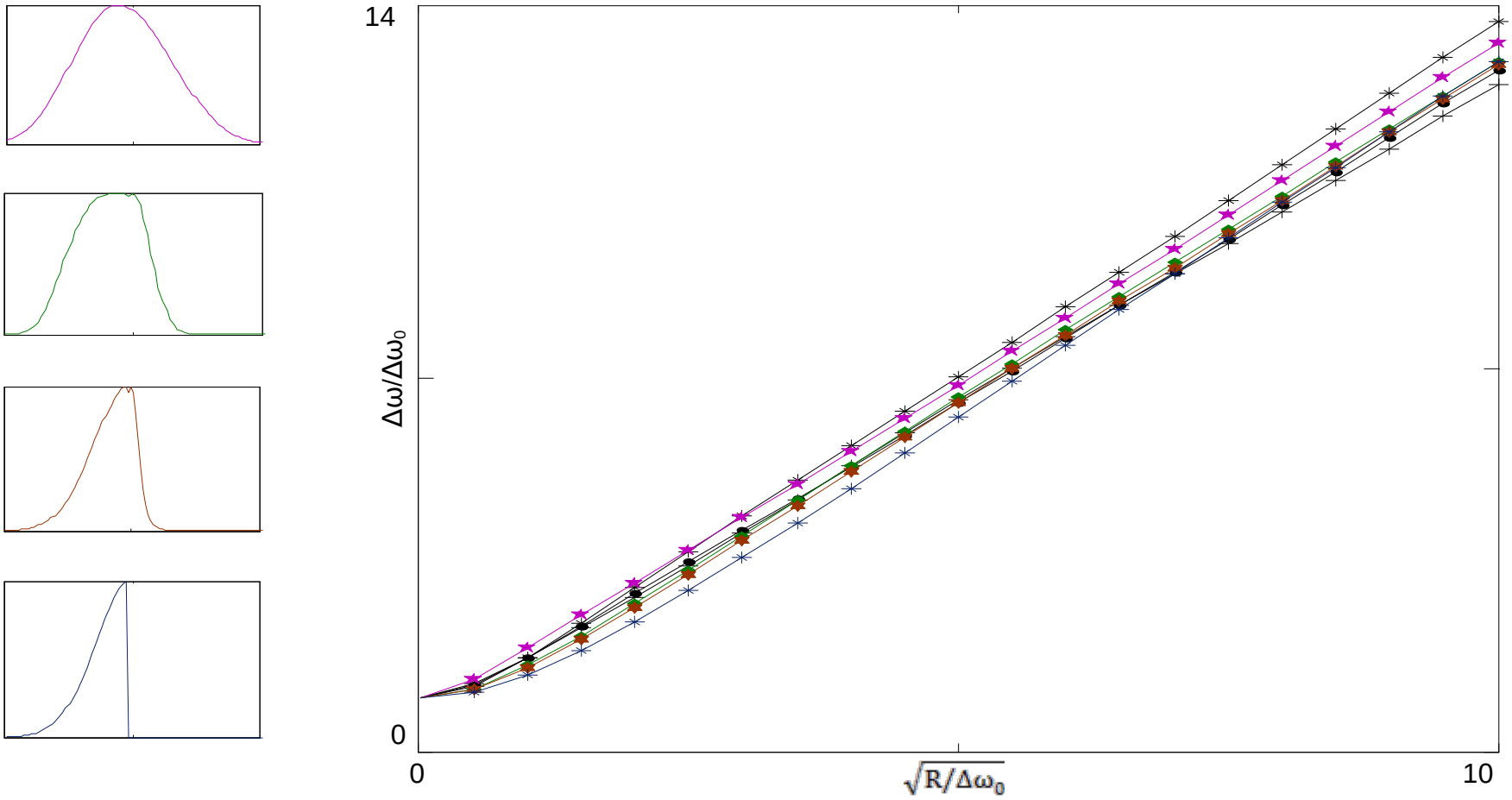

Figure 4.1. Dependence of similariton spectral width from $\sqrt{R}$ for various initial pulse forms (left column).

Figure 4.2 shows the dependence of the similariton spectral width $\Delta\omega_{base}$ from the input pulse duration Δt. The $\Delta\omega_{base}$ can be measured anywhere below 1/10 of the spectrum peak, but the results are better when this level is chosen lower. Here, the $\Delta\omega_{base}$ is measured at 1/100 of the peak intensity of the spectrum. The blue, red and green squares (fig. 4.2) correspond to the chirped Gaussian, super-Gaussian and $sech^2$ input pulses respectively. The orange and brown squares have triangle-like asymmetrical spectra. The dashed part of the linear approximation line stands for the region, for which similariton generation is not taking place due to low power. The durations of test pulses were changed by giving them linear chirp and temporally stretching them up to 4-5 times, which also results in change of the pulse shape.

Afterwards, the two-peak pulses were examined. For bell-shape pulse, the FWHM duration and spectral width are used. For complicated pulses, the standard deviation (SD) duration and spectral width are used. To calculate the SD of the parameter a, the following formula is used:

$$\sigma_a = \sqrt{\overline{a^2} - \overline{a}^2}. \tag{4.3}$$

In the case of complicated pulses, as for the bell-shape pulses, the numerical simulations show that the bandwidth of the similariton is proportional to the square root of nonlinearity parameter $\mathbb{R}$ (fig. 4.3). For all pulse forms, the SD of similariton spectrum is inverse proportional to square root of input pulse SD duration, with the coefficient independent from the pulse shape:

$$\sigma_\omega \sim \sqrt{E/\sigma_{\Delta t}}. \tag{4.4}$$

This relation was also checked for bell-shape pulses as well. Thus, for measurements by means of SD, there is a simple relation between the similariton bandwidth and the input pulse duration for both bell-shape and complicated pulses (fig. 4.3). The blue and red points of figure 4.3 correspond to similaritons generated from two-peak and three-peak pulses respectively, with various initial chirps. Green and red points correspond to pulses with Gaussian and $sech^2$ shapes and various initial chirps

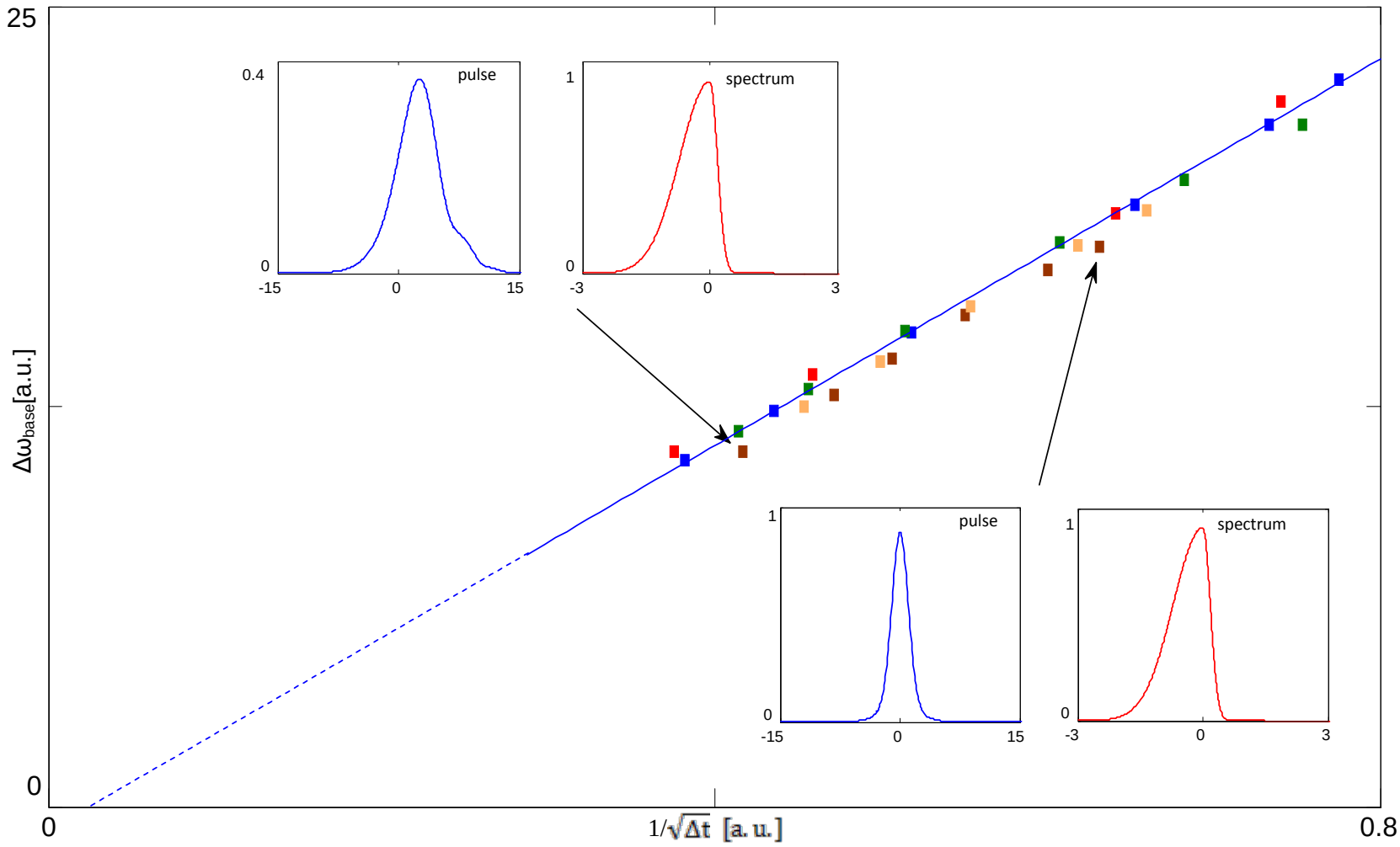

Figure 4.2. Results of numerical modeling for the dependence of similariton's spectral width (at the base) from the input pulse duration. Different color squares correspond to various initial temporal and spectral shapes.

To experimentally prove the study, the radiation of Mira 900F + Verdi V10 laser system with 100fs pulse duration at 800nm central wavelength and 76MHz repetition rate was used. Pulses first passed through dispersive medium of various lengths, resulting in shaping of pulses with different durations. After this, the pulse duration was measured by an autocorrelator (AC). The NL-D similariton was generated in a ~1m long SMF (Thorlabs 780HP). The $\Delta\lambda_{sim}$ bandwidth of the NL-D similariton was measured using an Ando AQ-6515A optical spectrum analyzer (OSA; fig. 4.4). Alternatively, the DFT method [15; 111] was used to provide the real-time performance. This method uses a large dispersive element to stretch the pulses, while keeping the stretched pulse duration proportional to its spectral width. In this experiment it was done by coupling the similariton pulses into a 600-m long SMF to stretch the pulses to nanosecond domain, and a nanosecond photodetector with a standard oscilloscope to measure the pulse duration.

First, the results of numerical studies were tested for laser pulses. Thereafter, initial pulses with different durations were shaped by passing through pieces of glass with different thicknesses. Also, the laser pulses were dispersively stretched and chirped, both positively and negatively, in an SF11-prism pair-based DDL. Studies were carried out for initial pulses with AC durations of Δt_0~150–550fs, in the range of radiation average powers of $\bar{p}$~ 50–500mW. Then, the relationship between the similariton spectral width and the input pulse AC duration was demonstrated. The input pulse AC duration at FWHM was used instead of the pulse duration, as the pulses in this experiment had similar shapes for different chirp slopes. Taking into account the coupled power and using the equation (4.2), the linear curve of figure 4.5 was obtained, which is in a good accordance with numerical results. Here, the X-axis is $\sqrt{\bar{p}/\Delta t_{in}}$, where $\bar{p}$ is the average power at the fiber output and Δt_{in} is the input pulse AC duration. The left and right columns in figure 4.5 are for the longest and shortest input pulses (with 146fs and 550fs AC-durations), respectively. On the top the AC traces and lower similariton spectra are shown. The similariton spectral bandwidths and input pulse durations are determined at the base, and FWHM, respectively. Figure 4.5 also contains the results of the measurements done by oscilloscope, for which the 600m-long SMF was used.

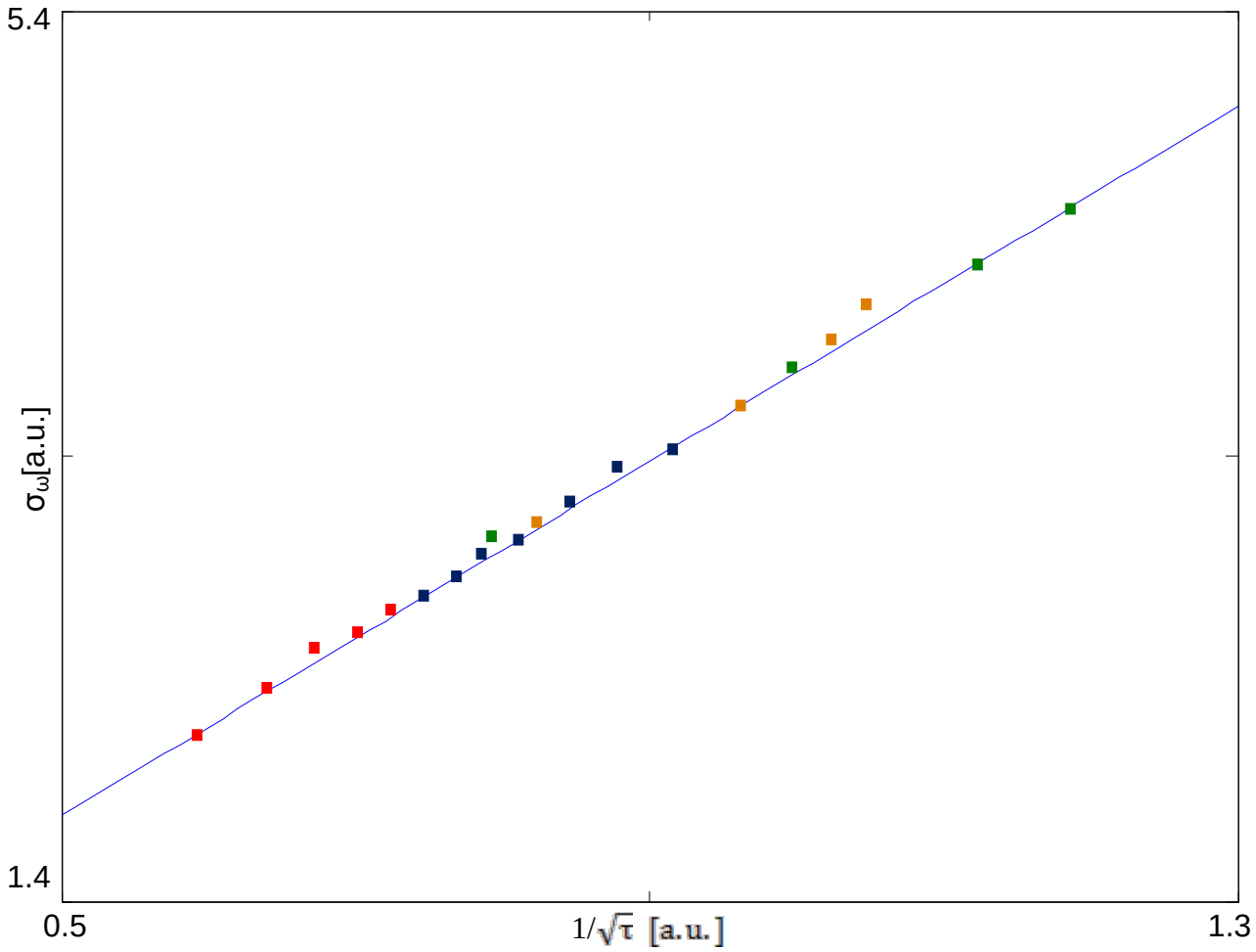

Figure 4.3. The dependence of the similariton spectral width from the SD duration for bell-shape (orange, green), two-peak (blue) and three-peak (red) input pulses.

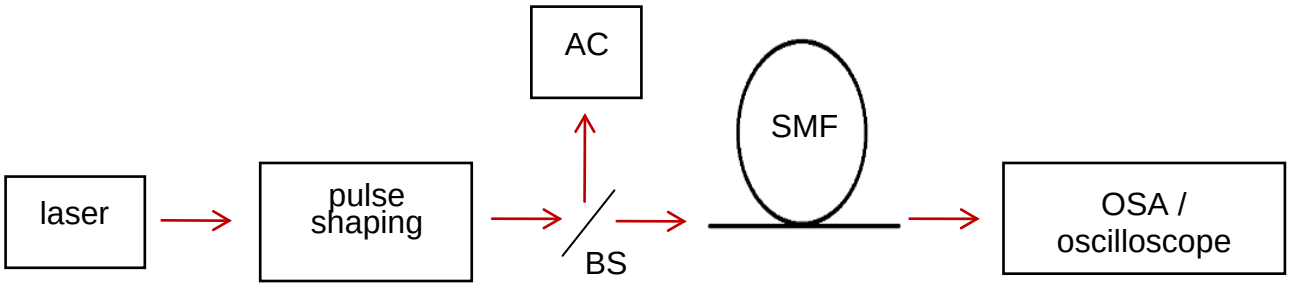

Figure 4.4. Experimental setup of pulse duration determination for bell-shaped pulses: AC – autocorrelator; BS – beam splitter; SMF – single-mode fiber; OSA – optical spectrum analyzer.

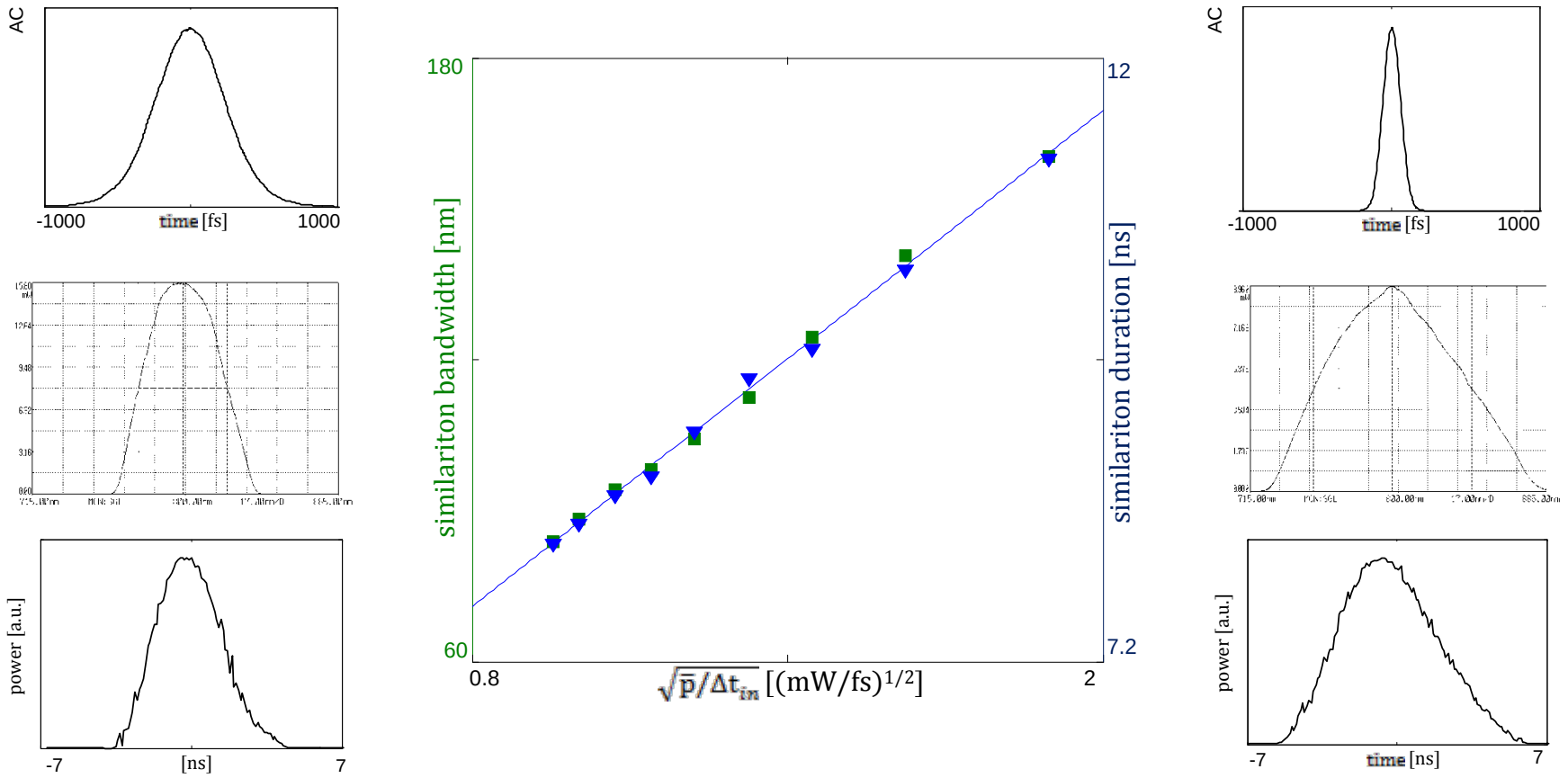

Figure 4.5. Experimental results of duration determination for bell-shape pulses: input pulse duration (central chart) versus $\sqrt{\bar{p}/\Delta t_{in}}$; green squares and blue triangles are the similariton OSA- and oscilloscope-measured bandwidths, respectively; blue line is for linear approximation. Left and right columns are the measurements for initial pulses with 550fs and 150fs AC durations. From top to bottom: input pulse AC, OSA- and oscilloscope-measured similariton spectra.

To examine the results of numerical analysis for complicated pulse forms, two-peak test pulses were shaped by inserting a thin microscope glass in a part of laser beam. The difference of refractive indexes causes a delay on a part of radiation, resulting in the formation of two-peak pulses. Then, the two-peak pulses were dispersively chirped in glasses with different lengths. Thereafter, the NL-D similaritons were generated from these pulses in an SMF, and the spectrum was measured (fig. 4.6). SD durations of pulses were ~180-250fs. The SD of the input pulse AC trace was used as an equivalent to the SD of the pulse, since it is equal to the pulse SD, with a coefficient of $\sqrt{2}$, for any pulse shape. The SD of similariton spectra was also calculated, which demonstrates a linear dependence (eq. 4.4) from the inverse of the square root of the tested pulse SD duration (fig. 4.7). The red points in figure 4.7 are for dispersively chirped two-peak pulses. Dispersion is applied to the pulses in order to change the pulse shape and obtain pulses with various durations. These measurements were compared with the ones of chirped laser pulses (green points). The blue line is the linear approximation.

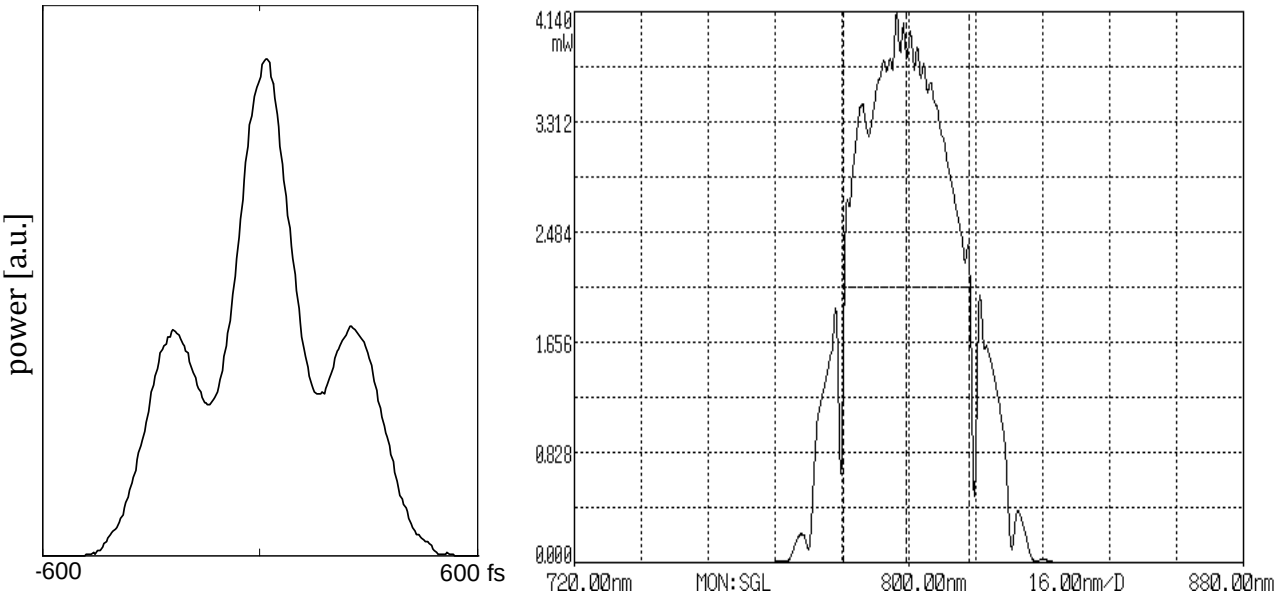

Figure 4.6. Experimental results of pulse duration determination for two-peak pulses: two-peak input pulse AC (left), and measured similariton spectrum (right).

Additionally, research was carried out for the compressed pulses, both numerically and experimentally. In the numerical modeling, the laser pulse compression and the similariton generation from this compressed pulse was studied. Figure 4.8 shows the results of simulation. The blue curves show input Gaussian pulse (fig. 4.8a) and spectrum (fig. 4.8b),

and the green ones are for the compressed pulse. The red spectrum in figure 4.8b is the similariton generated from the compressed pulse. The side lobes of the compressed pulse motivate the use of the SD formula (eq. 4.3) for pulse duration and spectral width calculations. Results of the numerical modelling, represented in figure 4.9, show that the dependence (eq. 4.4) of the similariton spectral width from the input pulse SD duration is also true for compressed pulses.

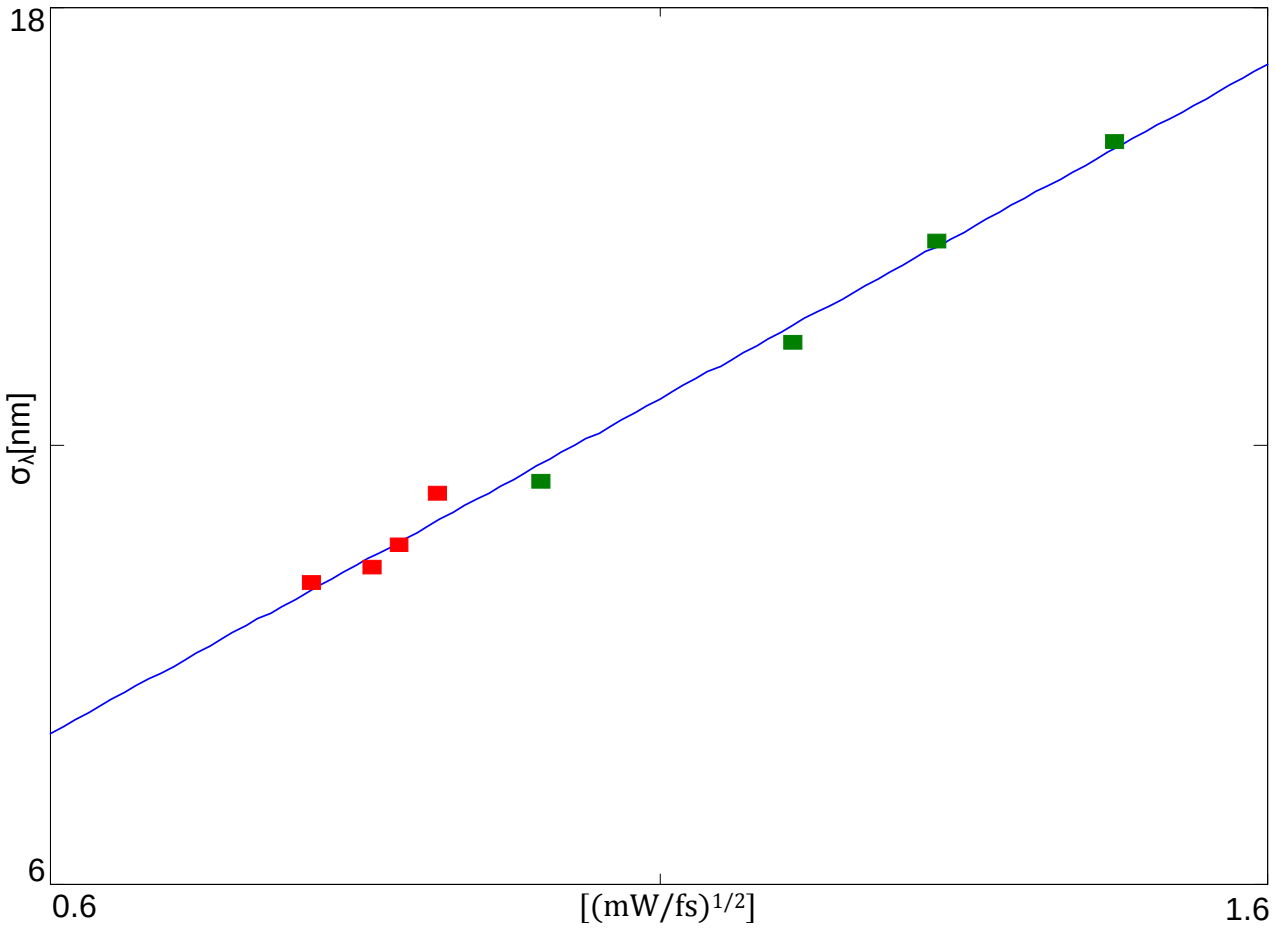

Figure 4.7. Experimental results for similaritons generated from chirped two-peak pulses (red) and chirped laser pulses (green).

Experimentally, the pulse compressor consisted of a short piece of SMF (~38cm Thorlabs-780HP), and a grating pair (groove density: 300mm^{-1}) based DDL. In this arrangement, the pulses were compressed down to ~64fs AC durations. By changing the amount of dispersion of the DDL, the compressed pulses were chirped both positively and negatively, resulting in pulses with ~64-160fs AC durations, with various pulse shapes. Afterwards, the compressed pulses were coupled into an LMA-5 large mode area fiber

(~3m) to generate the NL-D similariton (fig. 4.10). The fiber core diameter was 5µm, which is ~2x smaller than the core size of standard SMF, resulting in stronger nonlinearity. This fiber was used because of the drastic drop of the radiation power after the pulse compressor.

Thereafter, the compressed pulse SD durations were compared with the SD of the pulse AC. Figure 4.11 shows the dependence of the NL-D similariton spectrum SD from the radiation average power and the SD duration. The purple points are the measurements and the blue line is the linear approximation. The pulses after the compressor, i.e. the initial pulses for similariton generation, had different shapes, spectra and positive or negative chirp. This shows the large application range of the similaritonic technique, as it is applicable for various pulse cases.

The match of the results for compressed pulses and the results for the bell-shaped pulses was also checked. The SD of similariton spectra for the chirped laser pulses (~500mW average power) and compressed pulses (~50mW average power) were compared. The experimental measurements in these two cases are in a good agreement with each other (fig. 4.12). The blue line is the linear approximation, the green squares are measurements for laser pulses with AC durations of ~150-550fs and ~10nm initial spectral width. The purple triangles are for compressed input pulses with AC durations of ~70-100fs and ~40nm initial spectral width.

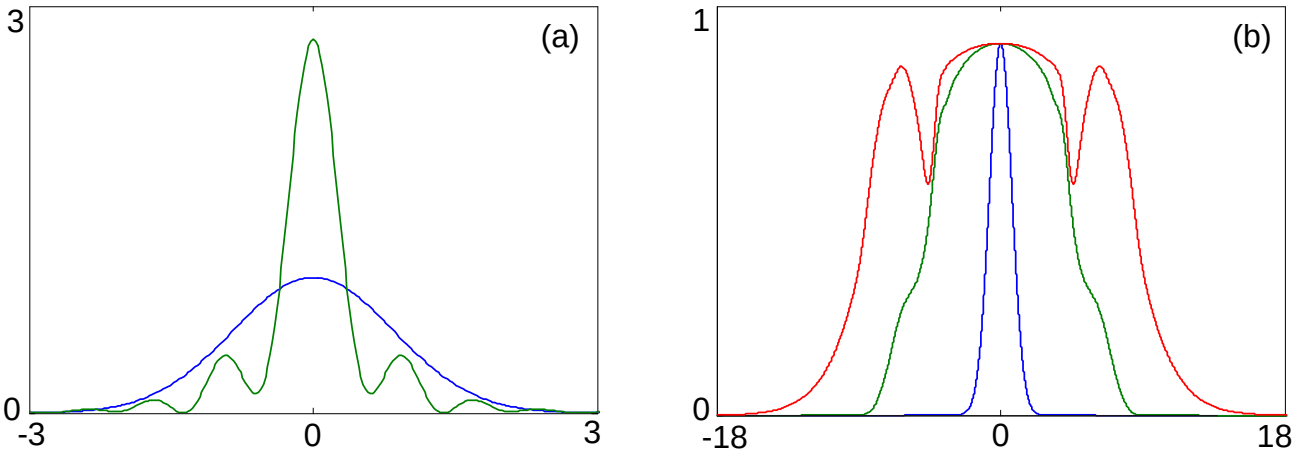

Figure 4.8. Spectrum of NL-D similariton generated from compressed input pulse. (a) Pulses and (b) spectra of input Gaussian pulse (blue), compressed pulse (green) and similariton (red).

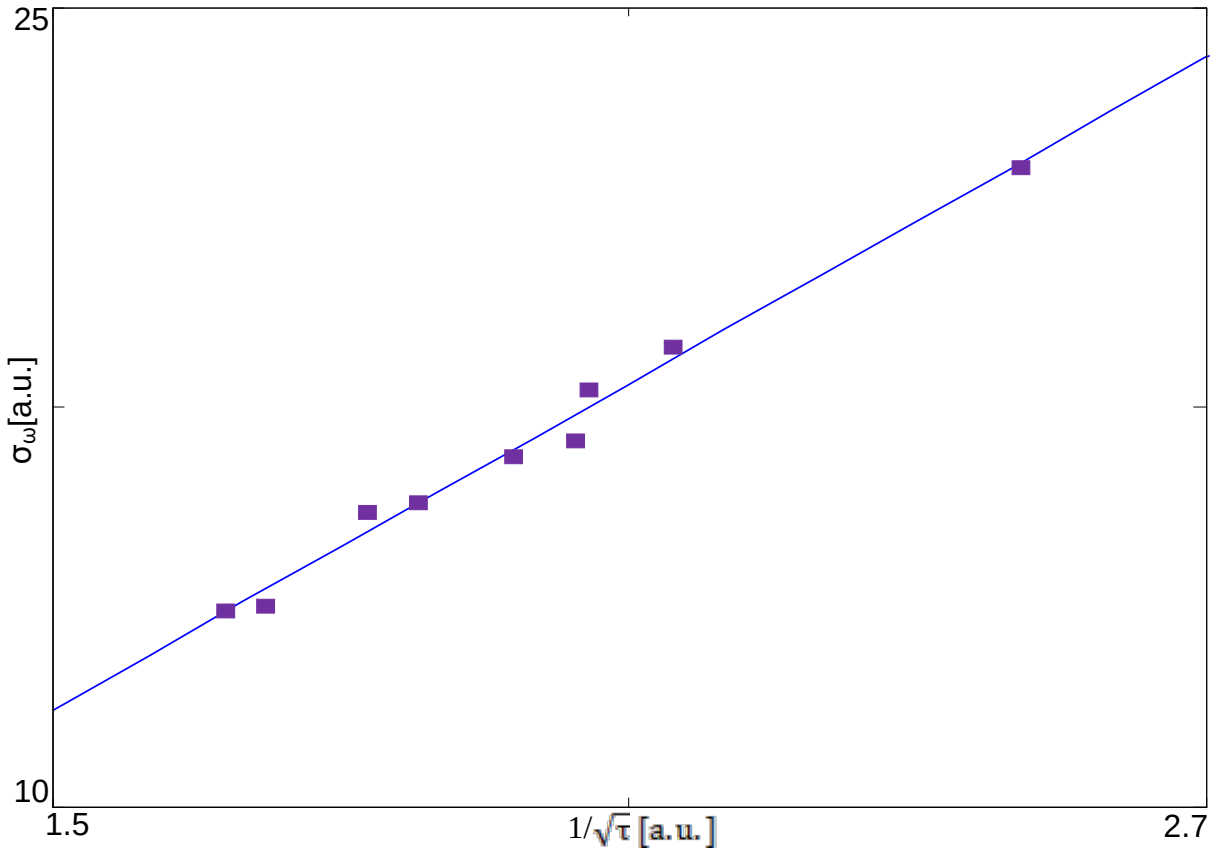

Figure 4.9. Results of numerical study of compressed pulses: the similariton spectral width versus the input pulse duration.

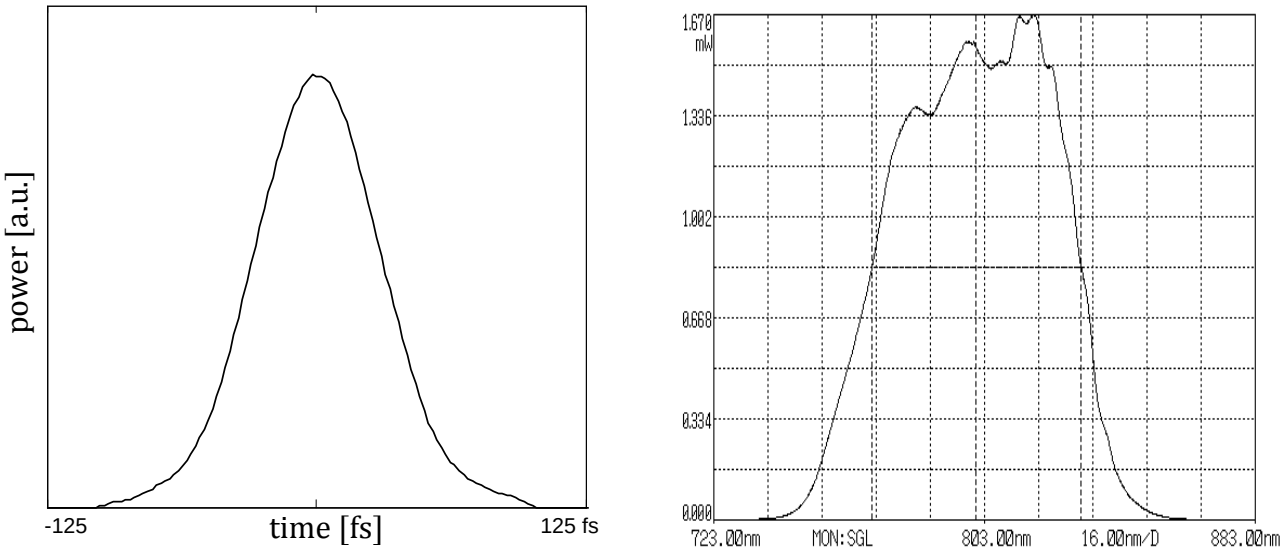

Figure 4.10. Experimental results for compressed input pulses: (left) input pulse AC, and (right) similariton spectrum.

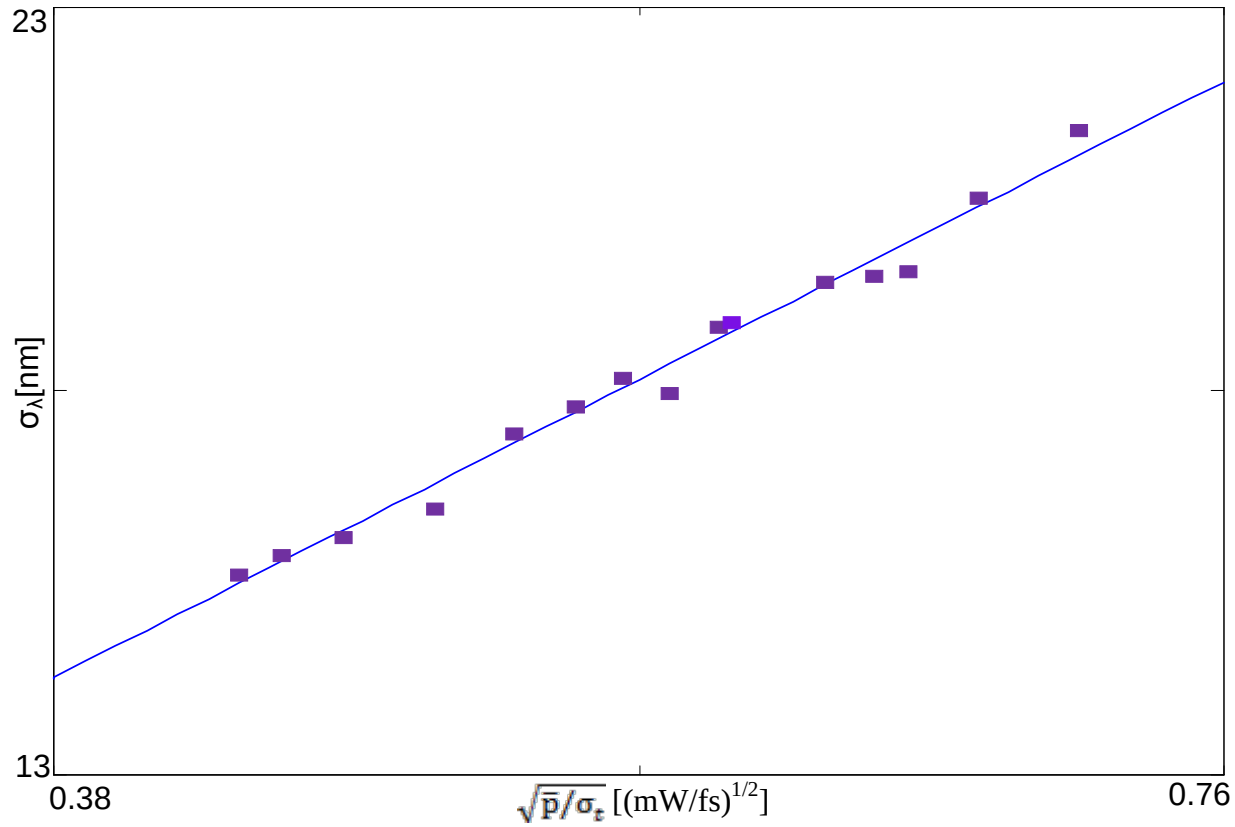

Figure 4.11. Experimental results for compressed pulses: dependence of the similariton spectrum SD from the coupled power and input pulse SD.

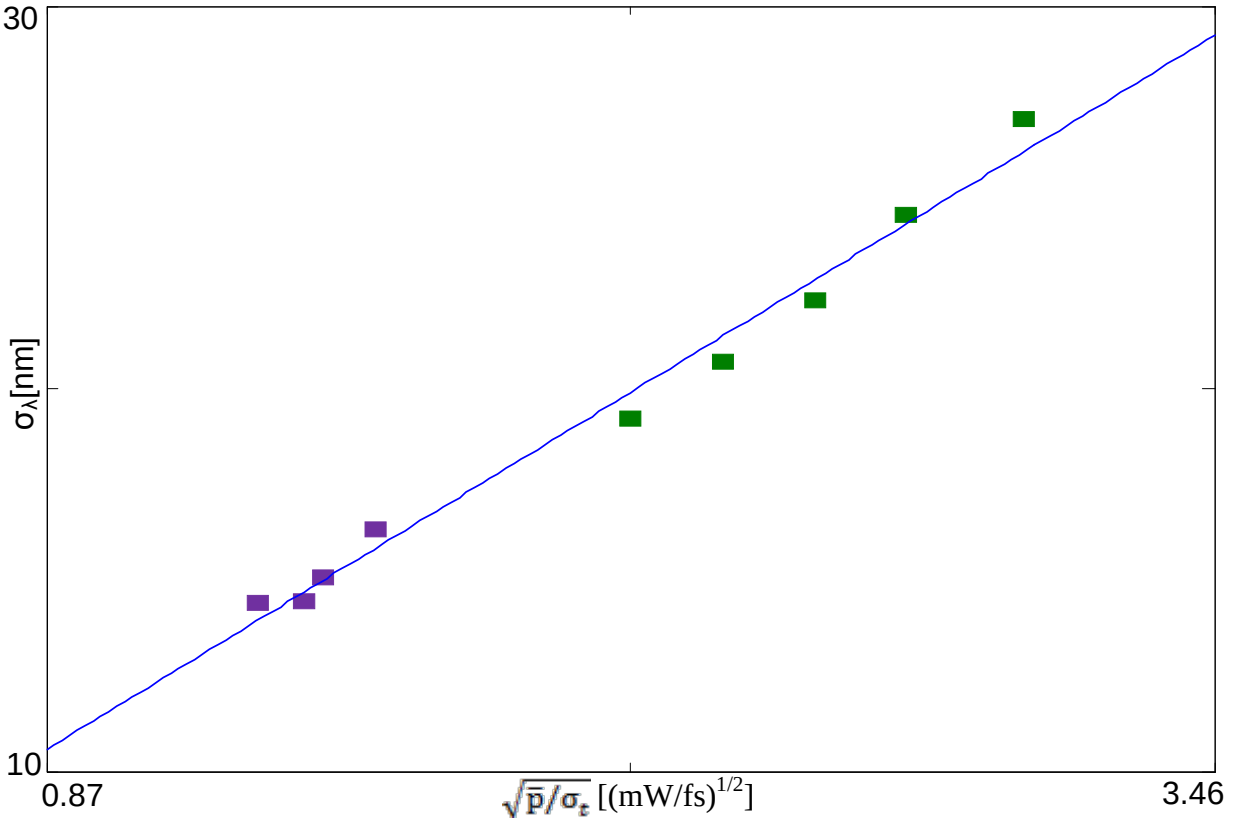

Figure 4.12. Results for bell-shape and compressed pulses: the similariton spectrum SD vs average power and SD duration of compressed pulses (purple) and chirped laser pulses (green).

4.2 Measurement of similariton bandwidth for femtosecond pulse duration determination

The numerical and experimental studies of paragraph 4.1 allow to implement the similaritonic technique of femtosecond pulse duration determination. The procedure for pulse duration determination includes coupling of the test pulse into an SMF and measurements of the coupled radiation average power and spectral width of the generated similariton or its duration (fig. 4.13). Using relations (4.1), (4.2) and (4.4), a general dependence of similariton spectral width from input pulse duration can be obtained:

$$\Delta t_0 \sim \bar{p}/\Delta\lambda_{sim}^2, \tag{4.5}$$

where $\bar{p}$ is the coupled radiation average power, $\Delta\lambda_{sim}$ is the spectral width of the similariton and Δt_0 is the test pulse duration. For pulses with bell-shape, Δt_0 is the pulse FWHM-duration, and $\Delta\lambda_{sim}$ is the spectral bandwith of similariton at its base. For test pulses with complicated shape, such as two-peak or compressed pulses, the SD Δt_0 and $\Delta\lambda_{sim}$ are used (eq. 4.4). As the energy loses in fiber are negligible, the average coupled power $\bar{p}$ can be measured at the output of the fiber, with use of a powermeter. As the similariton has linear chirp [11], its duration can be determined by multiplying its bandwidth and fiber length:

$$\Delta t_{sim} \sim z\Delta\lambda_{sim}, \tag{4.6}$$

This allows measuring the bandwidth by stretching the pulse in a long enough fiber, and registering it with a photodetector and an oscilloscope.

Figure 4.14 shows the measurements curve for a Thorlabs 780HP SMF as a medium for similariton generation. Here, the pulse energy is $E = 6.9x10^{-9}J$, which is calculated based on the coupled average power $\bar{p}$ and laser pulse repetition rate. Figure 4.14 also includes the curve for duration measurement by a nanosecond oscilloscope. For this, a 600m-long standard single-mode telecommunication fiber was used. This curve can be recalibrated for a different length of fiber by the use of relation (4.6).

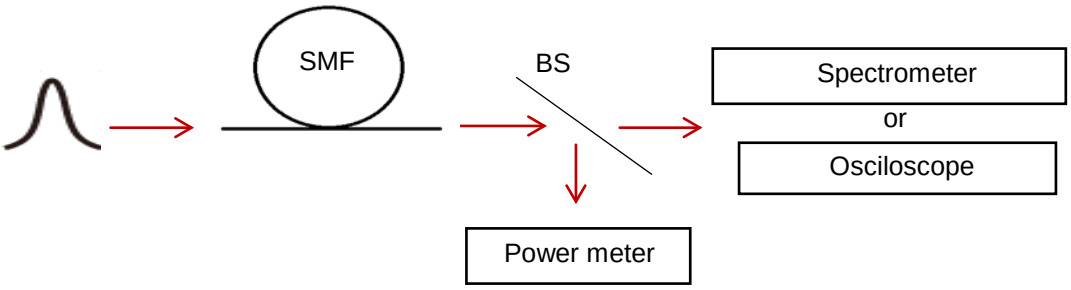

Figure 4.13. Setup of similaritonic technique for pulse duration determination: SMF – single-mode fiber, BS – beam splitter.

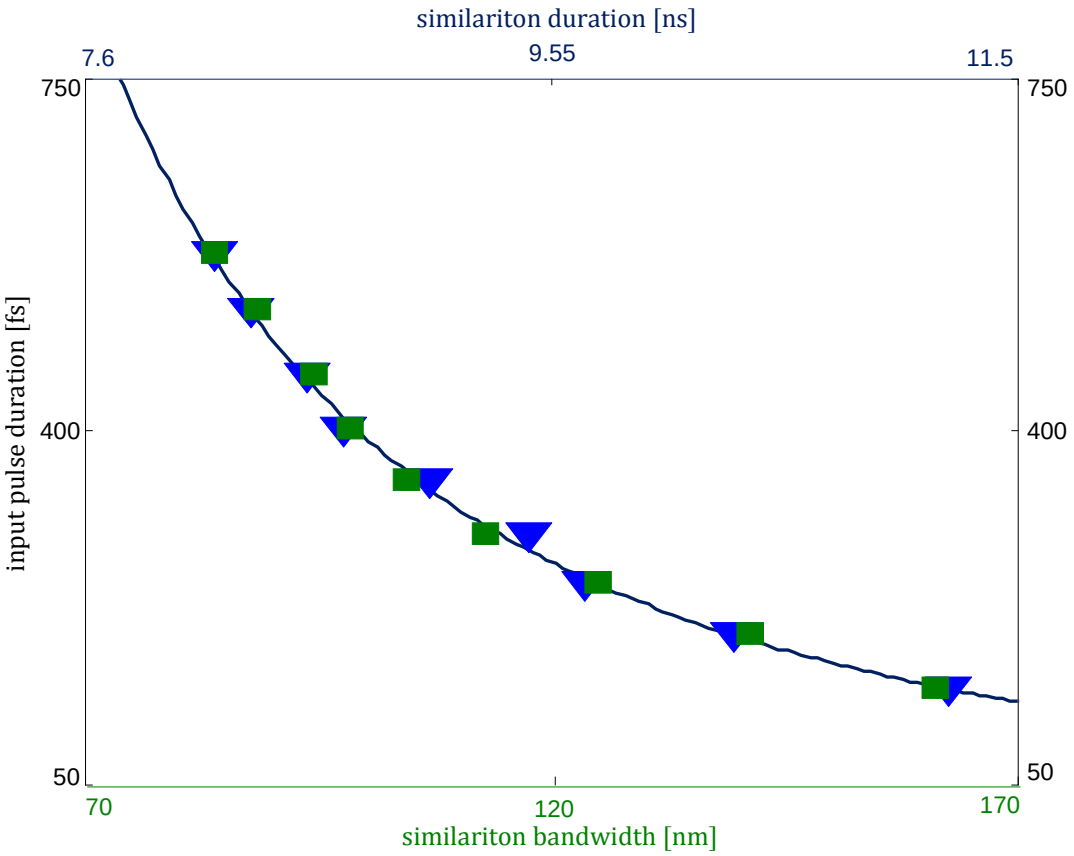

Figure 4.14. Duration measurements by similaritonic technique for a Thorlabs 780HP SMF. Green squares and blue triangles stand for spectrometer and oscilloscope measurements respectively.

4.3 Numerical study of spectron phase peculiarities

Here, the numerically studied phase peculiarities of spectron pulses in view of Dispersive Fourier Transformation are presented. In particular, it is shown that in the process of spectron shaping, the spectral information is transferred to temporal domain, not only for intensity, but also for the phase of the pulse. In the numerical studies, various pulses with different initial spectral phases were modeled as the input pulses at the entrance of the dispersive medium, from which the spectron pulses were shaped.

The spectron shaping process requires stretching of the pulse in the "far field of dispersion". The behavior of a pulse in this regime of dispersion ($\zeta = z/L_D \gg 1$), was examined mathematically: the Ψ complex slowly varying amplitude of a pulse has the following form

$$\Psi(\tau,\zeta) \approx \frac{1}{(i2\pi\zeta)^2} \exp\left(-\frac{i\pi^2}{2\zeta}\right)\tilde{\Psi}(\Omega,0), \qquad (\Omega = \tau/\zeta) \tag{4.7}$$

where $\tilde{\Psi}$ is the Fourier transform of Ψ, $\tau = (t - \frac{z}{v_g})/\Delta t_0$ – dimensionless running time, Ω – frequency ($\Omega = \tau/\zeta$), v_g – group velocity, $L_D = \Delta\tau^2/k_2$ – dispersive length, $\Delta\tau_0$ – duration of bandwidth-limited pulse, z – length of the dispersive medium and $\zeta = z/L_D$ – normalized length [11; 107]. The equation (4.7) describes the temporal amplitude and phase of the spectron pulse asymptotically:

$$|\Psi(\tau,\zeta)| \propto |\tilde{\Psi}(\Omega,0)|, \tag{4.8}$$

$$\varphi(\tau,\zeta) \approx \varphi(\Omega,0) - \Omega^2\zeta/2. \qquad (\Omega = \tau/\zeta) \tag{4.9}$$

Consequently, according to equations (4.8) and (4.9), the temporal intensity profile repeats the spectral one, and the temporal phase repeats the initial spectral phase, with additional parabolic component induced by dispersive medium: $\Omega^2\zeta/2 = \tau^2(2\zeta)^{-1}$**.** In practice, DDL consisting of pair of prisms or gratings, or fiber, for which the nonlinear impact is negligible, are used as a dispersive medium.

Numerical modeling was carried out, aimed at the research of process of spectron pulse formation from various initial pulse shapes. The dispersive equation in the 2nd approximation (parabolic equation) was numerically solved, with use of fast Fourier transformation algorithm [11]. The minimal length of dispersive medium ζ, required for

spectron shaping, was numerically examined for various input pulse forms, such as super-Gaussian (4^{th} order), asymmetric, and multi-peak pulses.

The shaping of spectron from a 4^{th} order super-Gaussian pulse (fig. 4.15a) was modeled first. After passing through a dispersive medium with a length of ζ=20, the resulting pulse at the output (fig. 4.15c) repeats the shape of the super-Gaussian pulse spectrum (fig. 4.15b): the spectron is shaped. For more complicated shapes, such as the asymmetric pulse (fig. 4.16a), the required minimum ζ tends to be more. In this case, the spectron (fig. 4.16.c) was shaped, and repeated the spectral shape (fig. 4.16b) after passing a dispersive medium with a length of ζ=25. Two- and three-peak pulses were also numerically modeled. These pulses were formed by overlaying Gaussian pulses with the different amplitudes and temporal delays. Figure 4.17a shows a tested two-peak pulse: the peaks' proportion is 1:2, and the time delay between the two peaks is equal to the double of the Gaussian pulse duration. Here, the spectron pulse (fig. 4.17c) was shaped on at length of dispersive medium ζ=60. The three-peak pulse (fig. 4.18a) was formed through overlaying of three Gaussian pulses, with peaks proportion of 1:2:4 and temporal delay between peaks each equal to the double of the Gaussian pulse duration. The spectron (fig. 4.18c) was shaped at the dispersive medium length of ζ=100, and repeats the spectral shape of the pulse (fig.4.18b).

Thereafter, the phase peculiarities of spectron pulses, generated from asymmetric, two-peak and three-peak input pulses were numerically modeled and examined. For the sake of simplicity, the parabolic components of spectron phases were subtracted. Figure 4.19a shows the shape of a tested asymmetric pulse. It had an initial spectral phase depicted in the figure 4.19b. After passing through ζ=25, the resulting spectron pulse had a temporal phase (fig. 4.19c), which repeated the spectral phase of the input pulse. The tested two-peak pulse is shown in figure 4.20a. It has the same proportions that had the two-peak pulse in figure 4.17a. The initial spectral phase of the two-peak pulse is shown in figure 4.20b. After passing through the dispersive element (ζ=60), the output spectron pulse had a temporal phase (fig. 4.20c) which repeated the spectral phase of the input pulse.

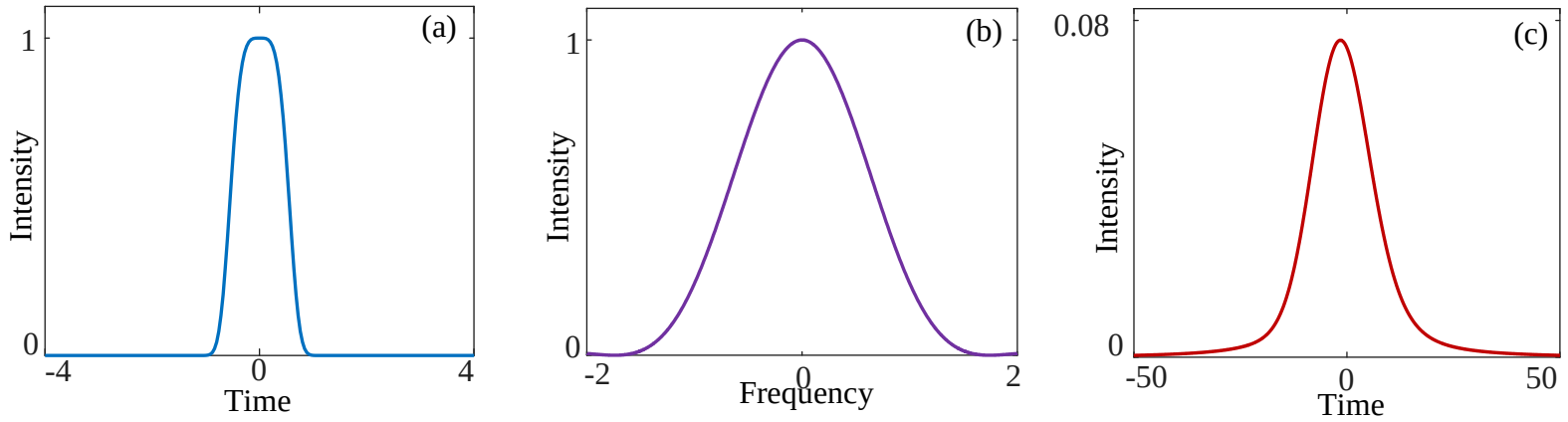

Figure 4.15. Spectron shaped from a 4th order super-Gaussian input pulse: (a) input pulse, (b) spectrum, and (c) spectron pulse, shaped at the length of ζ=20

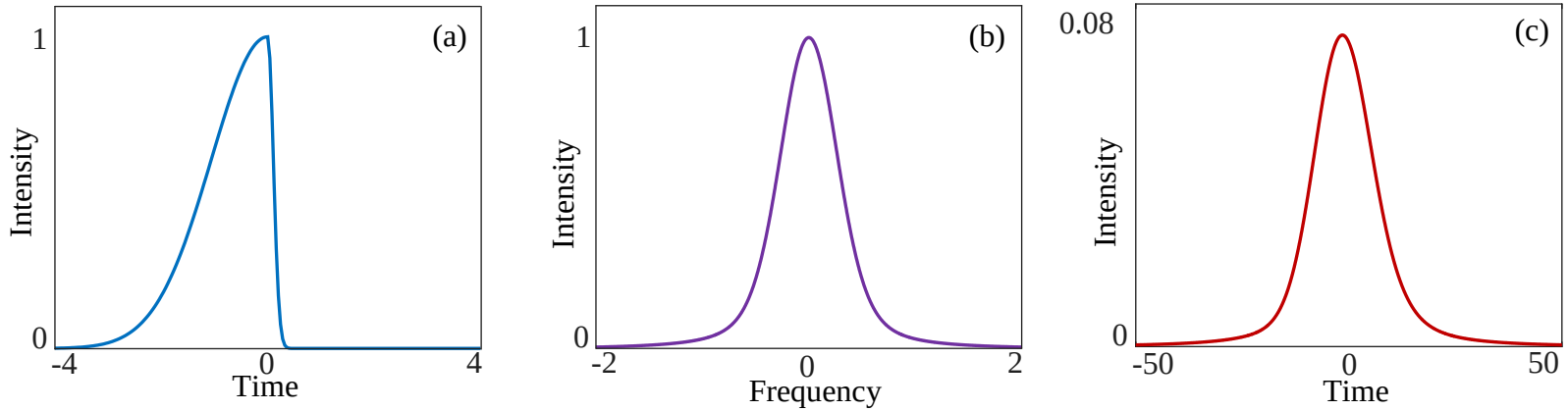

.

Figure 4.16. Spectron, shaped from an asymmetric input pulse: (a) input pulse, (b) spectrum, and (c) spectron pulse, shaped at the length of ζ=25.

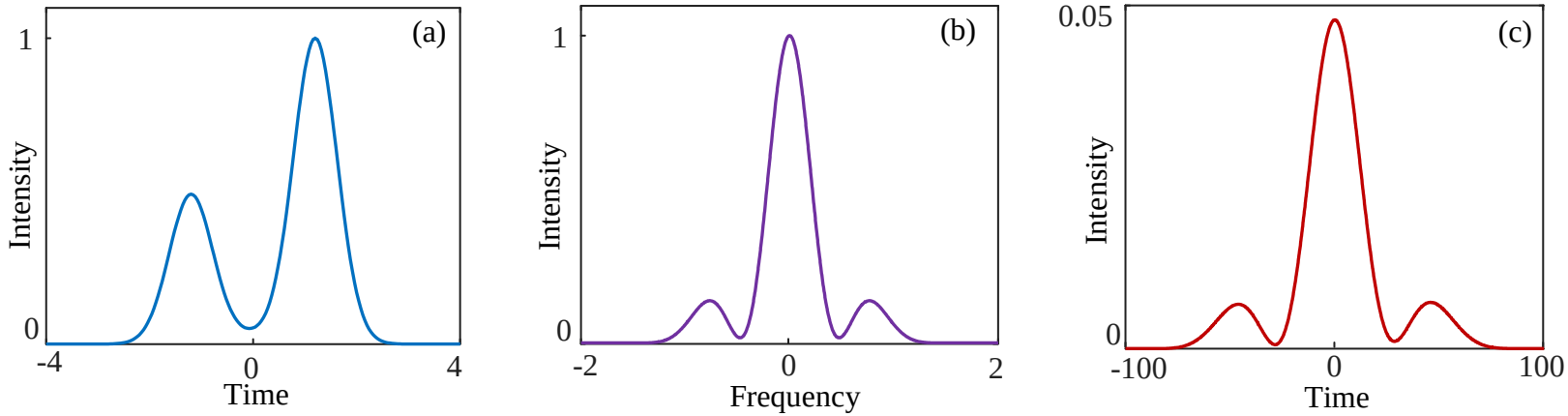

Figure 4.17. Spectron shaped from a two-peak input pulse: (a) input pulse, (b) spectrum, and (c) spectron pulse, shaped at the length ζ=60.

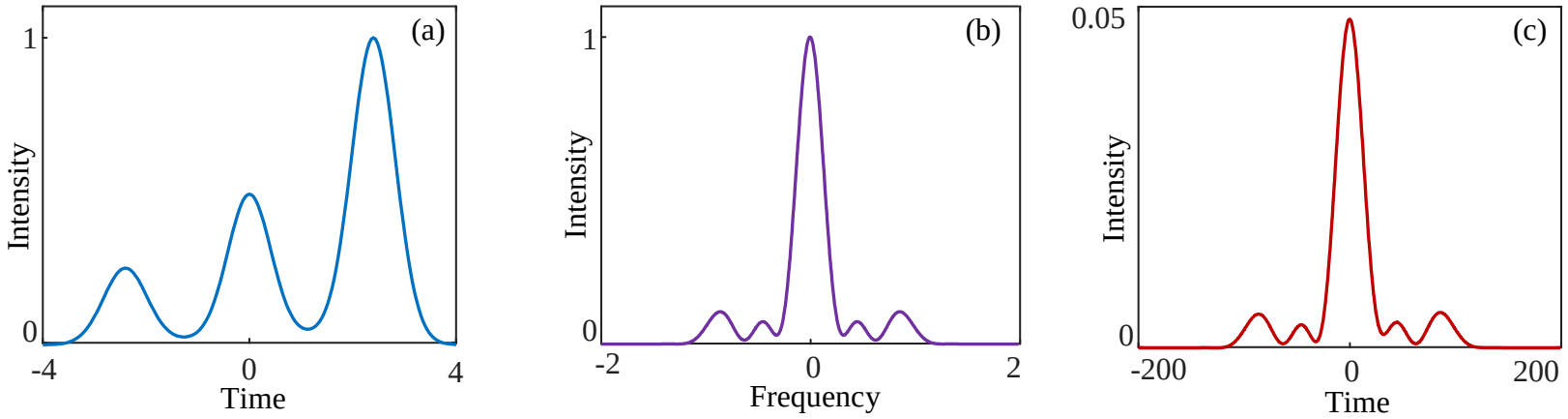

Figure 4.18. Spectron shaped from a three-peak input pulse: (a) input pulse, (b) spectrum, and (c) spectron pulse, shaped at the length ζ=100.

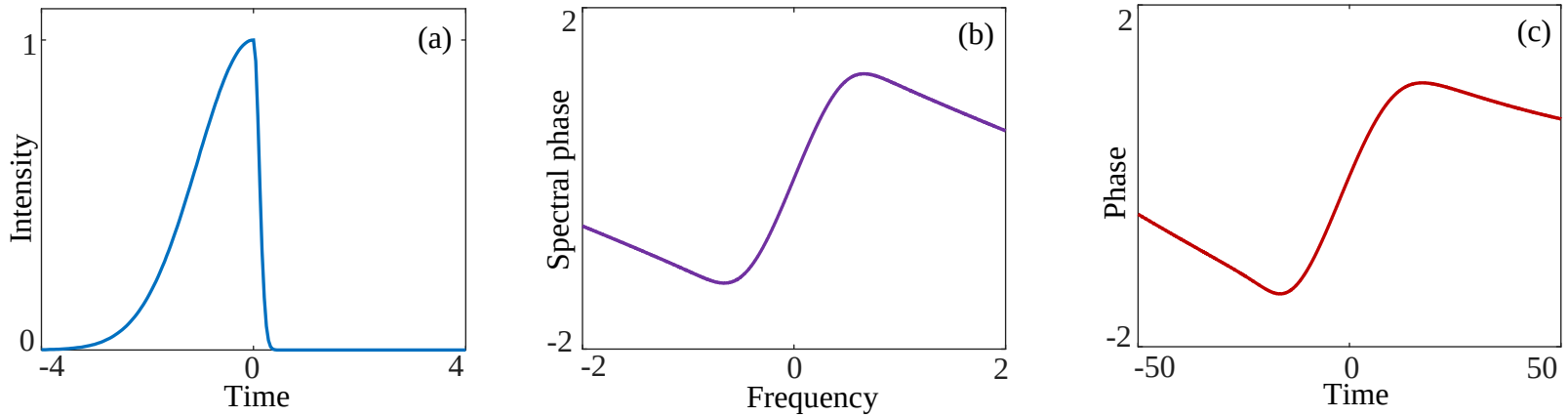

Figure 4.19. Spectron shaped from an asymmetric pulse: (a) input pulse, (b) spectral phase of the asymmetric pulse, and (c) spectron pulse temporal phase, shaped at the length ζ=25.

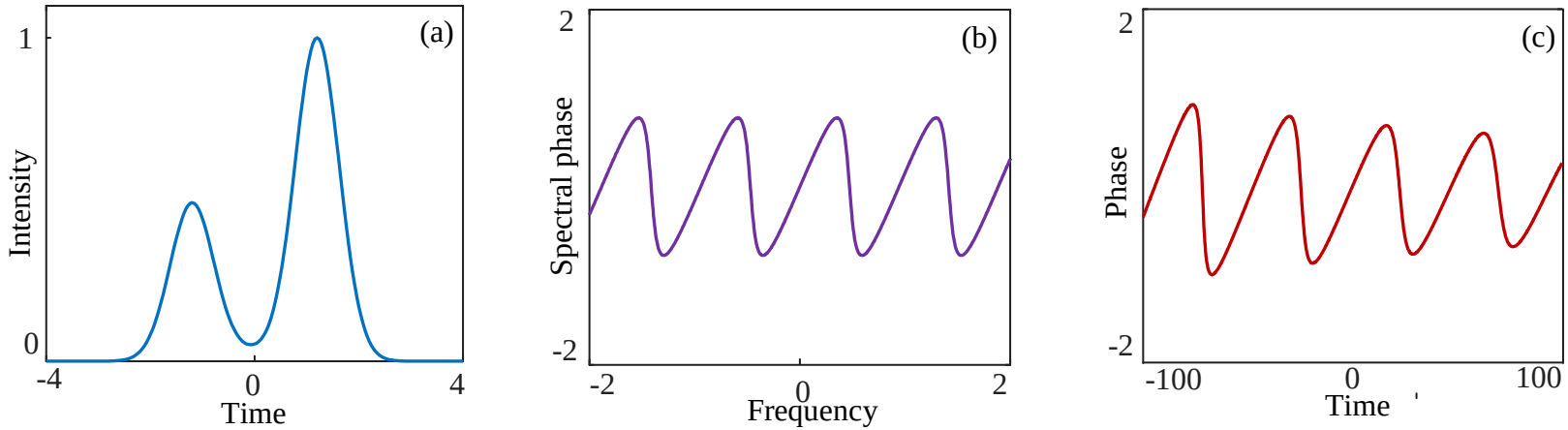

Figure 4.20. Spectron shaped from a two-peak pulse: (a) input pulse, (b) spectral phase of the two-peak pulse, and (c) spectron pulse temporal phase, shaped at the length ζ=60.

Finally, the phase peculiarities of the spectron generated from a three-peak pulse (fig. 4.21a) were studied. The proportions of three-peak pulse, again, was taken the same as in previous example (fig. 4.18a). The pulse passed through the ζ=100 dispersive element, which resulted in the shaping of the spectron pulse with temporal phase shown in figure 4.21c, which repeats the initial spectral phase (fig. 4.21b). These results show, that the spectron shaping process not only results in the intensity shape repeating the spectrum, but also the input pulse spectral phase reproduction by the temporal phase of the spectron pulse.

Thereafter, the formation of spectron from pulses with amplitude and phase modulations (AM and PM) was studied. The AM and PM were applied separately on a Gaussian spectra. The spectrum AM, with amplitude σ_{amp} and period T was given as

$$|\Psi(\Omega,0)| = |\Psi_0(\Omega)|\left[1+\sigma_{amp}\cos(T\Omega)\right], \tag{4.10}$$

and the spectrum PM (with amplitude σ_{ph} and period T) by the formula:

$$|\Psi(\Omega,0)| = \Psi_0(\Omega)\exp\left[i\sigma_{ph}\cos(T\Omega)\right]. \tag{4.11}$$

Applying the AM on the Gaussian spectrum resulted in pulse and spectrum shown in figure 4.22a and 4.22b (solid line), respectively. The minimum length ζ required for the spectron pulse shaping (to repeat the spectrum by the pulse intensity profile) is denoted as ζ_{amp}. The parameters of AM here were the following: $\sigma_{amp} = 0.5$; $T = 4\pi/\Delta\Omega$ ($\Delta\Omega$ is the spectral width). Figure 4.22b (dashed curve) shows the spectron, shaped at the length $\zeta_{amp} = 250$.

Figure 4.23 shows the formation of spectron pulse from a pulse with PM applied on its Gaussian spectrum. The resulting pulse and spectrum are shown in figure 4.23a and 4.23b (solid line), respectively.

The minimum length ζ required for the spectron pulse shaping in the meaning of phases (to repeat the initial spectral phase by the temporal phase profile of the output pulse) is denoted as ζ_{ph}. The PM parameters were the following: $\sigma_{ph} = 0.5$; $T = 4\pi/\Delta\Omega$. For these parameters, ζ_{ph} = 400. At this length, the temporal phase of the shaped spectron (fig. 4.23b, dashed line) repeats the shape of the input pulse spectral phase. Figure 4.23c shows the derivatives of the spectron temporal phase (dashed line) and the spectral phase

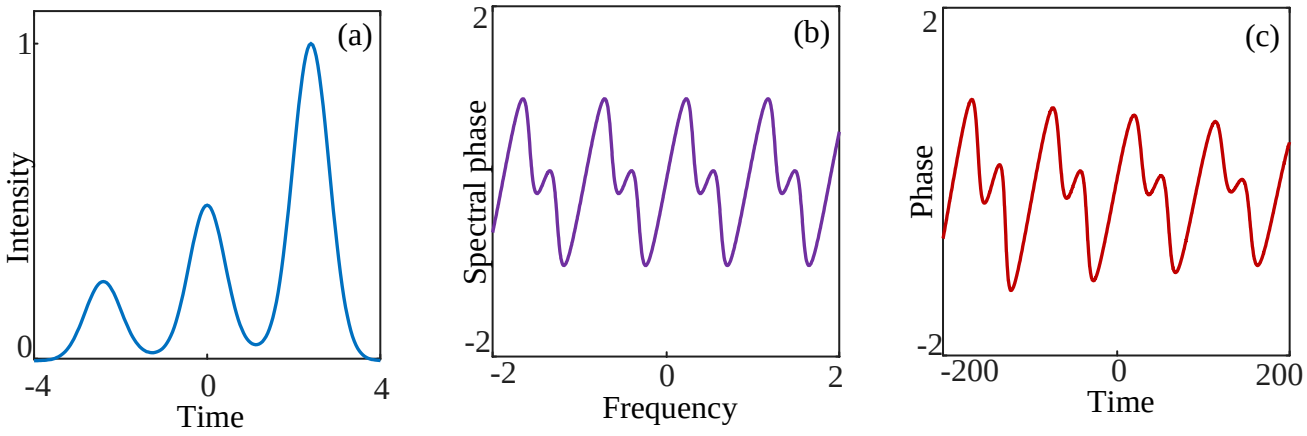

Figure 4.21. Spectron shaped from a three-peak pulse: (a) input pulse, (b) spectral phase of the three-peak pulse, and (c) spectron pulse temporal phase, shaped at the length ζ=100.

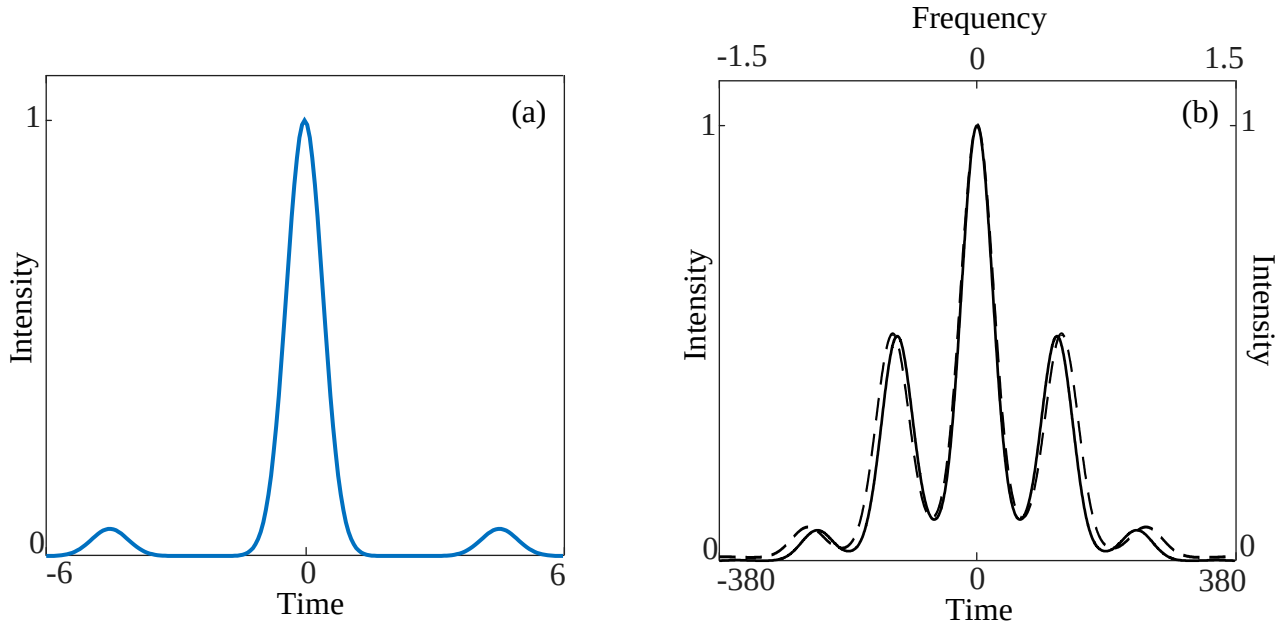

Figure 4.22. Spectron shaped from a pulse with AM of the Gaussian spectrum: (a) input pulse, (b) spectrum (solid line) and spectron pulse (dashed line) shaped at the length ζ_{amp} = 250.

of the input pulse (solid line).

The dependences of ζ_{amp} (fig. 4.24a) and ζ_{ph} (4.24b) from the parameters σ_{amp} and σ_{ph}, respectively, were studied as well. Both dependences are parabolic, with the higher values of ζ_{ph} than ζ_{amp} for the equal values of σ_{amp} and σ_{ph}.

Thereafter, the process of spectron shaping from two-peak pulse (fig. 4.25a) with initial SPM was numerically studied. The proportions of the two-peak pulse had a peak relation of 1:10 and temporal delay between two peaks equal to 2.5 times of the single pulse duration. The pulse had SPM-interaction in a short piece of fiber with the following parameters: $\zeta = 0.5$, $R = 8$, where $R = L_D/L_{NL}$ is the parameter of nonlinearity, and L_{NL} – the nonlinear length [11]. The spectrum at the output of the fiber had shape shown in figure 4.25b (solid line). The spectron pulse, shaped after a dispersive element with length of $\zeta = 70$ is shown in figure 4.25b (dashed line). The spectral phase of the input pulse and its derivative are shown in figure 4.25c and d (solid lines), respectively. Temporal phase of spectron and its derivative are shown in figure 4.25c and d (dashed lines), respectively. The phases and their derivatives have small mismatch, which is because of the impact of fiber dispersion.

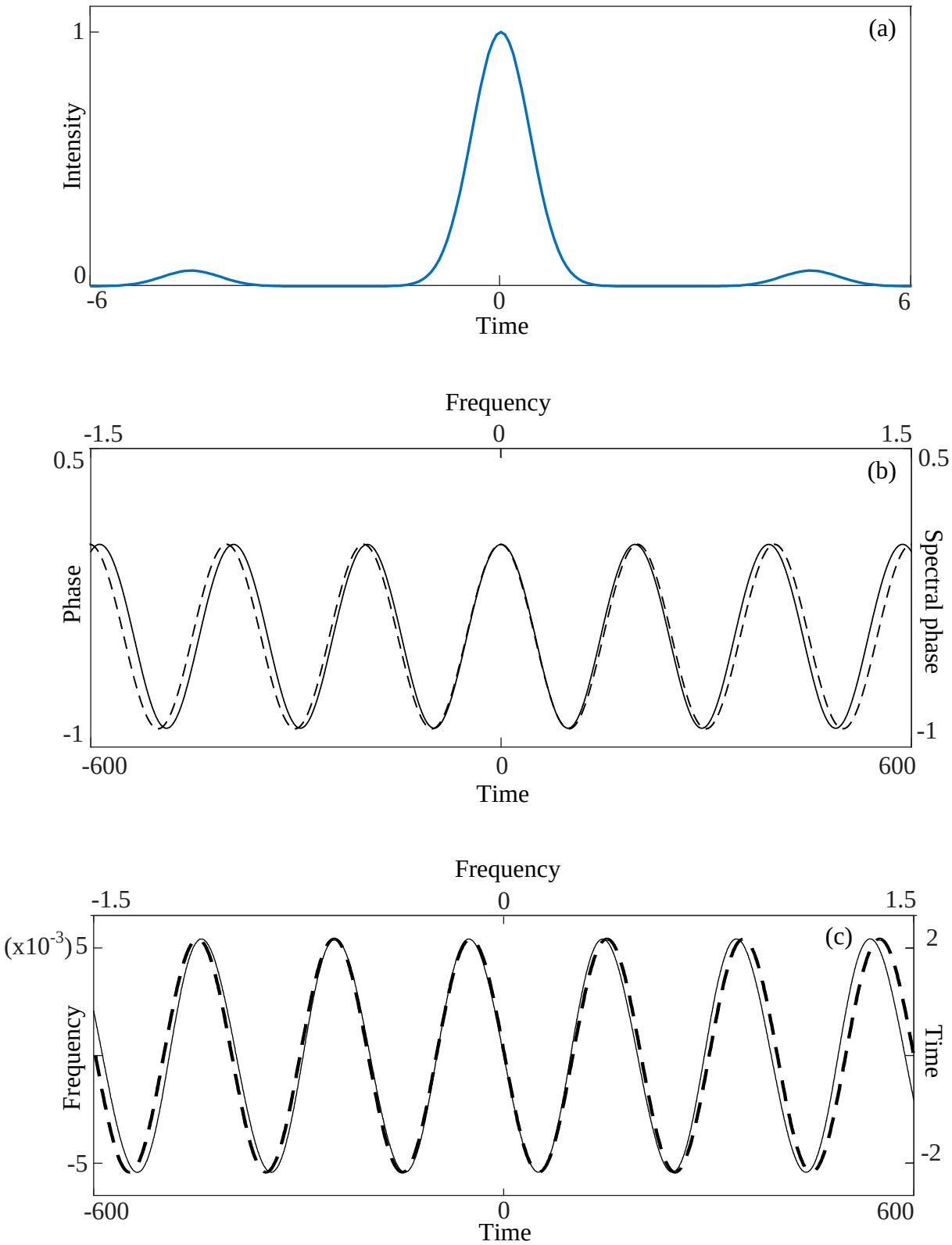

Figure 4.23. Spectron shaped from a pulse with the PM of the Gaussian spectrum: (a) input pulse, (b) initial spectral phase (solid line) and spectron's temporal phase (dashed line) shaped at length ζ_{ph}= 400, (c) derivatives of initial spectral phase (solid line) and temporal phase of the spectron (dashed line).

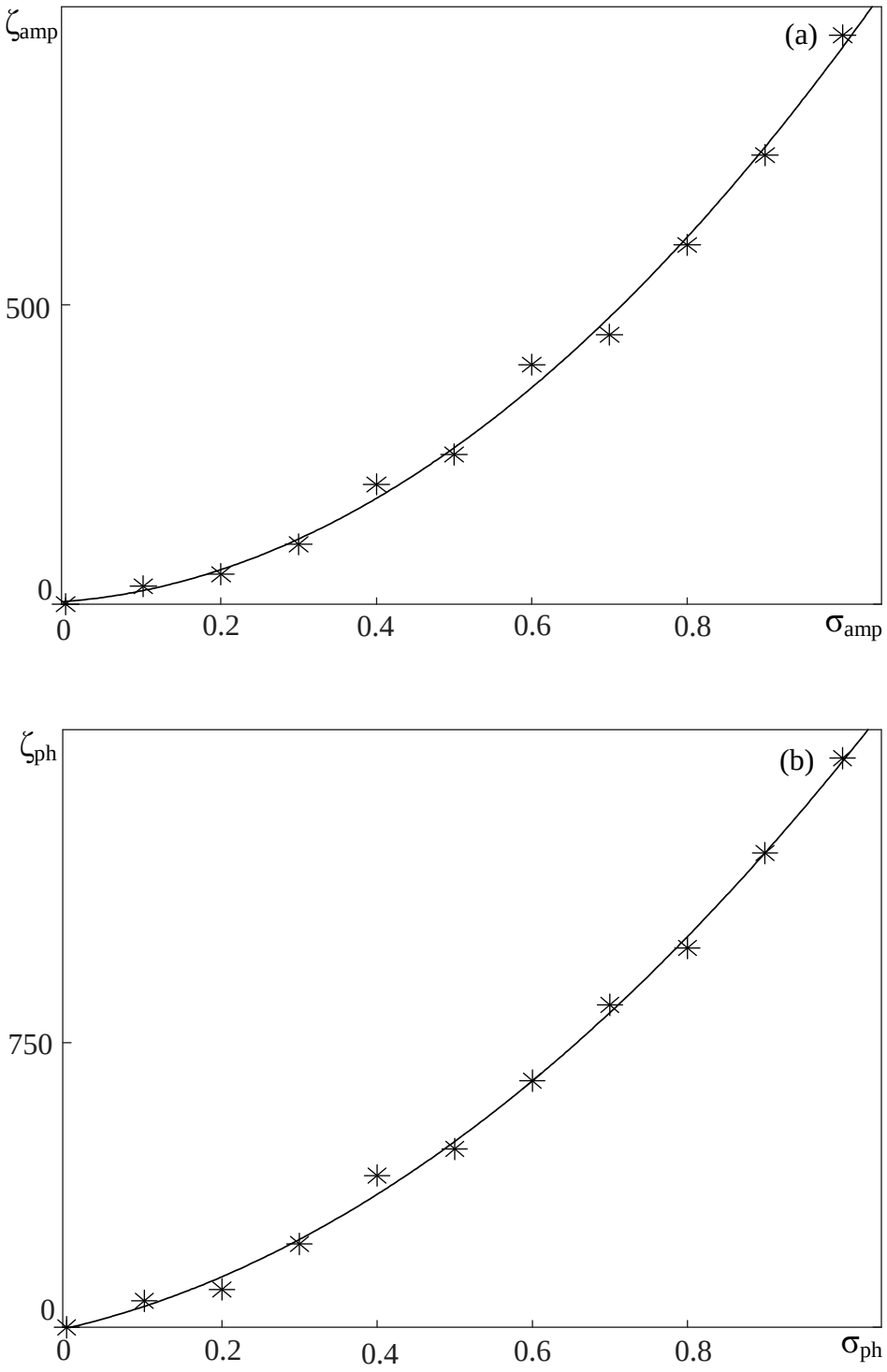

Figure 4.24. Dependence of (a) ζ_{amp} and (b) ζ_{ph} from parameters σ_{amp} and σ_{ph}, for spectron shaping from pulses with spectral AM and PM, respectively.

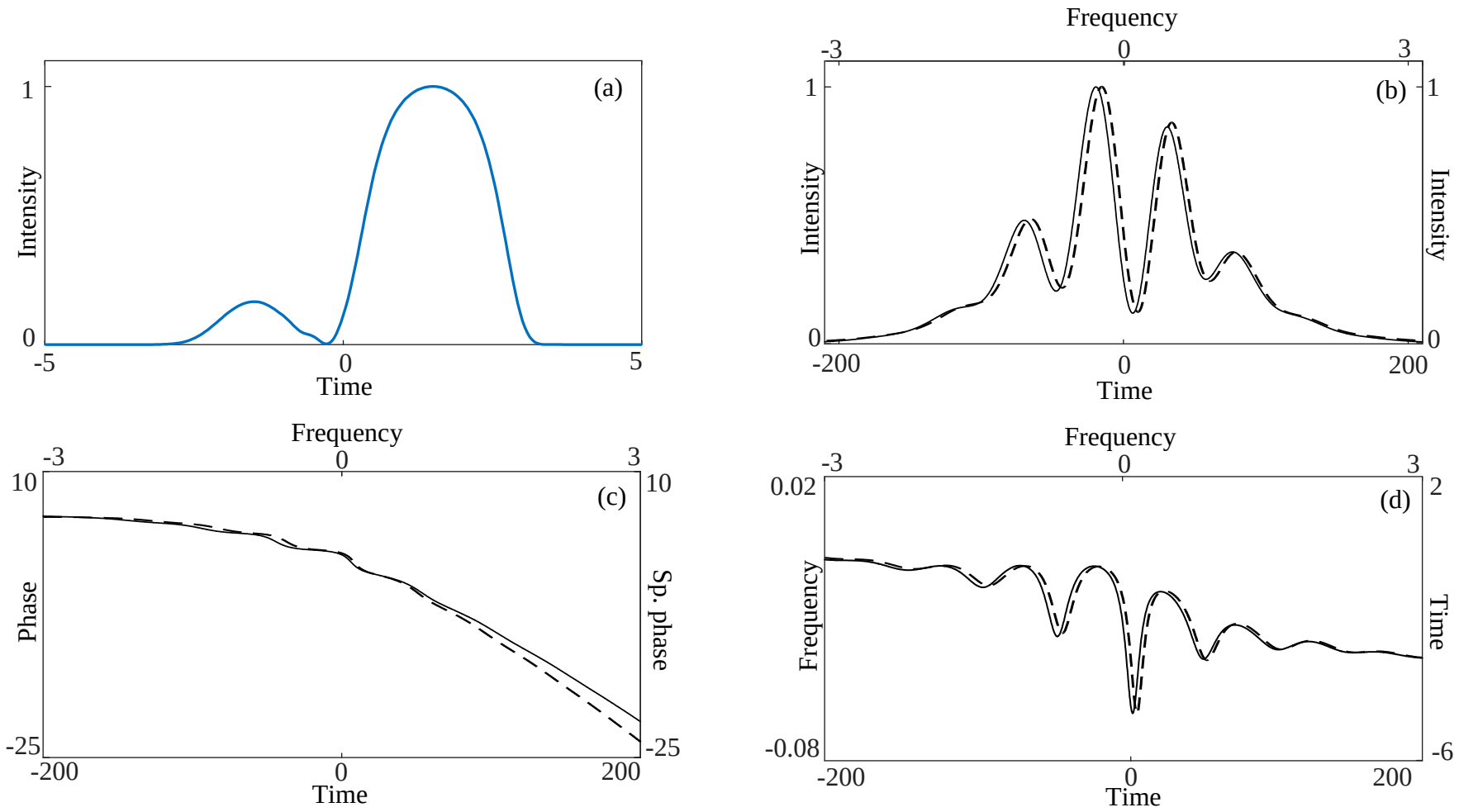

Figure 4.25. Spectron shaped from a two-peak pulse with SPM: (a) input pulse, (b) spectrum (solid line) and spectron pulse (dashed line) at $\zeta = 70$, (c) initial spectral phase (solid line) and spectron temporal phase (dashed line), (d) derivatives of initial spectral phase (solid line) and temporal phase of the spectron (dashed line).

Conclusion

This chapter is representing the research, aimed at development of femtosecond pulse duration measurement similaritonic technique, and study of spectron phase peculiarities. Results represented in this chapter are:

1. Numerical study of dependence of similariton spectral width from the energy and duration of input pulse. The relation is studied for bell-shaped, two-peak and compressed pulses. As a result, a general relation between the test pulse duration and energy, and similariton spectral width is found, for any pulse form.
2. Experimental study of similariton spectral width dependence from test pulse duration and average power for Gaussian, two-peak and compressed pulses, with various durations. The real-time performance of the technique was demonstrated for chirped laser pulses. The technical implementation curves of for Thorlabs 780HP SMF is also made.
3. Numerical demonstration of transfer of phase information from spectral to temporal domain in the process of spectron shaping. The phase peculiarities of spectron generated from various pulses (asymmetric, multi-peak, pulses with AM/PM of spectrum, two-peak pulses with SPM), were studied.

The duration measurement similaritonic technique can be used as an alternative to the autocorrelation technique. The advantages of this technique are the simplicity and the possibility of real-time measurements through stretching of the pulses and registration with an oscilloscope.

The transfer of phase information from spectral to temporal domain in the process of spectron shaping is of interest in context of pulse complex field complete characterization. This can serve as an alternative to spectral interferometric techniques of pulse characterization.

Summary

Classic, all-fiber and similaritonic techniques of spectral compression of femtosecond laser pulses are studied experimentally. The classic technique, using prism pair as a dispersive delay line, provided 12x SC. The all-fiber technique is implemented by replacing the prism pair with a hollow-core fiber with negative dispersion, providing 8.4x SC. The similaritonic technique, by compensating the chirp of dispersively stretched pulse with the chirp of the similariton pulse in the process of sum-frequency generation, is performed in an all-fiber configuration, with hollow-core fiber used instead of the prism pair, resulting in 11x SC.

Based on the detailed experimental studies of similaritonic technique of SC, a compact (30x30cm) commercial prototype of the spectrotemporal imaging device is developed. Moreover, the configuration of spectrotemporal imaging device with the hollow core fiber (instead of prism or grating disperive delay line) is also performed successfully.

The effect of spectral self-compression, a spectral analogue of the pulse solitonic self-compression, is demonstrated experimentally for the first time. The self-interaction of pulses at 800nm wavelength in a 2-m long HCF-800B hollow-core fiber resulted in a 30% narrowing of the spectrum with the increasing of pulse autocorrelation duration from 150fs to 1.3ps. A higher ratio spectral self-compression (~4x) is also registered in the initial experiment with the noisy supercontinuum radiation.

The detailed numerical studies of spectral peculiarities of the nonlinear-dispersive similariton showed the general dependence of the similariton spectral bandwidth from the seed pulse duration and its energy, allowing to develop a simple similaritonic technique of femtosecond pulse duration determination. This technique is tested for Gaussian, two-peak and compressed pulses, with results being in a quantitative agreement with the theoretical predictions.

The phase peculiarities of the spectron pulse are studied numerically. In particular, the transfer of spectral information to temporal domain for phases is studied, for a variety of test pulses, such as Gaussian, sech, asymmetric, multi-peak, etc. The results of the

study showed, that in the process of spectron shaping, the transfer of information (modulation) from spectral to temporal domain takes place not only for the amplitude, but also for the phase of the radiation field (i.e. the complete dispersive Fourier conversion occurs for complex field).

Acknowledgements

I would like to express thankfulness to my scientific advisor Prof. Levon Mouradian, who supported me at each point of this work with his wise advises and productive discussions. His experience and knowledge taught me everything I needed to accomplish this work.

I am grateful to Prof. Vasili Tsakanov for his help and encouragement during this work. My thesis would not be possible without his constant support.

I am also thankful to Aram Zeytunyan, who helped to take my first “steps” in scientific world.

Last but not least, I am thankful to my colleagues at Laboratory of Ultrafast Optics and Photonics, and CANDLE SRI for their brilliant collaboration.

References:

1. W.P. Leemans, A. J. Gonsalves, H. Mao, K. Nakamura, C. Benedetti, C. Schroeder, Cs. Tóth, J. Daniels, D. Mittelberger, S. Bulanov, J. Vay, C.G.R. Geddes, and E. Esarey, “Multi-GeV electron beams from capillary-discharge-guided subpetawatt laser pulses in the self-trapping regime”, Phys. Rev. Lett. 113 (24) (2014).
2. D. Powers, I. Ghebregziabher, G. Golovin, C. Liu, S. Chen, S. Banerjee, J. Zhang, D.P. Umstadter, “Quasi-monoenergetic and tunable X-rays from a laser-driven Compton light source”, Nature Photonics 8, 28–31 (2014).
3. E.A. Nanni, W.R. Huang, K. Hong, K. Ravi, A. Fallahi, G. Moriena, R. Dwayne Miller, and F. Kärtner, “Terahertz-driven linear electron acceleration”, Nature Communications 6, 8486 (2015).
4. R. Joel England, R. Nobel, Z. Wu, M. Qi, “Dielectric laser accelerators”, Rev. Mod. Phys. 86, 1337 (2014).
5. T. Shintake, H. Tanaka, T. Hara, T. Tanaka, K. Togawa, M. Yabashi, Y. Otake, Y. Asano, T. Bizen, T. Fukui, S. Goto, A. Higashiya, T. Hirono, N. Hosoda, T. Inagaki, S. Inoue, M. Ishii, Y. Kim, H. Kimura, M. Kitamura, T. Kobayashi, H. Maesaka, T. Masuda, S. Matsui, T. Matsushita, X. Maréchal, M. Nagasono, H. Ohashi, T. Ohata, T. Ohshima, K. Onoe, K. Shirasawa, T. Takagi, S. Takahashi, M. Takeuchi, K. Tamasaku, R. Tanaka, Y. Tanaka, T. Tanikawa, T. Togashi, S. Wu, A. Yamashita, K. Yanagida, C. Zhang, H. Kitamura, and T. Ishikawa, “A compact free-electron laser for generating coherent radiation in the extreme ultraviolet region”, Nature Photonics 2, 555-559 (2008).
6. Z. Huang, K.-J. Kim, “Review of x-ray free-electron laser theory” Physical Review Special Topics: Accelerators and Beams, 10, 034801 (2007).
7. I. Agapov, G.A. Blair, and M. Woodley, “Beam emittance measurement with laser wire scanners in the International Linear Collider beam delivery system”, Phys. Rev. ST 10 112801 (2007).
8. S. Antipov, M. Babzien, C. Jing, M. Fedurin, W. Gai, A. Kanareykin, K. Kusche, V. Yakimenko, and A. Zholents, “Subpicosecond Bunch Train Production for a Tunable mJ Level THz Source”, Phys. Rev. Lett. 111, 134802 (2013).

9. L.Kh. Mouradian, F. Louradour, V. Messager, A. Barthélémy, C. Froehly, “Spectro-temporal imaging of femtosecond events”, IEEE J. Quantum Electron. 36, 795-801 (2000).
10. L.Kh. Mouradian, A.V. Zohrabyan, V.J. Ninoyan, A.A. Kutuzian, C. Froehly, F. Louradour, A. Barthélémy, “Characterization of optical signals in fiber-optic Fourier converter,” Proc. SPIE 3418, Advances in Optical Beam Characterization and Measurements, (9 October 1998).
11. L. Mouradian and A. Barthelemy “Nonlinear-Dispersive Similaritons of Passive Fibers: Applications in Ultrafast Optics” Chapter 6 in “Shaping Light in Nonlinear Optical Fibers” Ed. S. Boscolo and Ch. Finot ©2017 John Wiley & Sons Ltd.
12. S.A. Akhmanov, V.A. Vysloukh, and A.S. Chirkin, “Optics of Femtosecond Laser Pulses”, AIP, New York (1992).
13. R. Salem, M. Foster, and A. Gaeta, “Application of space-time duality to ultrahigh-speed optical signal processing”, Advances in Optics and Photonics 5, 274–317 (2013).
14. K. Goda, B. Jalali, “Dispersive Fourier transformation for fast continuous single-shot measurements” Nature Photon. 7, 102–112 (2013).
15. D.R. Solli, J. Chou, and B. Jalali, “Amplified wavelength-time transformation for real-time spectroscopy”, Nature Photon. 2, 48–51 (2008).
16. D.R. Solli, C. Roper, P. Koonath, and B. Jalali, “Optical rogue waves”, Nature 450, 1054–1057 (2007).
17. D. R. Solli, C. Ropers, and B. Jalali, “Rare frustration of optical supercontinuum generation”, Appl. Phys. Lett. 96, 151108 (2010).
18. I. Petermann, B. Sahlgren, S. Helmfrid, and A.T. Friberg, "Fabrication of advanced fiber Bragg gratings by use of sequential writing with a continuous-wave ultraviolet laser source", Applied Optics. 41, 1051–1056 (2002).
19. G. Meltz, W.W. Morey, and W.H. Glenn, "Formation of Bragg gratings in optical fibers by a transverse holographic method", Opt. Lett. 14(15): 823–5 (1989).
20. E. Diebold, N. Hon, Z. Tan, J. Chou, T. Sienicki, C. Wang, and B. Jalali, “Giant tunable optical dispersion using chromo-modal excitation of a multimode waveguide”, Opt. Express, vol. 19, No. 24 (2011).

21. L. Mouradian, A. Zeytunyan, and G. Yesayan, “Similariton-based spectral interferometry for signal analysis on femtosecond time scale”. In Interferometry: Research and Applications in Science and Technology (ed. I. Padron). InTech, Moscow, pp. 99–124 (2012).
22. A. Pegoraro, A. Ridsdale, D. Moffatt, Y. Jia, J.P. Pezacki, A. Stolow, “Optimally chirped multimodal CARS microscopy based on a single Ti:sapphire oscillator”, Optics Express, 17, 2984 (2009).
23. E. Gershgoren, R. Bartels, J. Fourkas, R. Tobey, M. Murnane, and H. Kapteyn, “Simplified setup for high-resolution spectroscopy that uses ultrashort pulses”, Opt. Lett., 28, 361 (2003).
24. A. Zeytunyan, A. Muradyan, G. Yesayan, L. Mouradian, F. Louradour, and A. Barthélémy, “Generation of broadband similaritons for complete characterization of femtosecond pulses”, Optics Communications, Vol. 284, (15), 3742–3747, (2011).
25. L.Kh. Muradyan, N.L. Markaryan, T.A. Papazyan, and A.A. Ohanyan, “Self-action of chirped pulses: spectral compression”, Conference on Lasers and Electro-Optics, Vol. 7 of 1990 OSA Tech. Digest Series, paper CTUH32 (1990).
26. D.J. Kane and R. Trebino, "Characterization of arbitrary femtosecond pulses using frequencyresolved optical gating", IEEE J. Quantum Electron. 29, 571-579 (1993).
27. R. Trebino, “Frequency-Resolved Optical Gating. The Measurement of Ultrashort Laser Pulses”, Kluwer Academic Publishers, Dordrecht (2002).
28. N.L.Margaryan, L.Kh.Mouradian, and T.A. Papazyan, “Spectral compression of ultrashort laser pulses”, Sov. J. Quant. Electron. 21, 783–785 (1991).
29. D. Kane and R. Trebino, “Single-shot measurement of the intensity and phase of an arbitrary ultrashort pulse by using frequency-resolved optical gating”, Opt. Lett. Vol. 18, No. 10 (1993).
30. T. Mansuryan, A. Zeytunyan, M. Kalashyan, G. Yesayan, L. Mouradian, F. Louradour, and A. Barthélémy, “Parabolic temporal lensing and spectral imaging: a femtosecond optical oscilloscope”, J. Opt. Soc. Am. B, Vol. 25, No. 5 (2008).
31. L. Kh. Mouradian, A. V. Zohrabian, C. Froehly, F. Louradour, and A. Barthélémy, “Spectral imaging of pulses temoral profile”, in Conference on Lasers and Electro-

Optics (CLEO/Europe), OSA Technical Digest Series (Optical Society of America, 1998), paper CMA5.

32. L.Kh. Mouradian, F. Louradour, C. Froehly, and A. Barthélémy, “Self- and cross-phase modulation of chirped pulses: spectral imaging of femtosecond pulses”, in Nonlinear Guided Waves and Their Applications, Vol. 5 of OSA Technical Digest Series (Optical Society of America,1998), paper NFC4.
33. A.V. Zohrabyan, A.A. Kutuzian, V.Zh. Ninoyan, and L.Kh. Mouradian, “Spectral compression of picosecond pulses by means of cross phase modulation”, AIP Conf. Proc. 406, 395–401 (1997).
34. N. L. Markaryan and L. Kh. Muradyan, “Determination of the temporal profiles of ultrashort pulses by a fibre-optic compression technique”, Quantum Electron. 25, 668–670 (1995).
35. G. Yesayan, K. Palanjyan, T. Mansuryan, A. Zeytunyan, L. Mouradian, P. Kockaert, and P. Emplit, “Nonlinearspectronic similariton of single-mode fiber without gain,” in Nonlinear Photonics, OSA Technical Digest, paper JWA18 (2007).
36. J. Dudley, X. Gu, L. Xu, M. Kimmel, E. Zeek, P. O’Shea, R. Trebino, S. Coen, and R. Windeler, “Cross-correlation frequency resolved optical gating analysis of broadband continuum generation in photonic crystal fiber: simulations and experiments”, Opt. Express, Vol. 10, No. 21 (2002).
37. D. Reid, P. Loza-Alvarez, C. Brown, T. Beddard, and W. Sibbett, “Amplitude and phase measurement of mid-infrared femtosecond pulses by using cross-correlation frequency-resolved optical gating”, Opt. Letters, Vol. 25, No. 19 (2000).
38. S. Akturk, M. Kimmel, P. O’Shea, R. Trebino, “Measuring spatial chirp in ultrashort pulses using single-shot frequency-resolved optical gating”, Opt. Express 11, 68-78 (2003).
39. J. Piasecki, B. Colombeau, M. Vampouille, C. Froehly, J.A. Arnaud, "Nouvelle méthode de mesure de la réponse impulsionnelle des fibres optiques", Appl. Opt. 19, 3749-3755 (1980).
40. C. Iaconis and I.A. Walmsley, “Spectral phase interferometry for direct electric-field reconstruction of ultrashort optical pulses”, Opt. Lett. 23, 792-794 (1998).

41. M. Anderson, A. Monmayrant, S.-P. Gorza, P. Wasylczyk, and I.A. Walmsley, “SPIDER: A decade of measuring ultrashort pulses”, Laser Phys. Lett. 5, No. 4, 259–266 (2008).
42. C. Iaconis and I. Walmsley, “Self-referencing spectral interferometry for measuring ultrashort optical pulses”, IEEE J. Quant. Electron., Vol. 35, No. 4 (1999).
43. V. Messager, F. Louradour, C. Froehly, A. Barthélémy, “Coherent measurement of short laser pulses based on spectral interferometry resolved in time”, Opt. Lett. 28, 743-745 (2003).
44. M. Lelek, F. Louradour, A. Barthélémy, C. Froehly, T. Mansourian, L. Mouradian, J. P. Chambaret, G. Chériaux, B. Mercier, "Two-dimensional spectral shearing interferometry resolved in time for ultrashort optical pulse characterization", J. Opt. Soc. Am. B 25, A17-A24 (2008).
45. P. Kockaert, M. Haelterman, Ph. Emplit, and C. Froehly, “Complete characterization of (ultra)short optical pulses using fast linear detectors”, IEEE J. Sel. Top. Quantum Electron. 10, 206-212 (2004).
46. M. Asghari, Y. Park, J. Azana, “Complex-field measurement of ultrafast dynamic optical waveforms based on real-time spectral interferometry”, Opt. Express, Vol. 18, No 16 (2010).
47. J. Bromage, C. Dorrer, I. Begishev, N. Usechak, and J. Zuegel, “Highly sensitive, single-shot characterization for pulse widths from 0.4 to 85 ps using electro-optic hearing interferometry”, Opt. Lett. 31(23), 3523–3525 (2006).
48. P. Bowlan, P. Gabolde, A. Shreenath, K. McGresham, R. Trebino, and S. Akturk, “Crossed-beam spectral interferometry: a simple, high-spectral-resolution method for completely characterizing complex ultrashort pulses in real time,” Opt. Express 14(24), 11892–11900 (2006).
49. Y. Tong, L. Chan, and H. Tsang, “Fibre dispersion or pulse spectrum measurement using a sampling oscilloscope”, Electron. Lett. 33(11), 983–985 (1997).
50. J. Azaña, and M. A. Muriel, “Real-time optical spectrum analysis based on the time space duality in chirped fiber gratings”, IEEE J. Quantum Electron. 36(5), 517–526 (2000).

51. V. Lozovoy, I. Pastirk, M. Dantus, “Multiphoton intrapulse interference. IV. Ultrashort laser pulse spectral phase characterization and compensation,” Opt. Lett. 29, 775-777 (2004).
52. B. Xu, J.M. Gunn, M. Dela Cruz, V.V. Lozovoy, M. Dantus, “Quantitative investigation of the multiphoton intrapulse interference phase scan method for simultaneous phase measurement and compensation of femtosecond laser pulses”, J. Opt. Soc. Am. B 23, 750-759 (2004).
53. C. V. Bennett and B. H. Kolner, “Upconversion time microscope demonstrating 103x magnification of femtosecond waveforms”, Opt. Lett. 24, 783–785 (1999).
54. M.A. Foster, R. Salem, D.F. Geraghty, A.C. Turner-Foster, M. Lipson, and A.L. Gaeta, “Silicon-chip-based ultrafast optical oscilloscope”, Nature 456 81–4 (2008).
55. A. Zeytunyan, G. Yesayan, and L. Mouradian, “Pulse compression to 14 ds by third-order dispersion control in a hybrid grating-prism compressor”, App. Optics, Vol. 52, Issue 32, 7755-7758 (2013).
56. M. Oberthaler, R.A. Hopfel, “Special narrowing of ultrashort laser pulses by self-phase modulation in optical fibers”, Appl. Phys. Lett. 63, 1017–1019 (1993).
57. B.R. Washburn, J.A. Buck, and S.E. Ralph, “Transform-limited spectral compression due to self-phase modulation in fibers”, Opt. Lett. 25, 445–447 (2000).
58. L. Kh.Mouradian, A. V. Zohrabyan, A. Villeneuve, A. Yavrian, G. Rousseau, M. Piche, C. Froehly, F. Louradour, and A. Barthélémy, “Applications of temporal Kerr lensing to signal manipulation and analysis”, CLEO-Europe, Conf. Digest, v. 39 of OSA Trends in Optics and Photonics (OSA 2000), paper CTuH6.
59. E.R. Andresen, J.M. Dudley, D. Oron, C. Finot, and H. Rigneault, “Transform-limited spectral compression by self-phase modulation of amplitude-shaped pulses with negative chirp”, Opt. Lett. 36 707–709 (2011).
60. J. Fatome, B. Kibler, E. R. Andresen, H. Rigneault, and C. Finot, “All-fiber spectral compression of picosecond pulses at telecommunication wavelength enhanced by amplitude shaping”, Appl. Opt. 51 4547-4553 (2012).
61. A.A. Kutuzyan, T.G. Mansuryan, A.A. Kirakosyan, and L.K. Mouradian, “Self-forming of temporal dark soliton in spectral compressor”, Proc. SPIE 5135, Optical

Information, Data Processing and Storage, and Laser Communication Technologies, (3 September 2003).

62. S. W. Clark, F. Ö. Ilday, and F. W. Wise, “Fiber delivery of femtosecond pulses from a Ti:sapphire laser”, Opt. Lett. 26, 1320–1322 (2001).
63. F. Louradour, E. Lopez-Lago, V. Couderc, V. Messager, and A. Barthélémy, “Dispersive-scan measurement of the fast component of the third-order nonlinearity of bulk materials and waveguides”, Opt. Lett. 24, 1361–1363 (1999).
64. F. Audo, S. Boscolo, J. Fatome, B. Kibler, and C. Finot, “Nonlinear spectrum broadening cancellation by sinusoidal phase modulation”, Opt. Lett., Vol. 42, No. 15 (2017).
65. Y. Okawachi, J. Sharping, C. Xu, and A. Gaeta, “Large tunable optical delay voa self-phase modulation and dispersion”, Opt. Express, Vol. 14, No. 25 (2006).
66. R. Boyd and D. Gauthier, “‘Slow’ and ‘fast’ light”, Progress in Optics 43, E. Wolf, ed., (Elsevier, Amsterdam, 2002), Chap. 6, p. 497-530 (2002).
67. J.E. Sharping, Y. Okawachi, J. van Howe, C. Wang, A. Willner, and A. Gaeta, “All-optical, wavelength and bandwidth preserving, pulse delay based on parametric wavelength conversion and dispersion”, Opt. Express 13, 7872-7877 (2005).
68. P. Mamyshev, “All-optical data regeneration based on self-phase modulation effect”, in Proc. ECOC‘98, Madrid, Spain, 1, 475-476 (1998).
69. G. Agrawal, “Nonlinear fiber optics: its history and recent progress”, J. Opt. Soc. Am. B, Vol. 28, No. 12 (2011).
70. G. Agrawal, “Nonlinear Fiber Optics”, Academic Press (1989).
71. M. Foster, A. Gaeta, “Soliton-effect compression of supercontinuum to few-cycle durations in photonic nanowires”, Optics Express, 13, 6848 (2005).
72. E. Magi, P. Steinvurzel, and B. Eggleton, “Tapered photonic crystal fibers”, Opt. Express 12, 776-784 (2004).
73. S. Leon-Saval, T. Birks, W. Wadsworth, P. Russell, M. Mason, “Supercontinuum generation in submicron fibre waveguides”, Opt. Express 12, 2864 (2004).
74. M. Foster and A. Gaeta, “Ultra-low threshold supercontinuum generation in sub-wavelength waveguides”, Opt. Express 12, 3137 (2004).

75. T. Balciunas, C. Fouracade-Sutin, G. Fan, T. Witting, A. Voronin, A. Zheltikov, F. Gerome, G. Paulus, A. Baltuska, and F. Benabid, “A strong-field driver in the single-cycle regime based on self-compression in a Kagome fibre”, Nature Communications, 7117, (2015).
76. Y. Lin, C. Huang, “Large-scale and structure-tunable laser spectral compression in an optical dispersion-increasing fiber”, Opt. Express, Vol. 25, No 15 (2017).
77. G. Agrawal, “Nonlinear Fiber Optics”, 4th ed. (Academic, 2007).
78. Ph. Emplit, J. Hamaide, F. Reynaud, C. Froehly, and A. Barthélémy, "Picosecond steps and dark pulses through nonlinear single mode fibers", Opt. Commun. 62, 374-379 (1987).
79. A. Weiner, J. Heritage, R. Hawkins, R. Thurston, E. Kirschner, D. Leaird, W. Tomlinson, "Experimental observation of the fundamental dark soliton in optical fibers", Phys. Rev. Lett. 61, 2445-2448 (1988).
80. J. Rothenberg and H. Heinrich, "Observation of the formation of dark-soliton trains in optical fibers", Opt. Lett. 17, 261-263 (1992).
81. W. Zhao and E. Bourkoff, "Generation, propagation, and amplification of dark solitons", J. Opt. Soc. Am. B 9, 1134-1144 (1992).
82. J. Giannini and R. Joseph, "The propagation of bright and dark solitons in lossy optical fibers", IEEE J. Quantum Electron. QE-26, 2109-2114 (1990).
83. M. Lisak, D. Anderson, B. Malomed, "Dissipative damping of dark solitons in optical fibers", Opt. Lett. 16, 1936-1937 (1991).
84. W. Zhao, E. Bourkoff, "Interactions between dark solitons", Opt. Lett. 14, 1371-1373 (1989).
85. Ph. Emplit, M. Haelterman, J. Hamaide, "Picosecond dark soliton over a 1-km fiber at 850 nm", Opt. Lett. 18, 1047-1049 (1993).
86. A.B. Salem, R. Chief, and M. Zghal, “Soliton-self compression in highly nonlinear chalcogenide photonic nanowires with ultralow pulse energy” Opt. Express 19, 1995510 (2011).

87. A.A. Amorim, M.V. Tognetti, P. Oliveira, J.L. Silva, L.M. Bernardo, F.X. Kärtner, and H.M. Crespo, “Sub-two-cycle pulses by soliton self-compression in highly nonlinear photonic crystal fibers” Opt. Lett. 34, 3851 (2009).
88. L. Mollenauer, R. Stolen, and J. Gordon “Experimental-observation of picosecond pulse narrowing and solitons in optical fibers” Phys. Rev. Lett. 45, 1095 (1980).
89. L.Mollenauer, R. Stolen, J. Gordon, and W. Tomlinson, “Extreme picosecond pulse narrowing by means of soliton effect in single-mode fibers” Opt. Lett. 8/5, 289 (1983).
90. S.Boscolo, S.K.Turitsyn, and C.Finot, “Amplifier similariton fiber laser with nonlinear spectral compression,” Opt. Lett. 37, 4531 (2012).
91. R. Alfano and S. Shapiro, “Observation of self-phase modulation and small-scale filaments in crystals and glasses”, Phys. Rev. Lett. 24 (11), 592 (1970).
92. M. Bellini and T. Hänsch, “Phase-locked white-light continuum pulses: toward a universal optical frequency comb synthesizer”, Opt. Lett. 25 (14), 1049 (2000).
93. E. Goulielmakis, S. Koehler, B. Reiter, M. Schultze, A. Verhoef, E. Serebryannikov, A.M. Zheltikov, and F. Krausz “Ultrabroadband, coherent light source based on self-channeling of few-cycle pulses in helium”, Opt. Lett. 33 (13), 1407-1409 (2008).
94. H. Hundertmark, S. Rammler, T. Wilken, R. Holzwarth, T.W, Hänsch, and P. Russell, “Octave-spanning supercontinuum generated in SF6-glass PCF by a 1060 nm mode-locked fibre laser delivering 20 pJ per pulse”, Opt. Express 17 (3), 1919-1924 (2009).
95. R. Halir, Y. Okawachi, J. Levy, M. Foster, M. Lipson, and A. Gaeta, "Ultrabroadband supercontinuum generation in a CMOS-compatible platform", Opt. Lett. 37 (10) (2014).
96. R. Fork, C. Shank, C. Hirlimann, R. Yen, and W. Tomlinson, “Femtosecond white-light continuum pulses”, Opt. Lett. 8, (1) (1983).
97. B. Gross and J. Manassah, “Supercontinuum in the anomalous group-velocity dispersion region”, J. Opt. Soc. Am. B 9, 1813–1818 (1992).
98. J. Dudley, G. Genty, and S. Coen, “Supercontinuum generation in photonic crystal fiber”, Rev. Mod. Phys. 78, 1135 (2006).
99. A. Saliminia, S. Chin, and R. Vallée, “Ultra-broad and coherent white light generation in silica glass by focused femtosecond pulses at 1.5 μm”, Opt. Express 13 (15) (2005).

100. A. Brodeur and S. Chin, "Ultrafast white-light continuum generation and self-focusing in transparent condensed media", J. Opt. Soc. Am. B 16, 637-650 (1999).
101. D. Anderson, M. Desaix, M. Karlson, M. Lisak, and M.L. Quiroga-Teixeiro, “Wave-breaking-free pulses in nonlinear-optical fibers”, J. Opt. Soc. Am. B 10, pp 1185-1190 (1993).
102. C. Finot, G. Millot, C. Billet, J.M. Dudley, “Experimental generation of parabolic pulses via Raman amplification in optical fiber”, Opt. Express, Vol. 11, pp. 1547-1552 (2003).
103. V.I. Kruglov, A.C. Peacock, J.D. Harvey, and J.M. Dudley, “Self-similar propagation of parabolic pulses in normal-dispersion fiber amplifiers”, J. Opt. Soc. Am. B 19, pp. 461-469 (2002).
104. T. Hirooka, M. Nakazawa, “Parabolic pulse generation by use of a dispersion-decreasing fiber with normal group-velocity dispersion”, Opt. Lett., 29, 498-500 (2004).
105. A. Zeytunyan, G. Yesayan, L. Mouradian, P. Kockaert, P. Emplit, F. Louradour, and A. Barthelemy, “Nonlinear-dispersive similariton of passive fiber”, J. Europ. Opt. Soc. Rap. Public. 09009, Vol. 4 (2009).
106. A.S. Zeytunyan, “Bandwidth and duration of nonlinear-dispersive similariton”, Proc. of Yerevan State Univ. Phys. and Mathem. Sci., N 1, pp. 54-57 (2010).
107. С.А. Ахманов, В.А. Выслоух, А.С. Чиркин. Оптика фемтосекундных лазерных импульсов. Наука, Москва, (1988).
108. P.V. Kelkar, F.Coppinger, A.S. Bhushan, B. Jalali, “Time-domain optical sensing”, Electron. Lett., 35, 1661 (1999).
109. K. Goda, D.R. Solli, K.K. Tsia, B. Jalali, “Theory of amplified dispersive Fourier transformation”, Phys. Rev. A, 80 043821 (2009).
110. J. Azana, L.R. Chen, M.A. Muriel, and P.W.E. Smith, “Fiber Bragg grating period reconstruction using time-frequency signal analysis and application to distributed sensing”, Electron. Lett., 35, 2223 (1999).
111. A. Mahjoubfar, D.V. Churkin, S. Barland, N. Broderick, S.K. Turitsyn, B. Jalali, “Time stretch and its applications”, Nature Photon., 11, 341 (2017).
112. A.S. Zeytunyan, A. Muradyan, G.L. Yesayan, L.Kh. Mouradian, “Broadband similariton”, Laser Physics, 20, 1729 (2010).

List of abbreviations:

AC – autocorrelation

BBO crystal – beta-barium borate crystal

CARS – coherent anti-Stokes Raman scattering

CCD – charge-coupled device

CMD – chromo modal dispersion

DDL – dispersive delay line

DFT – dispersive Fourier transformation

FROG – frequency resolved optical gating

FWHM – full width at half maximum

GRENOUILLE – grating-eliminated no-nonsense observation of ultrafast incident laser light e-fields

GVD – group-velocity dispersion

HCF – hollow-core fiber

KLM laser – Kerr-lens modelocked laser

MIIPS – multiphoton intrapulse interference phase scan

NCHCF – negatively curved hollow-core fiber

NL-D similariton – nonlinear-dispersive similariton

OSA – optical spectrum analyzer

PCF – photonic crystal fiber

SC – spectral compression

Self-SC – spectral self-compression

SFG – sum-frequency generation

SHG – second-harmonic generation

SMF – single-mode fiber

SORBETS – superposition of optical radiation and beatings to extract the time signals

SPIDER – spectral phase interferometry for direct electric-field reconstruction

SPIRIT – spectral interferometry resolved in time

SPM – self-phase modulation

STI – spectrotemporal imaging